Predicting the Effect of Biofilm Growth on the Pressure Drop over a Biofilter

by

Jacoline van Jaarsveld

Thesis presented in partial fulfilment of the requirements for the degree
Master of Science in Applied Mathematics at
Stellenbosch University

Supervisor: Dr. Sonia Fidder-Woudberg
Faculty of Science
Department of Mathematical Sciences
Division of Applied Mathematics

December 2017

Declaration

By submitting this thesis electronically, I declare that the entirety of the work contained therein is my own, original work, that I am the sole author thereof (save to the extent explicitly otherwise stated), that reproduction and publication thereof by Stellenbosch University will not infringe any third party rights and that I have not previously in its entirety or in part submitted it for obtaining any qualification.

Date: December 2017

Abstract

Hydrogen sulphide is a poisonous gas produced by several industries. It is therefore crucial to investigate and mathematically model the environmentally friendly biofiltration process, which has the ability to remove poisonous gasses, such as hydrogen sulphide, from an air stream. In this study two approaches are used for modelling biofilm growth in three different biofilters, i.e. an empirical and analytical approach. In the empirical modelling approach, the pressure drop prediction of the Modified-Macdonald equation, the existing granular rectangular Representative Unit Cell (RUC) model and the model of Comiti and Renaud are used to determine the changes in biofilm affected porosity, specific surface area, tortuosity and biofilm thickness. The results are obtained by using Excel® Solver, which is based on an optimization method. Thereafter a sensitivity analysis is performed in order to analyze the effect of the sphericity. The analytical modelling approach involves only the RUC model. The first step is to predict the biofilm thickness. Thereafter, two methods are suggested for predicting the biofilm affected specific surface area. The first method is based on an approach suggested in the literature. In the second method, the RUC model is used to express the pressure drop in terms of the biofilm affected specific surface area, which yields the adapted RUC model. The biofilm affected specific surface area values are then obtained by making use of experimental pressure drop data and superficial velocity values. After incorporating both the analytically and empirically determined sphericity values into the adapted RUC model, the pressure drop results show the significant effect that the sphericity value has on the model predictions. Finally, a sensitivity analysis is performed on the input parameters to the model.

Opsomming

Verskeie nywerhede stel giftige waterstofsulfiedgas vry in die atmosfeer. Dit is dus noodsaaklik om die omgewingsvriendelike biofiltreringsproses, wat die vermoë het om giftige gasse, soos waterstofsulfied, vanuit die lugstroom te verwyder, te ondersoek en wiskundig te modelleer. Twee benaderings word gebruik in hierdie studie om die groei van biofilm in drie verskillende biofilters wiskundig te modelleer, d.i. 'n empiriese en 'n analitiese benadering. Die empiriese benadering behels die gebruik van die drukvalvoorspellings van die Gewysigde-Macdonald vergelyking, die bestaande korrelagtige reghoekige *Representative Unit Cell* (RUC) model en die model van Comiti en Renaud om die verandering in biofilm-geaffekteerde porositeit, spesifieke oppervlak-area, tortuositeit en biofilm dikte te bepaal. Die resultate is verkry deur gebruik te maak van Excel® Solver, wat gebaseer is op 'n optimeringsmetode. Daarna volg 'n sensitiwiteitsanalise op die effek van die bolvormigheid. Die analities gemodelleerde benadering is op slegs die RUC model gebaseer. Die eerste stap is om die dikte van die biofilm te voorspel. Daarna word twee metodes voorgestel vir die voorspelling van die biofilm-geaffekteerde spesifieke oppervlak-area. Die eerste metode is gebaseer op 'n benadering wat in die literatuur voorgestel word. Die tweede metode behels die gebruik van die RUC model om die drukval in terme van die biofilm-geaffekteerde spesifieke oppervlak-area uit te druk, wat die aangepaste RUC model produseer. Die biofilm-geaffekteerde spesifieke oppervlak-area waardes word dan bepaal deur gebruik te maak van die eksperimentele drukval data, asook die snelheidswaardes. Na die inkorporering van beide die analities- en empiries-bepaalde bolvormigheidswaardes in die aangepaste RUC model opgeneem is, wys die drukval resultate die aansienlike effek wat die bolvormigheidswaarde op die modelvoorspellings het. Ten slotte, word 'n sensitiwiteitsanalise op die invoer-parameters tot die model uitgevoer.

Acknowledgements

The support of the DST-NRF Centre of Excellence in Mathematical and Statistical Sciences (CoE-MaSS) towards this research is hereby acknowledged. Opinions expressed and conclusions arrived at, are those of the author and are not necessarily to be attributed to the CoE.

I would like to thank my supervisor, Dr. Sonia Fidder-Woudberg, for her guidance, time and all the opportunities that she made possible for me.
Sonia, jy is 'n inspirasie en 'n voorbeeld.

To my brother, Tinus. Thank you for all your advice and support when I needed it most.
Dankie dat jy altyd luister.

I would like to thank my parents, Martin and Sonia, for their endless love, for their endless support in all its forms and for giving me the opportunity to follow my dreams.
Dankie vir julle geduld, dankie vir al die gebede en dankie dat julle altyd daar is vir my - ek kon nie vir beter ouers gevra het nie.

Finally, I would like to thank God for a healthy mind without which I would not have been where I am today.
Markus 10:27: "Jesus het reguit na hulle gekyk en gesê: 'Vir mense is dit onmoontlik maar nie vir God nie, want vir God is alles moontlik.'"

Contents

Nomenclature

Standard characters

Notation:	Units:	Description:
a_f	[1/m]	biofilm affected SSA
a_o	[1/m]	initial SSA without biofilm
a_{vd}	[1/m]	SSA without taking biofilm growth into consideration
A	[ ]	empirical coefficient in Ergun equation
A_c	[m^2]	cross-sectional area of column
A_{fs}	[m^2]	fluid-solid interface without taking biofilm growth into account
A^*_{fs}	[m^2]	A_{fs}, taking overlapping into account
$(A_{fs})_b$	[m^2]	fluid-solid interface, taking biofilm growth into account
A_L	[m^2]	biofilm surface area lost with each point of contact
B	[ ]	empirical coefficient in Ergun equation
c_d	[ ]	drag coefficient in RUC model
C_1	[ ]	empirical coefficient in optimization method
C_2	[ ]	empirical coefficient in optimization method
d	[m]	cell dimension of RUC
d_s	[m]	solid width in RUC
D_p	[m]	particle diameter
D_v	[m]	diameter of hypothetical sphere
D_{vs}	[m]	mean spherical diameter
E	[ ]	roughness coefficient in Comiti and Renaud model
f	[ ]	friction factor
k	[m^2]	permeability

L	[m]	length of packed bed
L_e	[m]	length of flow path
L_f	[m]	biofilm thickness
m	[ ]	power of porosity in empirical models
M	[ ]	coefficient in Forchheimer equation
n	[ ]	coordination number
$\underline{\hat{n}}$	[ ]	streamwise direction in RUC model
N	[ ]	coefficient in Forchheimer equation
p	[Pa]	pressure
q	[m/s]	magnitude of superficial velocity
Q	[m^3/s]	volumetric discharge
r	[m]	radial coordinate in polar coordinate system
R	[m]	radius of sphere
Re_p	[ ]	particle Reynolds number
S_g	[m^2]	stagnant surfaces in RUC
S_p	[m^2]	outer surface area of particle
S_v^*	[1/m]	a_{vd} of spherical particles with rough surfaces
$S_{v,s}^*$	[1/m]	a_{vd} of spherical particles with smooth surfaces
$S_\parallel$	[m^2]	streamwise surfaces in RUC
$S_\perp$	[m^2]	transverse surfaces in RUC
S_1	[m^2]	total surface area of cones, excluding circular base area
S_2	[m^2]	total base areas of all cones on particle surface
U_f	[m^3]	total fluid volume in RUC
U_g	[m^3]	stagnant fluid volume in RUC
U_L	[m^3]	biofilm volume lost with each point of contact
U_o	[m^3]	total bed volume in RUC
U_p	[m^3]	volume of particle
U_s	[m^3]	solid volume in RUC
U_t	[m^3]	transfer volume in RUC
$U_\parallel$	[m^3]	streamwise volume in RUC
$U_\perp$	[m^3]	transverse volume in RUC

Greek symbols

Notation:	Units:	Description:
α	[ ]	average channel velocity ratio in RUC model
β	[ ]	surface roughness coefficient in RUC model
γ	[ ]	shape factor in Comiti and Renaud model
ϵ	[ ]	porosity
ϵ_{avg}	[ ]	average porosity
ϵ_{exp}	[ ]	experimentally determined porosity
ϵ_f	[ ]	biofilm affected porosity
ϵ_o	[ ]	initial porosity
ζ	[ ]	coefficient in RUC accounting for reduced $S_\perp$ area in fully staggered array
$\lambda_{w_\parallel}$	[Pa]	wall shear stress in RUC model
μ	[Pa.s]	fluid viscosity
ρ	[kg/m^3]	fluid density
τ	[ ]	geometrical tortuosity
ϕ	[ ]	sphericity
χ	[ ]	roughness factor
ψ	[ ]	geometric factor in RUC model

Acronyms

Notation:	Description:
PD	Percentage Difference
SSA	Specific Surface Area
SSR	Sum of Squared Residuals
RUC	Representative Unit Cell

List of Figures

List of Tables

Chapter 1

Introduction

Several industries are accountable for large quantities of chemical gasses being emitted to the atmosphere on a daily basis. Examples of such gasses are acetone, butanol, xylene, ammonia and hydrogen sulphide (H_2S). High concentrations of these gasses are a danger to not only the environment, but also to human health and plants [7]. Biofiltration is an environmentally friendly process by which pollution can be controlled. One of the main differences between the various biofiltration methods comes from the design of the bioreactor [8]. A biofilter consists of either an open or closed packed bed containing packing material and thin layers of moisture. In general, the most used biofilters are open bed biofilters. The latter are larger than closed bed biofilters and are mostly used outdoors while being exposed to a wide variety of weather conditions. Closed bed biofilters are normally used indoors and would typically be used to treat lower airflow ranges [8, 9].

One of the main elements of a biofilter is the packing material which acts like a filter when a polluted airstream passes through the packed bed. According to Delhoménie and Heitz [8], a characteristic of a packed bed that proves to be favourable to the performance of a biofilter is containing a packing material that consists of at least 60% particles with a diameter larger than 4 mm. Typical examples of packing materials include, for instance, rock and gravel, tree bark, compost, wood chips and soil (shown in Figure 1.1) [9, 10]. Composts, small scale wood chips and soil are most frequently used, since they are easily obtainable and at low cost. Characteristics of packing material that proves to be favourable to the performance of a biofilter include a large specific surface area (SSA), high porosity and a good water retention capacity. A large SSA provides a higher mass transfer rate which is beneficial to gas/biofilm exchange. A high porosity leads to a homogeneous distribution of the polluted gas through the packed bed. Good water

(a) Rock and Gravel

(b) Tree Bark

(c) Compost

(d) Wood Chips

(e) Soil

Figure 1.1. Typical examples of biofilter packing materials.

retention capacity is needed in order to avoid bed desiccation and gas flow channeling [8]. The thin layers of moisture, known as biofilm, consist of billions of living organisms that develop under optimized conditions. When contaminated gas is slowly being pumped through the biofilter it will come into contact with the moist biofilm layers. During this process the biofilm is responsible for consuming the biodegradable pollutants and biologically oxidizing the polluted gas [3, 5, 9]. In order for the polluted gas to be successfully biodegraded, it requires humidification of the packing material in order for the moist biofilm layers to be able to attach to the surface. Furthermore, making use of packing material with a large SSA allows more micro-organisms to grow and attach to its surface, which results in increasing biodegration of pollutants [3, 7].

Knowledge about biofilm growth and the effect it has on the operation of the biofilter can lead to improved biofilter designs that require less space, less energy, lower maintenance costs and optimize the ability to remove pollutants from the airstream. A better understanding of the physical phenomena underpinning biofilter operation can also help to identify specific operational shortcomings which can result in the formulation of measures for improvement [11].

Biofiltration has been proven to be an effective technology which has lower maintenance and operating costs compared to other more conventional filtration methods, such as air filtration. A biofilter can be designed according to any industrial layout and in any shape, form or size. The

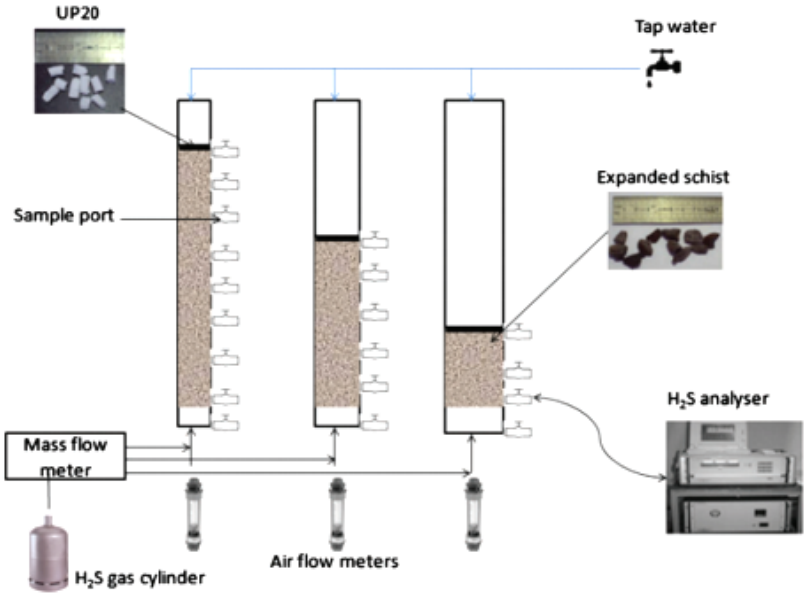

Figure 1.2. Schematic diagram of a biofilter. [1]

length of the packed beds in closed bed biofilters, for instance, can be increased vertically, rather than horizontally in diameter, in order to minimize the required space which will allow several reactors to operate next to one another. Subsequently, they will be able to operate more efficiently than one biofilter at a time [9, 12]. A disadvantage of using a biofilter is the requirement of a very large biofiltration system and the fact that the efficiency of the filtration system depends on humidification. Humidification is provided by saturating the gas before it enters the biofilter or by irrigating the packed bed with taps, positioned, for example, at the top of the biofilter (similar to the illustration shown in Figure 1.2). These systems are power consuming and when a power outage occurs, the packing material can become too dry which will cause it to crack. There are a few challenges regarding the micro-organisms: they can easily be poisoned and they only thrive in very specific temperatures and humidity [7]. The biofilm growth causes changes in the bed characteristics, e.g. an increase in pressure drop and a decrease in porosity, which, in turn, results in increasing maintenance costs over a long period of time [11, 13].

A typical biofiltration process, with the aim to remove H_2S from the air stream, is represented in Figure 1.2. The colourless H_2S is heavier than air, highly flammable and has an odorous smell that can be recognized at concentrations of less than 0.0047 ppm. It therefore requires the H_2S removal system to be efficient enough in order to remove 99% of the gas particles from the airstream to consequently remove the odour entirely. Health effects depend on the level of concentration and the amount of time a person is exposed to the gas. Exposure to low concentrations of H_2S may

only cause irritation to the eyes or the respiratory system, whereas exposure to concentrations of more than 10 ppm can cause shock, breathing difficulties, sudden unconsciousness or even death [10, 14, 15].

The three laboratory-scale biofilters in Figure 1.2 contain two different packing materials; UP20 and expanded schist, obtained by the thermal expansion of schist. UP20 is a synthetic packing material and schist is a coarse-grained rock. Organic packing materials are nowadays more commonly used in biofilters, since it costs less and contain more nutrients than inorganic or synthetic packing materials. Although inorganic packing materials, such as expanded schist, show better hydrodynamic and mechanical properties, they are however, much more expensive than organic packing materials, such as UP20, and also contain no nutrients in order for the biofilm to attach or grow on the surface of the packing material. Therefore, expanded schist requires additional inoculation of micro-organisms into the biofilter and is it optimal to use a combination of organic and inorganic packing materials [16].

The H_2S-contaminated airflow is regulated by a mass flow controller, as also indicated in Figure 1.2 and the air flow meters measure the volumetric discharge. The pressure drop is measured by different sampling ports, vertically separated by an equal distance apart.

1.1 Aims and Objectives

The aim of this study is to use mathematical modelling and an empirical optimization method, in order to investigate the effects that various parameters have on the pressure drop over a biofilter. Existing empirical and analytical porous media models will be used to predict the pressure drop over three different biofilters and to subsequently determine the changes in packed bed characteristics.

1.2 Layout of Thesis

In the following chapter the porous media parameters of relevance to this study will be discussed. This includes a discussion on the variables that are influenced by the changes in packed bed characteristics that occur during biofilter operation. In Chapter 3 a few modelling approaches from the literature are outlined.

Chapter 4 provides a discussion on the experimental procedures regarding three biofilters used by Dumont et al. [3], including the results obtained. The data presented in Chapter 4 will be used in this study for modelling purposes and will be graphically represented and evaluated against the model predictions in Chapter 5.

The empirical modelling approach used by Dumont et al. [3] is discussed in Chapter 6, followed by a discussion on the optimization method used in Excel®, as well as a sensitivity analysis on the sphericity.

The analytical approach is outlined in Chapter 7. The biofilm thickness is determined and subsequently the SSA in order to calculate the pressure drop. After comparing the results obtained from the empirical modelling approach with those obtained from the analytical modelling approach, an alternative approach for predicting the SSA is introduced, followed by a discussion on surface roughness. Thereafter follows a sensitivity analysis and finally, the conclusions drawn from this study are presented.

1.3 Publications Linked to this Study

The results obtained from the empirical approach obtained in Chapter 6 are published in: E. Dumont, S. Woudberg, and J. van Jaarsveld. Assessment of biofilm thickness in biofilters using porous media models. *Powder Technology*, 303: 76−89, 2016.

The results obtained from the analytical approach presented in Chapter 7 appear as: S. Woudberg, J. van Jaarsveld, and E. Dumont. Analytical determination of the effect of biofilm growth on the pressure drop over a biofilter. In *Proceedings of the World Congress on Momentum, Heat and Mass Transfer*, pages 105(1)−105(6) Prague, Czech Republic, 4-5 April, 2016.

A comparative analysis of the results obtained from the empirical and analytical approaches were presented by the author of this thesis at the 9th International Conference on Computational and Experimental Methods in Multiphase and Complex Flow in Tallinn, Estonia. The paper appears as: J. van Jaarsveld and S. Woudberg. An empirical versus analytical approach for modelling biofilm growth in biofilters. In *Multiphase Flow IX (Editors: P. Vorobieff and C. A. Brebbia), Proceedings of the 9th International Conference on Computational and Experimental Methods in Multiphase and Complex Flow*, pages 143-152, Tallinn, Estonia, 2017. WIT Press, UK.

Chapter 2

Porous Media Parameters

In this chapter, empirical laws for fluid transport of relevance to this study, i.e. Darcy's law and the Forchheimer equation, will be introduced. Thereafter, the variables that are influenced by changes in packed bed characteristics that occur during biofilter operation, such as porosity, tortuosity, sphericity and surface roughness, will be discussed.

2.1 Reynolds Number

The dimensionless particle Reynolds number indicates the contribution of turbulence relative to Darcy flow present in a system [17]. For fluid flow through a packed bed at a specific flow rate, it is important to take the pressure drop into account, which depends on the particle Reynolds number, Re_p, defined as

$$Re_p = \frac{\rho q D_p}{\mu}, \tag{2.1}$$

where q represents the magnitude of the superficial velocity, μ the fluid viscosity, D_p the particle diameter and ρ the fluid density [18, 19]. The numerator of equation (2.1) is defined as the inertial forces contributing to turbulence and the denominator as the viscous forces contributing to Darcy flow. When $Re_p > 100$, the flow is described as turbulent, whereas when $Re_p < 10$, the flow is considered laminar [18]. The latter values may vary in the literature, depending on the type of Reynolds number specified.

2.2 Darcy's Law

The permeability or hydraulic conductivity of a fluid, represented by k, is its capability to flow through a porous medium. The flow is either caused by gravity, a pressure drop over a certain distance or a combination of gravity and a pressure gradient. Henry Darcy formulated an empirical law describing the flow of a fluid through a porous medium known today as Darcy's Law [20], i.e.,

$$\frac{\Delta p}{L} = \frac{\mu q}{k}, \tag{2.2}$$

where $\frac{\Delta p}{L}$ represents the pressure drop, Δp, over a packed bed of length, L. The magnitude of the superficial gas velocity, q, defined as

$$q = \frac{Q}{A_c}, \tag{2.3}$$

is calculated by dividing, the volumetric discharge, Q, by the cross-sectional area of the column, A_c.

2.3 Forchheimer Equation

If the friction factor, $M = \frac{\mu}{k}$, is taken into consideration, Darcy's law can be written as follows,

$$\frac{\Delta p}{L} = Mq. \tag{2.4}$$

After taking higher velocities into account, equation (2.4) can be expressed as

$$\frac{\Delta p}{L} = Mq + Nq^2, \tag{2.5}$$

which is known as the Forchheimer equation, where the turbulent component, Nq^2, is considered to be the deviation from the linear Darcy term due to inertial effects. The Reynolds number (Section 2.1) can be used to indicate at which q-value this transition takes place. Although the non-linear term is often attributed to turbulence in the literature, only the time-independent laminar flow regime will be considered in this study.

2.4 Porosity

The void fraction of a packed bed, or the porosity, ε, is the ratio of spaces in the packed bed, not filled with solids, to the total volume of the packed bed, i.e.,

$$\varepsilon = \frac{U_f}{U_o}, \tag{2.6}$$

where $U_f = U_o - U_s$. The fluid volume is denoted by U_f, the volume of the solids by U_s and the total volume of the packed bed by U_o. The changes in ε over time not only affects the flow path through the packed bed, but the pressure drop over time as well.

2.5 Tortuosity

Tortuosity is a measure of the non-straightness of the flow path. The relationship between the length of the flow path, L_e, and the length of the packed bed, L, can be used to calculate the geometrical tortuosity, τ, [21] i.e.,

$$\tau = \frac{L_e}{L}. \tag{2.7}$$

Although there are different views in the literature concerning the tortuosity, based on streamlines or pathlines in a porous medium, the definition to be used in this study will be based on equation (2.7). Different equations for calculating τ will be discussed in Chapter 5.

2.6 Sphericity

Sphericity, ϕ, is known as a measure of the roundness of an object. Consider an object with volume, U_p, and outer surface area, S_p. The former and the latter are used to calculate ϕ, i.e.,

$$\phi = \frac{\pi^{\frac{1}{3}}(6U_p)^{\frac{2}{3}}}{S_p}, \tag{2.8}$$

where the numerator of equation (2.8) represents the surface area of a sphere with the same volume, U_p, as the original object. If $\phi = 1$, the object is a sphere and otherwise for $\phi < 1$ [3].

2.7 Surface Roughness

The surface roughness of a particle describes the texture and appearance of the exterior of the particle. The degree of roughness can vary between smooth, e.g the surface of an ideal glass sphere, and rough, e.g. a surface consisting of irregularities.

According to a study by Jian-Chao et al. [22], the relationship between the rough and smooth surfaces is known as the roughness factor, represented by χ. The study of Jian-Chao et al. [22] is based on fractal analysis including the assumption that the roughness configuration on a spherical particle is in the form of conical peaks, as shown in Figure 2.1.

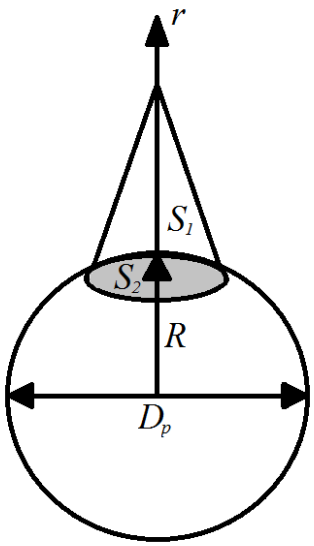

Figure 2.1. A spherical particle with surface roughness in the form of a conical peak.

The roughness factor is defined by the latter authors as

$$\chi = \frac{S_1 + \pi D_p^2 - S_2}{\pi D_p^2}, \tag{2.9}$$

where S_1 represents the total surface area of cones, excluding the circular base area, and S_2 is defined as the total base areas of all the cones on a particle surface, as indicated in Figure 2.1. Although only one cone is shown in Figure 2.1, in principle, there may be more cones covering the particle.

Jian-Chao et al. [22] proposed a dimensionless relationship between the surface of particles being

smooth and completely covered with peaks:

$$S_v^* = \chi S_{v,s}^*, \tag{2.10}$$

where S_v^* and $S_{v,s}^*$ represent the dimensionless SSA for a porous medium of spherical particles with rough surfaces and smooth surfaces, respectively. Jian-Chao et al. [22] showed that at higher porosities, the SSA is greater when the surface roughness is taken into consideration than when the particles are considered to be smooth ($\chi = 1$). At higher porosities, e.g. $\varepsilon = 0.800$, the effect of the surface roughness is negligible, whereas it is important to be taken into account at lower values of ε. Considering the effect of porosity on the SSA, Jian-Chao et al. [22] found that when ε ranges between 0.100 and 0.800, χ falls in the range 1 to 1.33. These values are, however, based on analytical fractal analysis and not on data of actual particles. In the present study the effect of surface roughness of the packing material on the pressure drop will be investigated. Thereafter follows a comparison between the calculated roughness factors and the roughness range reported by Jian-Chao et al. [22].

Chapter 3

Modelling Approaches from the Literature

Different models from the literature are to be considered in this study in order to determine the change in pressure drop over a biofilter for several days of operation. In this chapter the Ergun equation and variations thereof used, will be introduced. In addition, the Comiti and Renaud and granular RUC models will be included in the discussion.

3.1 Ergun Equation

A superposition of the Carman-Kozeny and Burke-Plummer equations is known as the Ergun equation. The Ergun equation is based on flow through a capillary tube wherein the fluid flowing through the porous medium is considered to have cylindrical, tortuous flow paths [23]. The flow is therefore regarded as Poiseuille flow in which a tortuosity factor is introduced, according to the Dupuit-Forchheimer relationship.

If $Re_p < 10$, the flow through the packed bed is regarded as laminar (Section 2.1) and can be calculated with the Carman-Kozeny equation [24], i.e.,

$$-\frac{dp}{dx} = A\frac{(1-\varepsilon)^2}{\varepsilon^3}\frac{\mu q}{D_p^2\phi^2}, \tag{3.1}$$

where the pressure gradient, $-\frac{dp}{dx} = \frac{\Delta p}{L}$, is directly proportional to the magnitude of the superficial velocity, q, and indirectly proportional to the square of D_p. The empirical coefficient, A, is equal to 150. If $Re_p > 100$, the flow through the packed bed is said to be turbulent and the pressure

drop can be calculated with the Burke-Plummer equation [24], i.e.,

$$-\frac{dp}{dx} = B\frac{(1-\varepsilon)}{\varepsilon^3}\frac{\rho q^2}{D_p\phi}, \tag{3.2}$$

where the empirical coefficient, B, is equal to 1.75. A superposition of equations (3.1) and (3.2) yields the empirical Ergun equation, i.e.,

$$-\frac{dp}{dx} = A\frac{(1-\varepsilon)^2}{\varepsilon^m}\frac{\mu q}{D_p^2\phi^2} + B\frac{(1-\varepsilon)}{\varepsilon^m}\frac{\rho q^2}{D_p\phi}, \tag{3.3}$$

which is widely used to calculate the pressure drop for both Darcy and inertial flow, where $m = 3$. According to Comiti and Renaud [24], inertial flow is present when the particle Reynolds number is in the range 0.4 to 1000.

Three additional variations of the Ergun equation will be considered in this study, i.e., the Macdonald equation, the Modified-Macdonald equation [21] and the Delhoménie et al. model [25].

3.2 Macdonald Equation

Macdonald et al. [21] modified the original Ergun equation by respectively adjusting the empirical coefficients, A, B and m. These modifications where made empirically in order to take the surface roughness into account, as well as to fit the data more accurately. Macdonald et al. [21] verified that the Ergun equation is successful for predicting the pressure drop when the coefficient values are changed to $A = 180$ and $B = 1.8$ instead of $A = 150$ and $B = 1.75$, i.e.,

$$-\frac{dp}{dx} = 180\frac{(1-\varepsilon)^2}{\varepsilon^3}\frac{\mu q}{D_p^2\phi^2} + 1.8\frac{(1-\varepsilon)}{\varepsilon^3}\frac{\rho q^2}{D_p\phi}. \tag{3.4}$$

D_p is equal to the equivalent mean spherical diameter, D_{vs}. The latter is defined as

$$D_{vs} = \phi D_v = 6\frac{U_p}{S_p},$$

where ϕ is the sphericity (as discussed in Section 2.6). D_v denotes the diameter of a hypothetical sphere with the same average volume of the actual packing material, U_p. Macdonald et al. [21] used $\phi = 0.6$ for gravel media. The value of the coefficient A in the Macdonald equation is considered to be independent of surface roughness, whereas the coefficient B is dependent on surface roughness. Equation (3.4) is widely recognized as an improvement to the Ergun equation [26].

3.3 Modified-Macdonald Equation

The Modified-Macdonald equation, based on an adaptation of equation (3.4), is a model described by Morgan-Sagastume et al. [26] as one that provides a good estimate for the biofilm affected porosity and pressure drop in a biofilter. The power of the porosity, m, is changed to 3.6. As proposed by Macdonald et al. [21], the value of A is set to 180, and similarly to equation (3.4), is considered to be independent of surface roughness. The coefficient B, however, is dependent on surface roughness and may vary between 1.8 and 4.0. Hence, the Modified-Macdonald equation is given by

$$-\frac{dp}{dx} = 180\frac{(1-\varepsilon)^2}{\varepsilon^{3.6}}\frac{\mu q}{D_p^2\phi^2} + B\frac{(1-\varepsilon)}{\varepsilon^{3.6}}\frac{\rho q^2}{D_p\phi}. \tag{3.5}$$

If the particle surface is considered to be smooth, $B = 1.8$, whereas if it is rough, $B = 4.0$ [26]. Morgan-Sagastume et al. [26] made use of a packing material with a considerably rough surface and accordingly set the value of B equal to 4.0. This results in a factor 2 difference between the inertial term for smooth and rough particles [26]. The value of ϕ for nearly spherical sand is 0.95 and 0.75 for an average of various sand types. They therefore used the average value of 0.85 for the sphericity of their pellets.

3.4 Delhoménie et al. Equation

Delhoménie et al. [25] performed an experiment on two biofilters with the aim to remove toluene from the airstream. Both biofilters consisted of packed beds containing mature compost and an organic binder. Initially, the Ergun equation, without ϕ, was used to predict the porosity of the packed beds. Regardless of the sphericity being excluded from the predictions, the packing material particles were described as spherical, therefore the value of $\phi = 1$ would not have affected the results. It was found that the Ergun equation under-predicted the experimental porosity values (measured by Delhoménie et al. [25]). Therefore, in order to fit the experimental data satisfactorily, Delhoménie et al. [25] proposed the following empirical version of the Ergun equation:

$$-\frac{dp}{dx} = \sigma\left(150\frac{(1-\varepsilon)^2}{\varepsilon^m}\frac{\mu q}{D_p^2} + 1.75\frac{(1-\varepsilon)}{\varepsilon^m}\frac{\rho q^2}{D_p}\right), \tag{3.6}$$

with σ known as the correction factor. According to Delhoménie et al. [25], the power of the porosity, m, takes into account the errors made in the experimental determination of ε. The values of σ and m were determined with data fitting and respectively found to be 0.9 and 6. Since the value of $m = 6$ is double the value of m used in the original Ergun equation, Delhoménie et

al. [25] made the conclusion that the initial under-prediction of the experimental porosity values is a result of the errors made in the experimental determination of ε. The aim of the present study, however, is to find physical reasoning behind possible deviations, rather than introducing coefficients in order for the results to fit the experimental data satisfactorily.

3.5 Comiti and Renaud Model

Comiti and Renaud [24] performed an empirical study concerning the behaviour of a fluid flowing through a packed bed. They compared the use of parallelepipedal particles and spherical particles as packing material. Comiti and Renaud [24] defined the SSA, without taking biofilm growth into consideration, as

$$a_{vd} = \frac{A_{fs}}{U_o}, \tag{3.7}$$

where A_{fs} is defined as the fluid-solid interfaces and U_o as the total bed volume. Comiti and Renaud [24] also defined A^*_{fs} as the fluid-solid interfaces of the parallelepipedal particles taking overlapping into account. Although the experiments were performed on both parallelepipedal particles and spherical particles, for the purpose of this study, only non-overlapping fluid-solid interfaces will be considered.

Comiti and Renaud [24] made use of the following Forchheimer-type equation (refer to Section 2.3) in order to determine the values of the parameters, M and N, by making use of the measured pressure drop values, defined as

$$-\frac{1}{q}\frac{dp}{dx} = Mq + N, \tag{3.8}$$

together with the measured q-values. Considering that equation (3.8) matches the general equation of a straight line, M and N are defined as the slope and the y-intercept, respectively.

Comiti and Renaud [24] proposed a correction for wall effects. According to Dullien [27], if the average diameter of the cylindrical column divided by the diameter of the packing material is greater than or equal to 10, the wall effects can be ignored. Therefore, since the column diameter of the biofilter used in this study is 0.1 m and the average particle diameter of schist is 0.01 m, i.e. $0.1/0.01 = 10$, the proposed correction for wall effects will be excluded, even though the value coincides with the value distinguishing the two wall effect regimes.

For $Re_p < 10$, the pressure gradient is based on the equation for Poiseuille flow, i.e.,

$$-\frac{dp}{dx} = 2\gamma\tau^2\mu a_{vd}^2\frac{(1-\varepsilon)^2}{\varepsilon^3}q, \tag{3.9}$$

where τ denotes the tortuosity (Section 2.5) and γ is defined as a shape factor that depends on the geometry of the pores. For cylindrical pores, $\gamma = 1$, which also represents the mean value for various shapes of channels.

In order to take the numerous directional changes of the flow into account when $Re_p > 100$, Comiti and Renaud [24] made the assumption that the pores are rough channels. The roughness of these channels, denoted by the coefficient E, is assumed to have the same range of magnitude as the average diameter, D_p. For explanatory purposes, Comiti and Renaud [24] compared this roughness concept of cylindrical pipes with friction factors and subsequently revealed that the Nikuradse formula, i.e.,

$$\frac{1}{\sqrt{f/2}} = 2.46 \ln \frac{D_p}{2E} + 4.92, \tag{3.10}$$

can be used to calculate the friction factor, f. Hence, the pressure gradient for high Reynolds numbers is approximated as follows:

$$-\frac{dp}{dx} \simeq 0.0968 \tau^3 a_{vd} \frac{1-\varepsilon}{\varepsilon^3} \rho q^2, \tag{3.11}$$

since $f/2 \simeq 0.0968$, which is based on the assumption that $E \simeq D_p$.

A superposition of equations (3.9) and (3.11), followed by division through q, yields:

$$-\frac{1}{q}\frac{dp}{dx} = 0.0968 \tau^3 \rho a_{vd} \frac{1-\varepsilon}{\varepsilon^3} q + 2\gamma\tau^2 \mu a_{vd}^2 \frac{(1-\varepsilon)^2}{\varepsilon^3}. \tag{3.12}$$

Since equation (3.12) is written in the form of equation (3.8), Comiti and Renaud [24] defined M and N as

$$M = 0.0968 \tau^3 \rho a_{vd} \frac{1-\varepsilon}{\varepsilon^3}, \tag{3.13}$$

and

$$N = 2\gamma\tau^2 \mu a_{vd}^2 \frac{(1-\varepsilon)^2}{\varepsilon^3}, \tag{3.14}$$

respectively. The experimental values of M and N were determined by linear regression from the graph of $-\frac{1}{q}\frac{dp}{dx}$ as a function of q. Subsequently, Comiti and Renaud [24] solved equations (3.13) and (3.14) simultaneously in order to determine the values of τ and a_{vd}.

3.6 Granular Representative Unit Cell Model

The RUC model, developed at Stellenbosch University, is the smallest rectangular representation of the average geometrical properties of a granular packed bed (as schematically shown in Figure 3.1).

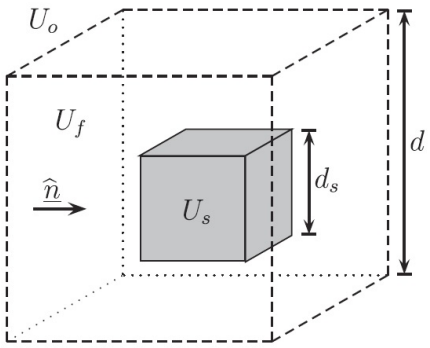

Figure 3.1. The granular RUC model [2].

In Figure 3.1 $\underline{\hat{n}}$ is the streamwise direction which can be in any of the three principal directions. The solid volume and the fluid volume are respectively denoted by U_s and U_f. The total volume of the unit cell is denoted by U_o. The dimension, d_s, is defined as the average particle diameter and can be expressed in terms of the porosity, ε, and the dimension, d, of the RUC, i.e.,

$$d_s = (1-\varepsilon)^{\frac{1}{3}} d, \tag{3.15}$$

where the porosity is defined as in Section 2.4. As opposed to Comiti and Renaud [24] assuming Poiseuille flow, in this study plane-Poiseuille flow is assumed. This is due to the rectangular characteristics which in turn is a result of the assumption of piece-wise straight streamlines between parallel plates. Although not indicated in Figure 3.1, the parallel plate geometry is formed by the surfaces of solids neighbouring the one in the RUC.

The different regions of the fluid domain include streamwise and transverse volumes with adjacent streamwise and transverse surfaces, respectively. The streamwise volume, $U_{\parallel}$, is defined as the region wherein the flow is parallel to the streamwise direction, whereas the transverse volume, $U_{\perp}$, is the region wherein the flow is perpendicular to the streamwise direction. The transfer volume, U_t, is the region without any adjacent fluid-solid interfaces. The streamwise surfaces, $S_{\parallel}$, are known as the surfaces parallel to the streamwise direction, whereas the transverse surfaces, $S_{\perp}$, are the surfaces perpendicular to the streamwise direction. Stagnant fluid volumes (if present) are presented by U_g with the corresponding surfaces parallel to these volumes, known as the stagnant surfaces, denoted by S_g.

The volume partitioning of the fluid domain is presented in Table 3.1 which contains the various volumes and surface areas expressed in terms of d_s and d [2]. In the granular RUC model two arrays are considered, i.e. regular arrays and fully staggered arrays. Staggering is defined as

Table 3.1. Volume and surface partitioning table of the granular RUC model.

Variables	**Granular RUC model**	
	Fully staggered array	**Regular array**
U_o	d^3	d^3
U_s	d_s^3	d_s^3
U_f	$d^3 - d_s^3$	$d^3 - d_s^3$
$U_\parallel$	$2\,d_s^2\,(d - d_s)$	$2\,d_s^2\,(d - d_s)$
S_{fs}	$6\,d_s^2$	$6\,d_s^2$
$S_\parallel$	$4\,d_s^2$	$4\,d_s^2$
$U_\perp$	$d_s^2\,(d - d_s)$	0
$S_\perp$	$2\,d_s^2$	0
U_g	0	$d_s^2\,(d - d_s)$
S_g	0	$2\,d_s^2$

the measure of deviation with respect to the average flow direction that the fluid undergoes to circumvent the solid obstacles. A regular array contains stagnant regions and consists of no staggering. The fluid enters and leaves the RUC in the streamwise direction. In a fully staggered array, however, the fluid entering the RUC in the streamwise direction slightly undergoes a shift in the transverse directions before exiting the RUC again in the streamwise direction. There are no stagnant regions in a fully staggered array. Even though the RUC model is applicable to volumes containing stagnant regions, for the purpose of the present study, the assumption will be that there are no stagnant fluid volumes in the packed bed of a biofilter. Therefore, the focus will be on staggered arrays only.

The geometric factor, ψ, can be expressed in terms of the fluid, streamwise and transfer volumes, i.e.,

$$\psi = \frac{U_f}{U_\parallel + U_t}. \tag{3.16}$$

Equation (3.16) can be expanded by defining the fluid volume in terms of $U_\parallel$, U_t, $U_\perp$ and U_g, i.e.,

$$\psi = \frac{U_\parallel + U_t + U_\perp + U_g}{U_\parallel + U_t}. \tag{3.17}$$

The geometric factor can also be expressed in terms of the porosity by application of equation (3.15) together with the expressions presented in Table 3.1, i.e.,

$$\psi = \frac{\varepsilon}{1 - (1 - \varepsilon)^{2/3}}. \tag{3.18}$$

When stagnant fluid volumes are absent, ψ equals the geometric tortuosity, τ. The tortuosity, τ,

discussed in Section 2.5, can then be expressed as

$$\tau = \frac{U_{\parallel} + U_t + U_{\perp}}{U_{\parallel} + U_t}. \tag{3.19}$$

The pressure gradient over a packed bed with randomly distributed granules, obtained by application of the RUC model, is given by

$$-\frac{dp}{dx} = \frac{S_{\parallel} + \alpha\zeta S_{\perp}}{\varepsilon U_o}\lambda_{w_{\parallel}}\psi + \frac{S_{\perp}\psi^2}{2\varepsilon^3 U_o}c_d\rho q^2, \tag{3.20}$$

and is based on a drag model, as opposed to the model of Comiti and Renaud [24] and the Ergun equation, which are based on a capillary tube model. The variables, α and ζ, are respectively set equal to $\sqrt{2}$ and $1/4$ when considering fully staggered arrays [2]. The wall shear stresses are quantified as follows:

$$\lambda_{w_{\parallel}} = \frac{6\mu q\psi}{\varepsilon(d - d_s)}. \tag{3.21}$$

The drag coefficient is denoted by c_d [2]. For a cube orientated perpendicular to the streamwise direction and $Re_p > 10^4$, the value of c_d is 1.1. For a square rod under the same conditions, $c_d = 2.0$ [2]. The value of c_d can therefore vary between 1.1 and 2.0. A value of 1.9 provided exact correspondence for the higher Reynolds number term of the RUC model to the higher Reynolds number term of the Macdonald equation (discussed in Section 3.2). The assignment of $c_d = 1.9$ was the most empirical aspect of the modelling procedure of Du Plessis and Woudberg [2]. Consequently, $c_d = 1.9$ will be used in the present study. By making use of Table 3.1 and equation (3.15), equation (3.20) can be rewritten in terms of ε and d_s, i.e.,

$$-\frac{dp}{dx} = \frac{25.4(1-\varepsilon)^{4/3}\mu q}{d_s^2(1-(1-\varepsilon)^{1/3})(1-(1-\varepsilon)^{2/3})^2} + \frac{(1-\varepsilon)c_d\rho q^2}{2d_s\varepsilon(1-(1-\varepsilon)^{2/3})^2}, \tag{3.22}$$

In equation (3.22) the particle diameter, $d_s = D_p$. In this study (as opposed to the model presented in the study of Du Plessis and Woudberg [2]) the sphericity, ϕ (defined in Section 2.6), will be incorporated as well as the coefficient, β, which accounts for surface roughness (discussed in Section 2.7), to yield:

$$-\frac{dp}{dx} = \frac{25.4(1-\varepsilon)^{4/3}\mu q}{D_p^2\phi^2(1-(1-\varepsilon)^{1/3})(1-(1-\varepsilon)^{2/3})^2} + \frac{\beta(1-\varepsilon)c_d\rho q^2}{2D_p\phi\varepsilon(1-(1-\varepsilon)^{2/3})^2}. \tag{3.23}$$

Recall from Section 3.3 that Morgan-Sagastume et al. [26] have set the value of B equal to 4.0 which results in a factor 2 difference between the inertial term for smooth and rough particles [26]. Therefore, in order to incorporate the same relative difference in magnitude, the value of $\beta = 2$ was chosen for the RUC model.

Chapter 4

Experimental Procedure and Results

This chapter includes a discussion on the experimental data and procedures followed by Dumont et al. [3]. This data will be used in subsequent chapters for modelling purposes. Bed and fluid properties, as well as measured values will be given. The results obtained from Biofilters 1, 2 and 3 will be graphically represented and analyzed.

4.1 Experimental Setup

The biofiltration system, shown in Figure 4.1, was used by Dumont et al. [3] to remove the poisonous and life threatening H_2S gas, from the air stream. The bed and fluid properties (shown in Table 4.1) for the three respective biofilters were provided by Dumont [28] from the École des Mines de Nantes, in France. Porosity is not included in Table 4.1, since the biofilm growth affects the porosity over time and therefore changes.

Table 4.1. Biofilter properties.

Expanded schist particle diameter (m)	0.01
UP20 particle diameter (m)	0.007
UP20 particle length (m)	0.01
Column diameter (m)	0.1
Air density, ρ (kg.m^{-3})	1.2
Air viscosity, μ (Pa.s)	1.80×10^{-5}
Packed bed height (m)	0.87
Column cross-sectional area (m^2)	0.0079

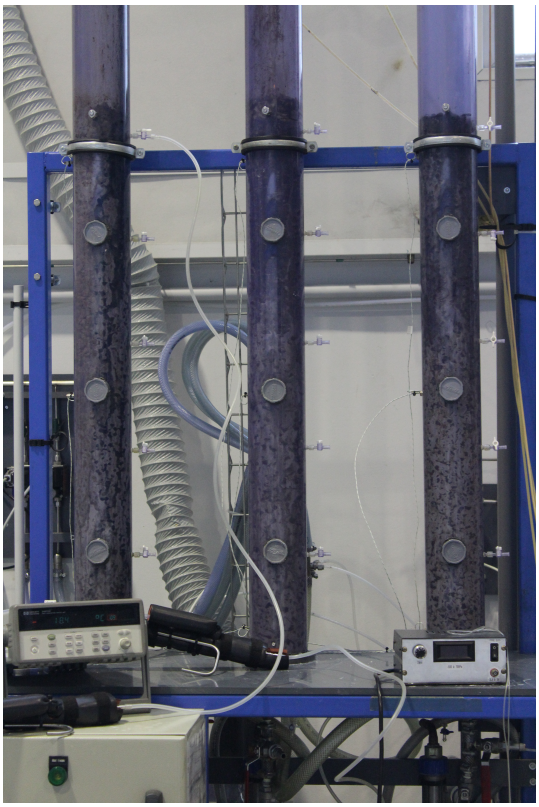

Figure 4.1. From left to right: Biofilter 1, Biofilter 2 and Biofilter 3 [3].

The pressure was measured on seven different days (i.e. days 0, 19, 39, 57, 71, 92 and 106) over a period of 110 days by five different sampling ports, vertically separated by a distance of 20 cm, starting at the bottom. Pressure values between 10 and 80 Pa/m were observed. Volumetric airflow rates in the range 0.5 to 1.8 m^3/h were measured which correspond to superficial velocities in the range 89 to 229 m/h.

As mentioned in Section 2.2, the superficial gas velocity is calculated by dividing Q, the volumetric discharge, by the cross-sectional area of the biofilter, A_c. Since Q is measured in m^3/h, the units of q are m/h which were then converted to m/s. The three cylindrical columns, shown in Figure 4.1, all had a diameter of 0.1 m and a height of 1.5 m. Biofilter 1 was inoculated with activated sludge and contained 3.97 kg of expanded schist which formed a packed bed of 0.87 m in height. Biofilter 2 was however not inoculated, but also contained 3.97 kg of expanded schist. Biofilter 3 was inoculated with activated sludge and contained 3.97 kg of expanded schist, as well as 0.48 kg of UP20 which formed packed bed heights of 0.77 m and 0.1 m, respectively. It is important to

(a) Expanded schist (b) UP20

Figure 4.2. Packing materials used in experiment.

note that the pressure drop was only measured over the sections of the packed bed that contained expanded schist. It is assumed that expanded schist, shown in Figure 4.2(a), is a roughly round, non-porous particle of 10 mm in diameter with a SSA of 600 1/m. Expanded schist has a larger SSA than ordinary schist for biofilm to grow on, and was therefore chosen as packing material for Biofilters 1, 2 and 3. UP20, shown in Figure 4.2(b), is a synthetic packing material that makes the addition of extra buffer and nutrient solutions unnecessary.

4.2 Assumptions

Dumont et al. [4] made the assumption that the biofilm growth is homogeneous, and that the biofilm development on the surface of the packing material did not change the shape of the expanded schist. The assumption was also made that the entire packed bed was evenly covered with tap water, and that the changes over time in pressure drops are related to the changes over time in particle roughness as a result of the biofilm development.

4.3 Results

The initial bed porosity, ε_o, experimental porosity, ε_{exp}, range and average porosity, ε_{avg}, of Biofilters 1, 2 and 3 are shown in Table 4.2. According to Dumont [28], a deviation of about 1% in the measured porosity values is reasonable and is shown in Figure 4.3. A continuous decrease in porosity over time, although minimal, is expected as a result of the increasing biofilm growth in the packed bed. Figure 4.3, however, shows an alternating decrease and increase in porosity in

Table 4.2. Packed bed porosity.

Biofilter	**Initial bed porosity, ε_o**	**Experimental porosity, ε_{exp}**	**Average porosity, ε_{avg}**
1	0.423	0.398 to 0.423	0.404
2	0.422	0.410 to 0.422	0.420
3	0.415	0.401 to 0.415	0.407

Biofilters 1 and 3.

The sudden decrease in porosity on day 19 and day 92 for Biofilter 1 may be attributed to the assumption that the entire bed was evenly covered with tap water, which may not be true [3]. Except for day 0, when no biofilm is present, the porosity in Biofilter 2 undergoes an intermittent decrease over time.

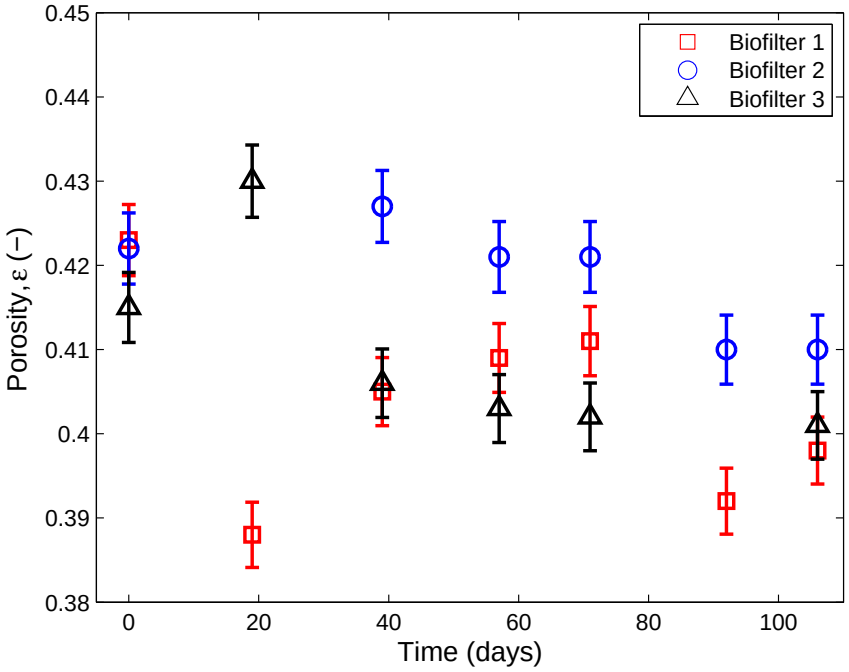

Figure 4.3. Change in packed bed porosity over time.

In order to determine the porosity of the biofilter, two containers of equal size were filled with a certain volume of fluid. After adding a volume of solids, U_s, to the second container, the same amount of fluid was displaced. Note that the total volume of the packed bed, $U_o = U_f + U_s$. In this specific case the porosity can be calculated as

$$\varepsilon = \frac{U_f}{U_f + U_s}. \tag{4.1}$$

Equation (4.1) was used by Dumont [28] to experimentally calculate the porosity values graphically displayed in Figure 4.3. Figures 4.4, 4.5 and 4.6 represent the pressure gradient measurements for Biofilters 1, 2 and 3, respectively, over the entire period of 110 days. The pressure gradient values are plotted as a function of the superficial velocity.

Note that water accumulation in the pipes may cause disturbances and lead to a malfunction of the differential pressure sensor. Therefore, pressure drop data is missing for Biofilter 2 on day 19 and for Biofilter 3 on day 92. From Figures 4.4, 4.5 and 4.6 it is clear that when a specific q-value is considered, an increase in the pressure drop over time is observed, which is due to the increasing biofilm concentration [3]. As a result of inoculation, Biofilter 1 and 3 are similar when considering the rapidly increasing pressure drop values over time. Recall that Biofilter 2 was not inoculated with activated sludge. Hence, in comparison with the other biofilters, the increase in pressure drop in this biofilter was marginally slow. According to Dumont et al. [4], irrigation was the probable cause of biofilm development in Biofilter 2.

After observing a non-linear trend in Figures 4.4, 4.5 and 4.6, it is evident that inertial effects cannot be neglected. These effects will therefore be included in the prediction of the pressure drop.

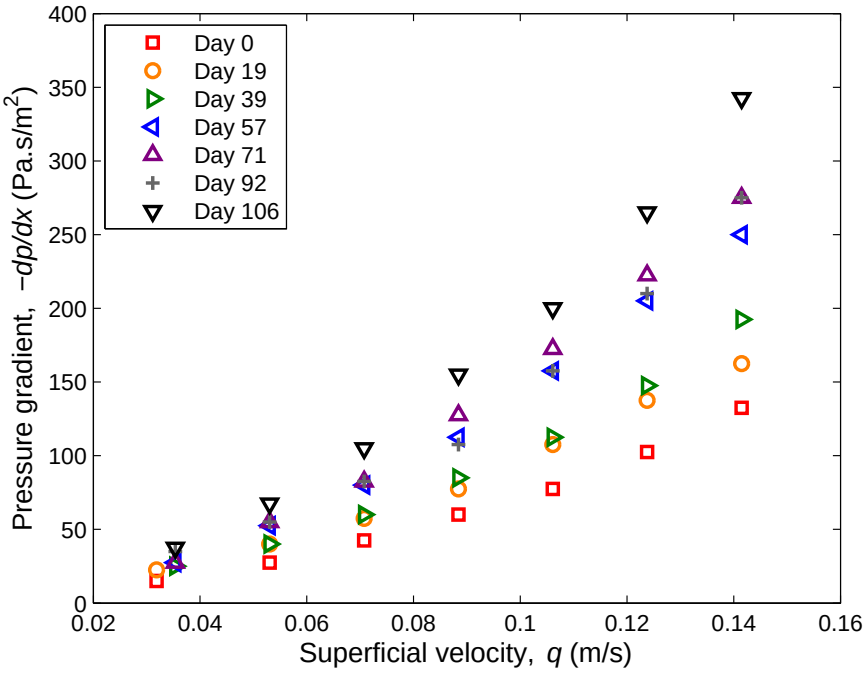

Figure 4.4. Biofilter 1: Pressure gradient versus superficial velocity.

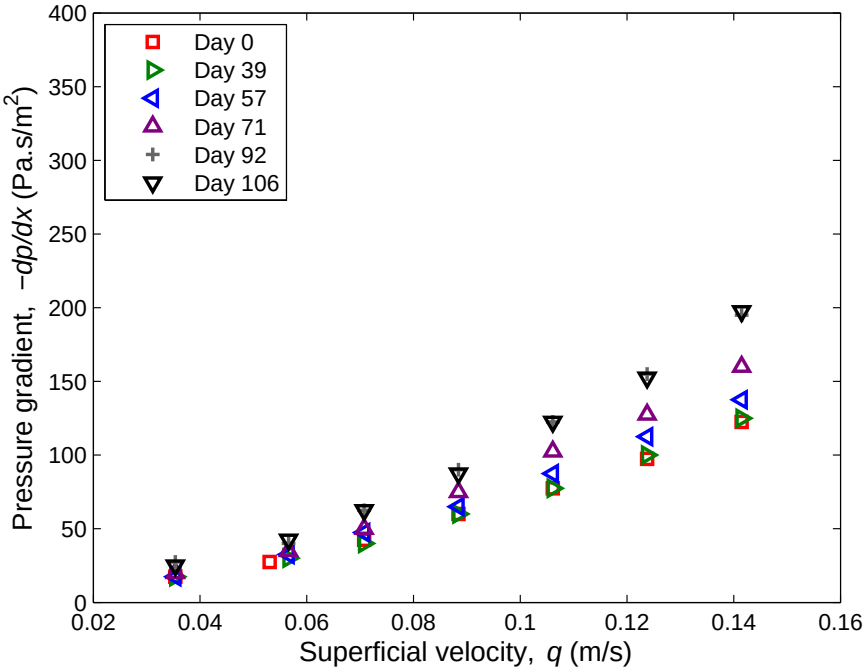

Figure 4.5. Biofilter 2: Pressure gradient versus superficial velocity.

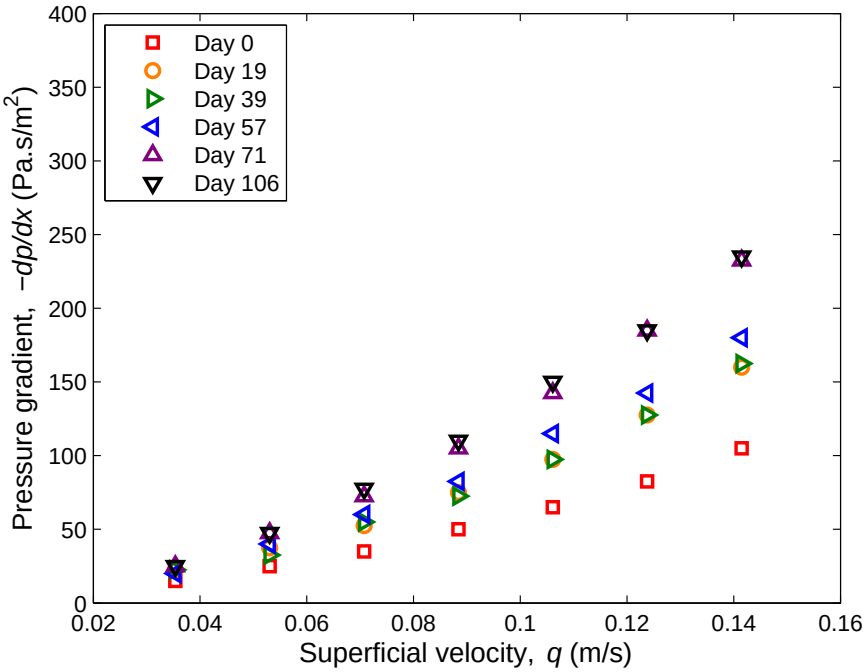

Figure 4.6. Biofilter 3: Pressure gradient versus superficial velocity.

Chapter 5

Comparison Between Modelling Approaches

In this chapter the results obtained from the different models discussed in Chapter 3 will be compared when evaluated against the experimental data presented in Chapter 4. This includes the graphical representation of the behaviour of the pressure drop and tortuosity values throughout the entire experiment.

5.1 Pressure Drop Prediction

Different variations of the Ergun equation were considered in Chapter 3. As already mentioned, the differences between the equations lie in the empirical coefficient values, A and B, as well as in the power of the porosity, m. The corresponding coefficient values for the Ergun equation, Macdonald equation and Modified-Macdonald equation are summarized in Table 5.1.

The model predictions for the pressure gradient over the superficial velocity, q, along with the experimental data for day 0, are graphically represented in Figures 5.1, 5.2 and 5.3 for Biofilters

Table 5.1. Different variations of Ergun equation.

Equation	**A**	**B**	**m**
Ergun	150	1.75	3
Macdonald	180	1.8	3
Modified-Macdonald	180	$1.8 - 4.0$	3.6

1, 2 and 3, respectively.

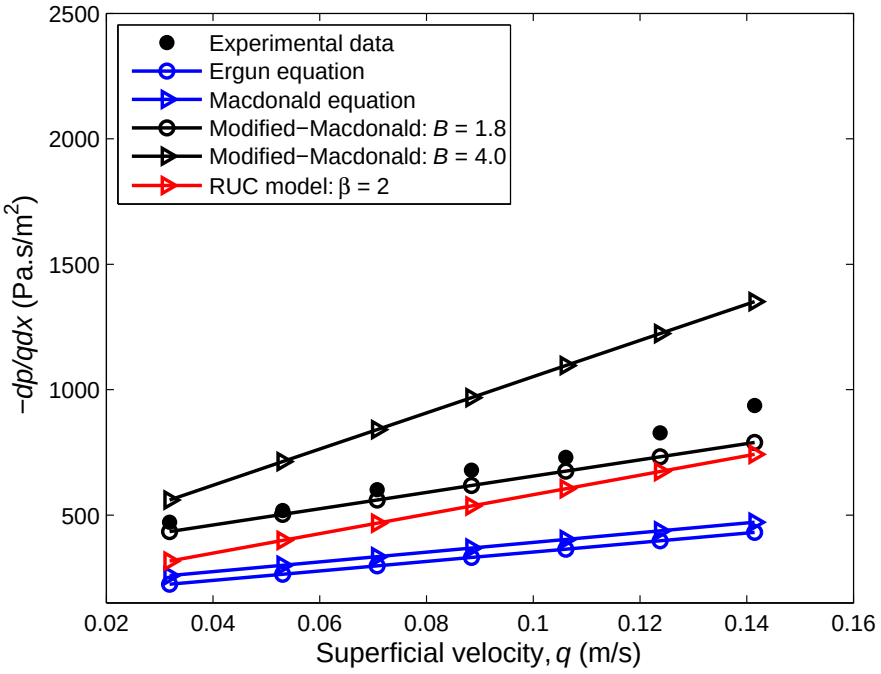

Figure 5.1. Biofilter 1: Model predictions for day 0.

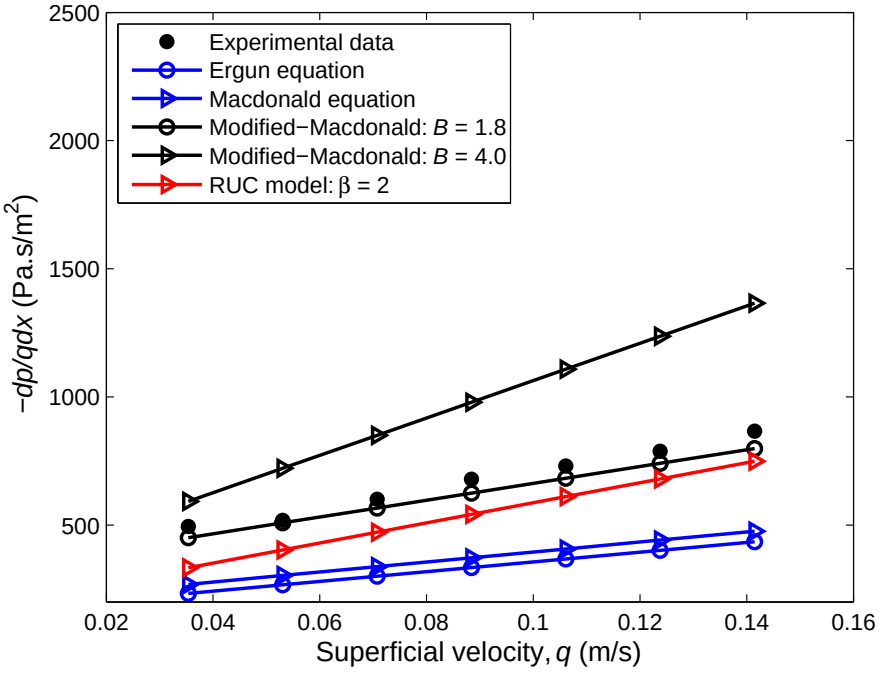

Figure 5.2. Biofilter 2: Model predictions for day 0.

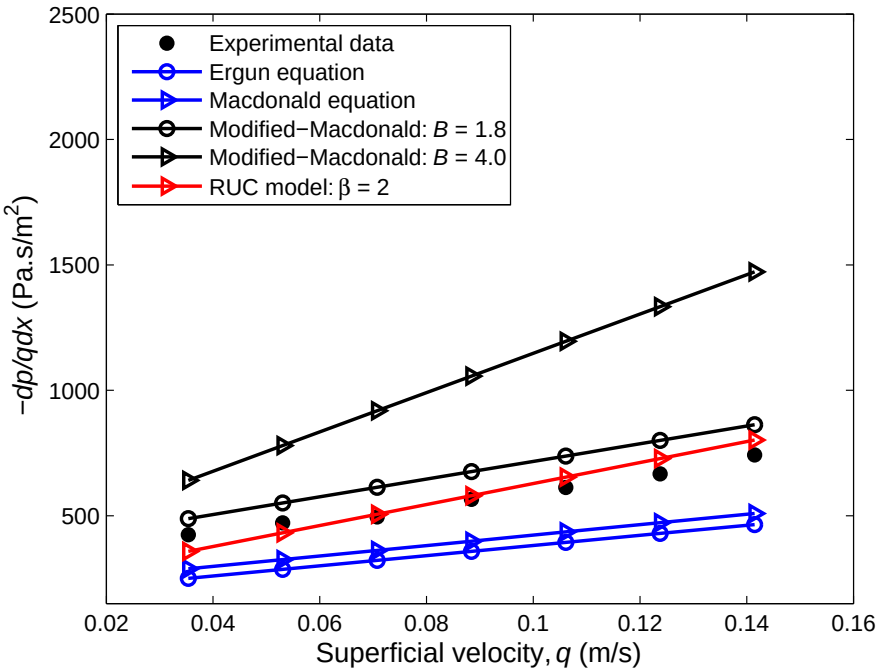

Figure 5.3. Biofilter 3: Model predictions for day 0.

The different models used to predict the pressure gradient in these figures are equations (3.3), (3.4), (3.5) and (3.23), corresponding to the Ergun equation, Macdonald equation, Modified-Macdonald equation and RUC model, respectively, with $\phi = 0.85$. For comparison, the two limiting values of B were used for the Modified-Macdonald equation, i.e. $B = 1.8$ and $B = 4.0$. Similar figures for the other days on which data was recorded are presented in Appendix A.

Considering the performance of the Ergun and Macdonald equations on day 0, the results under-predict the experimental data. This is observed throughout the entire experiment. Therefore, these models were excluded from the plots for days 19-106 in Appendix A.

When considering the results obtained from Biofilter 1, the Modified-Macdonald equation with $B = 1.8$ give the most accurate results on days 0 and 19, after which it starts to under-predict the experimental data. The Modified-Macdonald equation with $B = 4.0$ over-predicts the data for days 0 to 39, whereas on days 57 to 106 it yields the most accurate predictions. The RUC model under-predicts the experimental data throughout the entire experiment.

When considering Biofilter 2, the Modified-Macdonald equation with $B = 1.8$ give more accurate results on days 0 to 57, compared to the other models. On days 71 to 106, the model under-predicts the experimental data. Furthermore, the Modified-Macdonald equation with $B = 4.0$

over-predicts the data on days 0 to 57. For days 71 to 106 the over-prediction becomes less, leading to satisfactory results. Similar to Biofilter 1, the results obtained from the RUC model under-predict the experimental data throughout the entire experiment.

For Biofilter 3 the RUC model yields the best results on day 0, compared to the other model predictions. It does, however, under-predict the data throughout the rest of the experiment. Except for day 0, the Modified-Macdonald equation with $B = 1.8$ under-predicts the data throughout the entire experiment. Considering the results obtained from the Modified-Macdonald equation with $B = 4.0$, the experimental data is over-predicted on days 0, 39 and 57, whereas the model gives accurate predictions on days 19, 71 an 106.

When considering the overall performance of the three models over the entire experiment and all three biofilters, the Modified-Macdonald equation with $B = 4.0$ yields the most accurate results. Furthermore, the Modified-Macdonald equation with $B = 1.8$ mostly under-predicts the experimental data. Except for the accurate results for Biofilter 3 on day 0, the RUC model under-predicts the data throughout the entire experiment.

5.2 Tortuosity Prediction

Biofilm growth affects the porosity of the packed bed and since the tortuosity is a function of porosity, the biofilm growth also has an affect on the tortuosity [29]. An increase in biofilm concentration affects the flow path which, in turn, affects the tortuosity. Thus, according to Dumont et al. [3], it can be assumed that the changes in tortuosity as a result of biofilm growth can be related to the pressure drop measurement.

Lanfrey et al. [30] proposed the following relationship in order to calculate the tortuosity in a packed bed filled with uniform particles, i.e.,

$$\tau = 1.23\frac{(1-\varepsilon)^{\frac{4}{3}}}{\varepsilon\phi^2}, \tag{5.1}$$

where the value of 1.23 is an empirical coefficient. Dias et al. [31] also proposed a relationship between tortuosity and porosity: Equation (5.2), with m an empirical constant, is used by the latter authors to calculate the tortuosity in a packed bed filled with non-uniform particles, i.e.,

$$\tau = \frac{1}{\varepsilon^m}, \tag{5.2}$$

where $0.4 \leq m \leq 0.5$ [31].

Dumont et al. [3] made use of the empirical capillary-tube model proposed by Comiti and Renaud [24] to calculate the tortuosity and the SSA through the empirical coefficients M and N (as discussed in Section 3.5). Similar to the models proposed by Lanfrey et al. [30] and Dias et al. [31] to predict the tortuosity, Comiti and Renaud [24] did not take biofilm growth into consideration in equations (3.13) and (3.14).

The tortuosity predicted by the RUC model is given by equation (3.19). Taking the sphericity, ϕ, into consideration in equation (3.19), it follows furthermore from Table 3.1 that

$$\tau = \frac{d^3 - d_s^3}{\phi(2d_s^2(d - d_s) + (d - d_s)^2(d + 2d_s))}, \tag{5.3}$$

which leads to

$$\tau = \frac{\varepsilon}{\phi(1 - (1 - \varepsilon)^{2/3})}, \tag{5.4}$$

by application of equation (3.15). Equation (5.4) is identical to equation (3.18), except for the sphericity, ϕ, in equation (5.4).

Dumont et al. [3] compared the models of Comiti and Renaud [24], Lanfrey et al. [30] and Dias et al. [31] by plotting the changes in tortuosity over time for Biofilter 3. A similar plot is given by Figures 5.4, 5.5 and 5.6 for Biofilters 1, 2 and 3, respectively, but with tortuosity as a function of porosity, instead of time and with $\phi = 0.85$ instead of $\phi = 0.87$. The RUC model (equation (5.4) (with $\phi = 1$ and $\phi = 0.85$)) was also added for comparison. Note that the tortuosity values obtained from the model of Comiti and Renaud [24] and shown in Figures 5.4 to 5.6 were determined by Dumont et al. [3] and are given in their Table 2. The use of $\phi = 1$ is equivalent to disregarding ϕ in the tortuosity equations.

For the entire operation of Biofilter 1, the tortuosity values obtained from the RUC model together with the models of Lanfrey et al. [30] and Dias et al. [31] decrease slightly with an increase in porosity. The results obtained with the Dias et al. [31] and Lanfrey et al. [30] ($\phi = 1$) models give tortuosity values in the range 1.4 to 1.7. The Lanfrey et al. [30] ($\phi = 0.85$) model ranges between 1.9 and 2.3. The predictions made by Comiti and Renaud [24] can be considered as less accurate when compared to the other models, since the values of τ show no specific trend. Considering the decrease in τ, a similar observation can be made for Figures 5.5 and 5.6. In Figure 5.5, the Dias et al. [31] and Lanfrey et al. [30] ($\phi = 1$) models give tortuosity values in the range 1.3 to 1.6. The Lanfrey et al. [30] ($\phi = 0.85$) model provides tortuosity values ranging between 1.9 and 2.1. Referring to the results shown in Figure 5.6, the Dias et al. [31] and Lanfrey et al. [30] ($\phi = 1$)

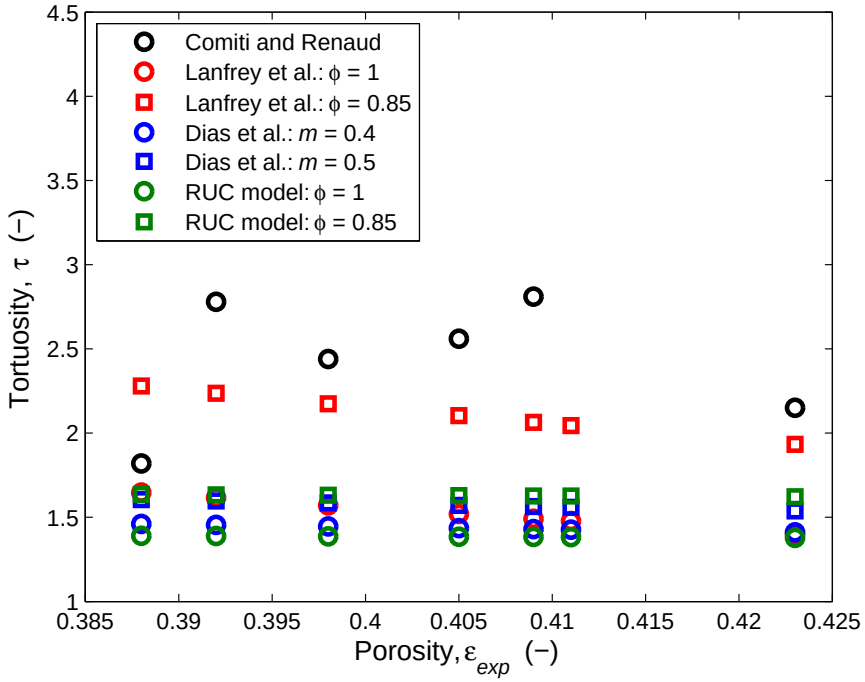

Figure 5.4. Biofilter 1: Tortuosity as a function of porosity.

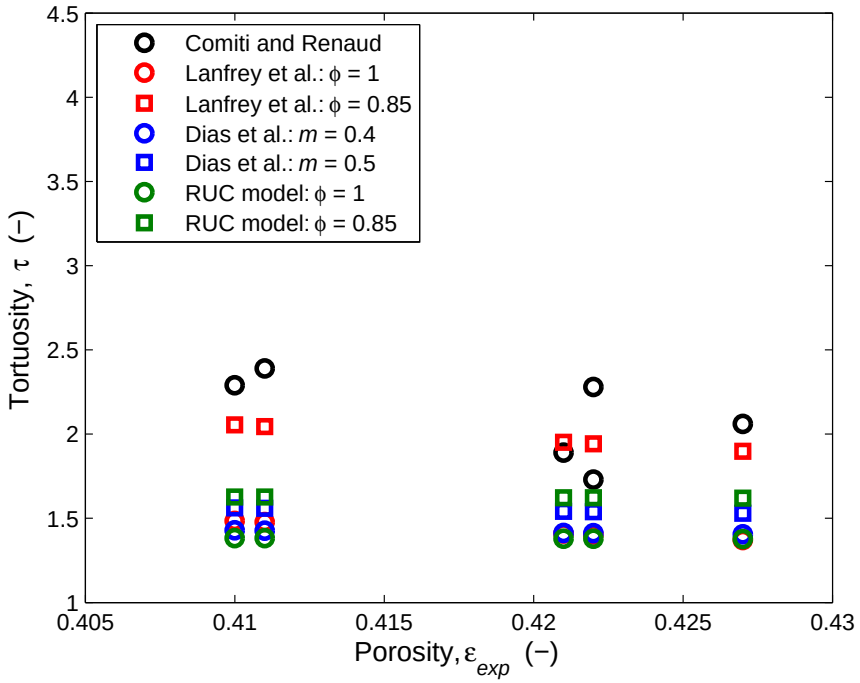

Figure 5.5. Biofilter 2: Tortuosity as a function of porosity.

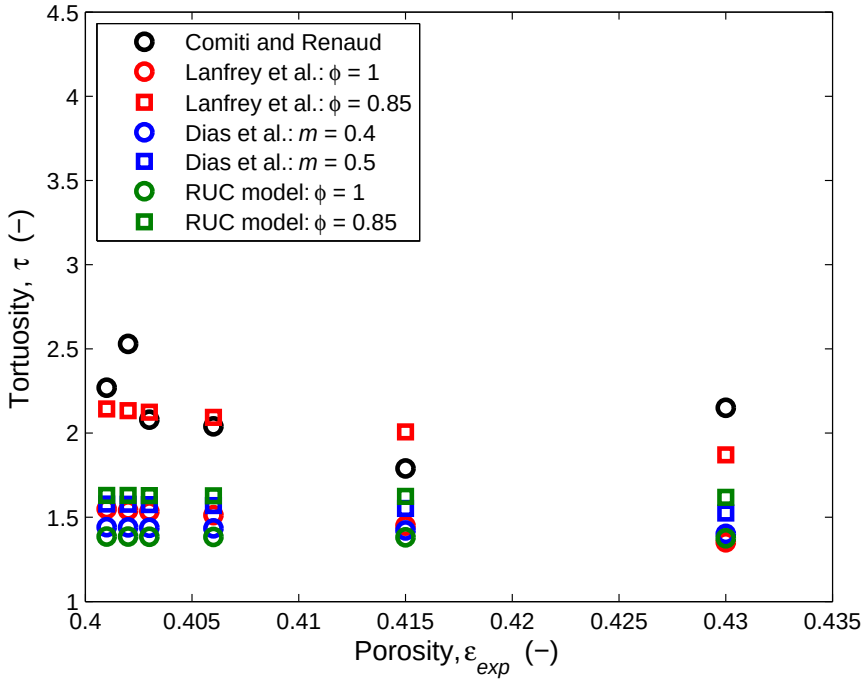

Figure 5.6. Biofilter 3: Tortuosity as a function of porosity.

models give tortuosity values in the range 1.3 to 1.6. The Lanfrey et al. [30] ($\phi = 0.85$) model provides tortuosity values ranging between 1.8 and 2.2.

Considering all three biofilters, the changes in the τ-values obtained from the RUC model are insignificant. As the porosity increases, the tortuosity only decreases with a value of 0.01-0.02 over time. The small decrease in tortuosity can be attributed to equation (5.4), since a small change in ε leads to a small change in τ. Although Dumont et al. [3] assumed that the changes in tortuosity as a result of biofilm growth can be related to the pressure drop measurement, the RUC model prediction remains unaffected by biofilm growth, but this does not imply that the pressure drop is also unaffected. The tortuosity predictions of the RUC model is still in line with the model predictions of Dias et al. [31] and Lanfrey et al. [30]. The tortuosity is, however, only one of the parameters contributing to the pressure gradient.

Chapter 6

Empirical Modelling Approach

In order to assess development of the biofilm thickness, SSA, tortuosity and biofilm affected porosity over time, Dumont et al. [4] performed an empirical study with the aim to apply different porous media models to experimental pressure drop measurements carried out in biofilters. The empirical modelling approach followed will be discussed in this chapter which involves an optimization method used in Excel®, as well as a sensitivity analysis on the sphericity.

6.1 Optimization Method

Similarly to the present study, Dumont et al. [4] made use of the Modified-Macdonald equation, the Comiti and Renaud model and the RUC model, in order to fit the experimental pressure drop measurements and subsequently determine the change in porosity, SSA and tortuosity over time, as well as the development of the biofilm thickness. The experimental procedure and results were discussed in Chapter 4.

Due to the inconsistent decrease in measured porosity values (indicated in Figure 4.3), the three porous media models will be used to determine the biofilm affected porosity, ε_f, that show a more consistent decrease over time. In order to empirically calculate the biofilm affected porosity on each day that pressure drop data was recorded, the following Forchheimer-type equation, discussed in Section 2.3, was used to empirically fit the experimental pressure drop data obtained from the three respective models:

$$-\frac{1}{q}\frac{dp}{dx} = C_1 f_1(\varepsilon) + C_2 f_2(\varepsilon) q, \tag{6.1}$$

with $M = C_2 f_2(\varepsilon)$ and $N = C_1 f_1(\varepsilon)$. The empirical coefficients, C_1 and C_2, and the functions

Table 6.1. Comparison of coefficients defining equation (6.1) for each model [4].

Model	C_1	$f_1(\varepsilon)$	C_2	$f_2(\varepsilon)$
Modified-Macdonald	$180\frac{\mu}{D_p^2\phi^2}$	$\frac{(1-\varepsilon)^2}{\varepsilon^{3.6}}$	$B\frac{\rho}{D_p\phi}$	$\frac{(1-\varepsilon)}{\varepsilon^{3.6}}$
Comiti and Renaud	$2\tau^2\mu a_{vd}^2$	$\frac{(1-\varepsilon)^2}{\varepsilon^3}$	$0.0968\tau^3\rho a_{vd}$	$\frac{(1-\varepsilon)}{\varepsilon^3}$
RUC	$25.4\frac{\mu}{D_p^2\phi^2}$	$\frac{(1-\varepsilon)^{4/3}}{(1-(1-\varepsilon)^{1/3})(1-(1-\varepsilon)^{2/3})^2}$	$\beta c_d\frac{\rho}{2D_p\phi}$	$\frac{(1-\varepsilon)}{\varepsilon(1-(1-\varepsilon)^{2/3})^2}$

depending on porosity, $f_1(\varepsilon)$ and $f_2(\varepsilon)$, are defined in Table 6.1 for each of the three models.

Dumont et al. [4] graphically represented the linear change in pressure drop over the three biofilters, according to equation (6.1). Similar figures are graphically represented in Figures 6.1, 6.2 and 6.3. The linear regression, R^2, slope and intercept values have been determined for each day for all three biofilters and are given in Table 6.2 and also indicated in Figures 6.1, 6.2 and 6.3.

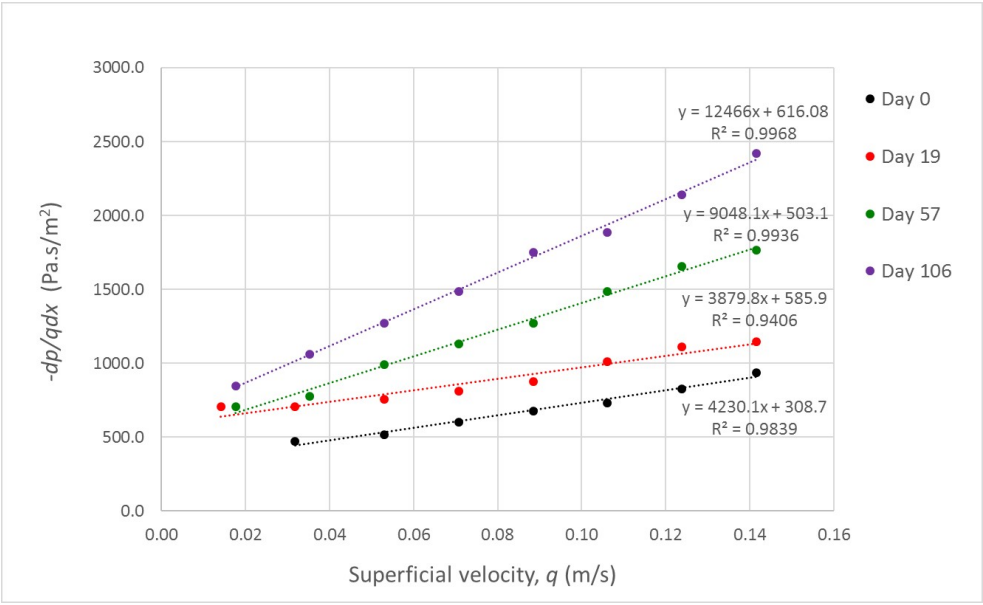

Figure 6.1. Linear regression of pressure drop data for Biofilter 1.

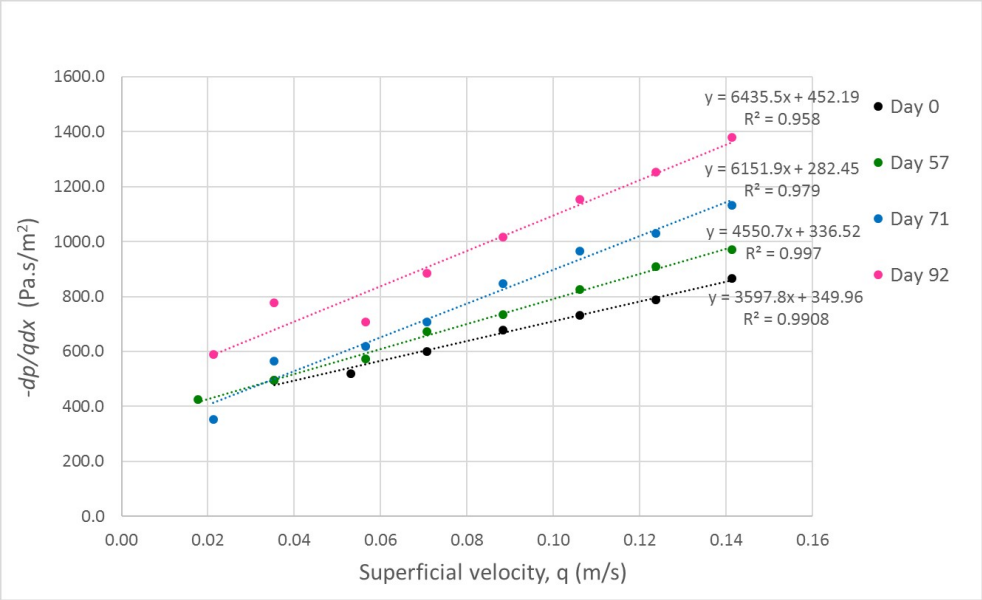

Figure 6.2. Linear regression of pressure drop data for Biofilter 2.

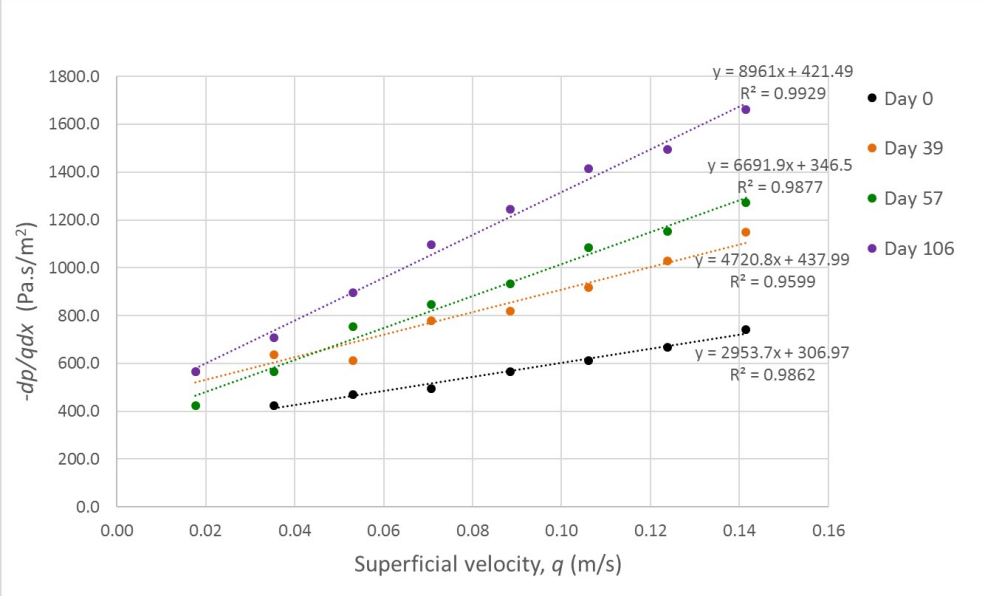

Figure 6.3. Linear regression of pressure drop data for Biofilter 3.

Table 6.2. Slope, y-intercept and R^2-values of the linear regression in pressure drop for Biofilters 1, 2 and 3.

	Biofilter 1			**Biofilter 2**			**Biofilter 3**		
Day	**Intercept**	**Slope**	R^2	**Intercept**	**Slope**	R^2	**Intercept**	**Slope**	R^2
0	308.70	4230.10	0.9839	349.96	3597.80	0.9908	306.97	2953.70	0.9862
19	585.90	3879.80	0.9406	No recorded data			535.73	3823.80	0.8990
39	557.73	5064.90	0.9238	425.76	2961.90	0.8781	437.99	4720.80	0.9599
57	503.10	9048.10	0.9936	336.52	4550.70	0.9970	346.50	6691.90	0.9877
71	514.23	10218.00	0.9943	282.45	6151.90	0.9790	411.78	8744.50	0.9993
92	749.44	7324.70	0.8702	452.19	6435.50	0.9580	No recorded data		
106	616.08	12466.00	0.9968	431.46	6604.00	0.9863	421.49	8961.00	0.9929

Considering the data displayed in Figures 6.1 to 6.3, it is once again clear that the pressure drop increases over time. This illustrates the influence of the biofilm growth inside the biofilter. For the sake of easy readability, not all the lines (i.e. for all the days) are shown in Figures 6.1 to 6.3. According to Dumont et al. [4] the straight lines fitted to $-\frac{1}{q}\frac{dp}{dx}$ versus q are satisfactory, since the linear regression based on the least squares approach fitted the experimental data very well, as indicated by the lower R^2-values in Table 6.2, except for Biofilter 1 on day 92, Biofilter 2 on day 39 and Biofilter 3 on day 19. Recall that data is missing for Biofilter 2 on day 19 and for Biofilter 3 on day 92.

The difference between the porosity functions, $f_1(\varepsilon)$ and $f_2(\varepsilon)$, according to the three pressure drop models is shown in Figures 6.4 and 6.5, respectively. In Figure 6.4 the curves obtained from the Modified-Macdonald equation and the Comiti and Renaud model show close correspondence. Referring to Table 6.1, an explanation for this phenomenon is the fact that the only difference in $f_1(\varepsilon)$ and $f_2(\varepsilon)$ for the two models lie in the value of m (i.e. the exponent of the porosity). In the case of the Modified-Macdonald equation, $m = 3.6$, whereas in the case of the Comiti and Renaud model, $m = 3$. The RUC model, however, predicts values for $f_1(\varepsilon)$ that are significantly higher than those predicted by the other two models. Figure 6.5 shows different results. Even though the $f_2(\varepsilon)$-functions (given in Table 6.1) are again similar when considering the Modified-Macdonald equation and the Comiti and Renaud model, the Modified-Macdonald equation and RUC model predict similar values for $f_2(\varepsilon)$, while the Comiti and Renaud model predicts values that are considerably lower. However, the models should not be evaluated based on the independent performance of the $f_1(\varepsilon)$- and $f_2(\varepsilon)$-functions. The combined effect is what determines the overall performance of the pressure drop, according to equation (6.1).

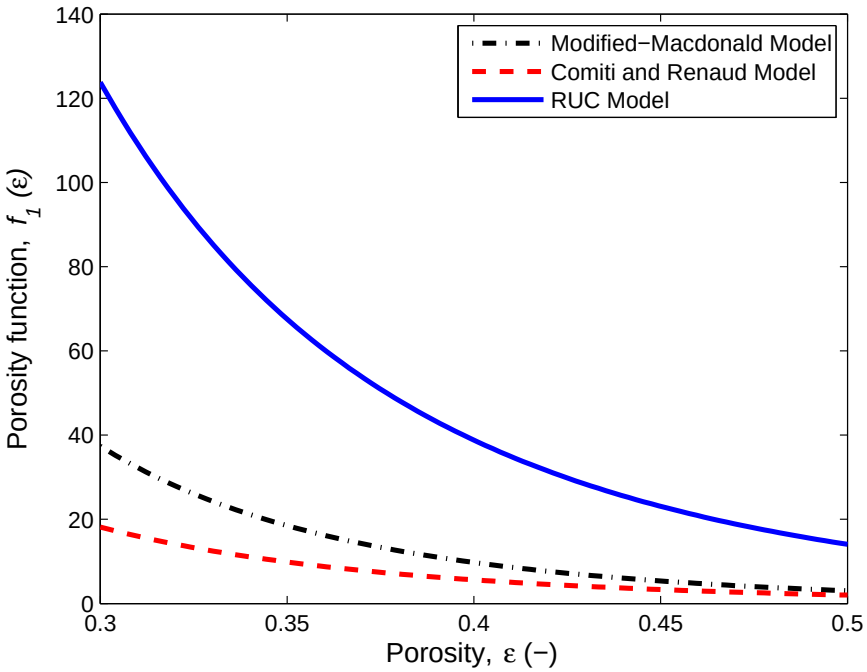

Figure 6.4. Comparison of model predictions for the porosity function, $f_1(\varepsilon)$ [4].

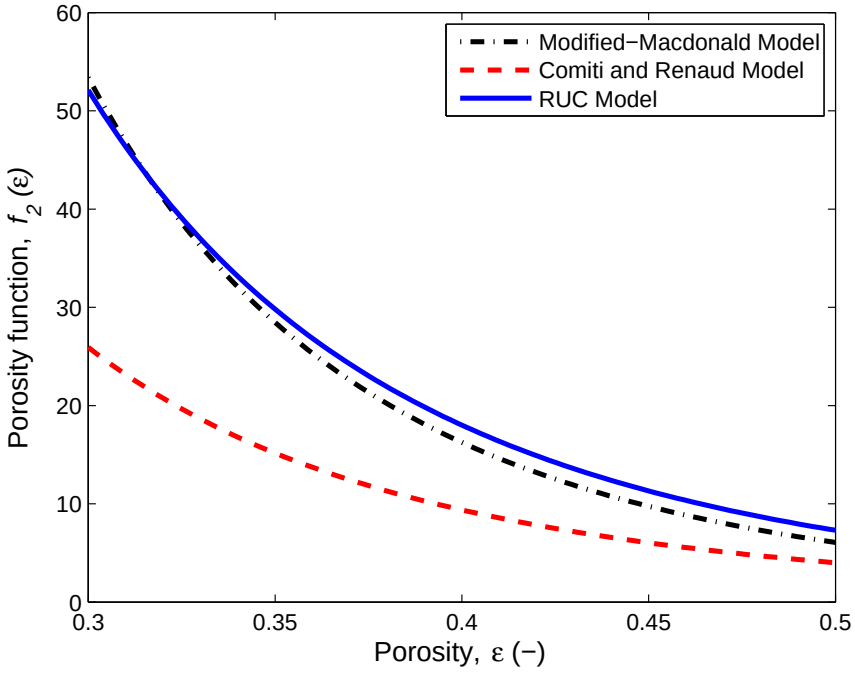

Figure 6.5. Comparison of model predictions for the porosity function, $f_2(\varepsilon)$ [4].

Recall that the Modified-Macdonald equation depends on the porosity, sphericity and the particle

roughness coefficient. Prior to the presence of biofilm in any packed bed, the initial porosity can be measured (as discussed in Section 4.3). The initial porosities for the three biofilters, i.e. on day 0, are given in Table 4.2. On any other day of the experiment, however, the porosity has to be determined without disturbing the packed bed with biofilm. Since ε_o is known, the sphericity factor (which is the only unknown in this model on day 0) can be obtained from the pressure drop measurement results obtained on the first day of the experiment, day 0.

Dumont et al. [4] used the Modified-Macdonald equation, Excel® Solver and the sum of the squared residuals (SSR), i.e.,

$$\text{SSR} = \sum_{i=1}^{7} \left\{ \left(\frac{\Delta p}{Lq} \right)_i^{exp} - \left(\frac{\Delta p}{Lq} \right)_i^{model} \right\}^2, \tag{6.2}$$

in order to determine that $\phi = 0.85$, which is consistent with the value used by Morgan-Sagastume et al. [26]. In equation (6.2), $(\frac{\Delta p}{Lq})_i^{exp}$ is defined as the pressure drop values determined experimentally and $(\frac{\Delta p}{Lq})_i^{model}$ as the pressure drop values determined by the porous media model under consideration. The symbol, i, indicates the number of airflow rates recorded per day that were used to determine the $\frac{\Delta p}{Lq}$-curves, of which there are 7 in total. Recall from Section 4.2 that Dumont et al. [4] made the assumption that the biofilm development on the surface of the packing material did not change the shape of the expanded schist. This allowed Dumont et al. [4] to keep the sphericity value constant over time. For all the other days on which data was recorded, there are two unknowns to be determined in the Modified-Macdonald equation, i.e. B and ε.

Two cases were considered for the initial guessed values when examining the Modified-Macdonald equation, i.e. $B = 2$ and $B = 3$ with ε set equal to the value of the experimentally determined porosity, ε_{exp}. After optimization, it was established that ε and B were independent of the initial guessed values.

Considering the Comiti and Renaud model, equation (3.12) depends on ε, τ and the SSA (i.e. a_{vd}, without taking biofilm growth into consideration). Dumont et al. [4] used Excel® Solver to determine ε, τ and a_{vd} (i.e. three unknowns) for all the other days after day 0. Two arbitrarily chosen combinations of initial guessed values were tested in the present study, i.e. Case 1: (τ; a_{vd}) = (1.5; 500) and Case 2: (τ; a_{vd}) = (1.3; 600). The investigation of the influence of different initial guessed values were not performed by Dumont et al. [4].

Equation (3.23), representing the RUC model, depends on the porosity, the sphericity, the drag coefficient and the particle roughness coefficient. In order for the calculation procedure with the RUC model to be in direct comparison with that of the Modified-Macdonald equation, Dumont

Table 6.3. Porous media models and the corresponding optimized variables.

Variables that were optimized	**Modified-Macdonald**	**Comiti and Renaud**	**RUC**
$\boldsymbol{\varepsilon}$	√	√	√
$\boldsymbol{B}$	√		
$\boldsymbol{a_{vd}}$		√	
$\boldsymbol{\tau}$		√	

et al. [4] also used $\phi = 0.85$ as input parameter for the RUC model. As discussed in Section 3.6, Du Plessis and Woudberg [2] suggested the use of $c_d = 1.9$. Subsequently, Dumont et al. [4] used Excel® Solver to determine ε (the only unknown) for all the other days of biofilter operation. The porous media models and the corresponding variables that were optimized in Excel® are indicated in Table 6.3.

The first step in the optimization method is to find the SSR (refer to equation (6.2)). The second step is to setup Solver. Solver offers three different solving methods, i.e. GRG Nonlinear, Simplex LP and Evolutionary. GRG Nonlinear requires that the objective cell or at least one of the constraints has to be a smooth nonlinear function, whereas Simplex LP and Evolutionary are selected for linear and non-smooth problems, respectively. In this case the objective cell contains equation (6.2), which is a smooth nonlinear function, therefore, GRG Nonlinear was selected. The program presents the option to either minimize or maximize the SSR-value. In this case the aim is to minimize the squared difference between $(\frac{\Delta p}{Lq})_i^{exp}$ and $(\frac{\Delta p}{Lq})_i^{model}$. The third step is to choose the cells in Excel® containing variables that Solver can change, i.e. the constraints, in order to subsequently minimize the SSR. For this step to be possible, the user has to enter initial guessed values in the cells containing the unknown variables, before running Solver. It is important to note that in every case for every model and in all three biofilters, the experimentally determined porosity value for the specific day being considered, was used as an initial guess for this variable.

6.2 Optimized Porosity Results

The differences between the optimized porosity values and the effects of the different initial guessed values are graphically represented in Figures 6.6, 6.7 and 6.8 for the three biofilters, respectively. Note that only one set of data points is reflected for the Modified-Macdonald equation, since it is unaffected by the initial guessed B-values. After optimization the Comiti and Renaud model showed to be dependent on the initial guessed values chosen, even though the differences are

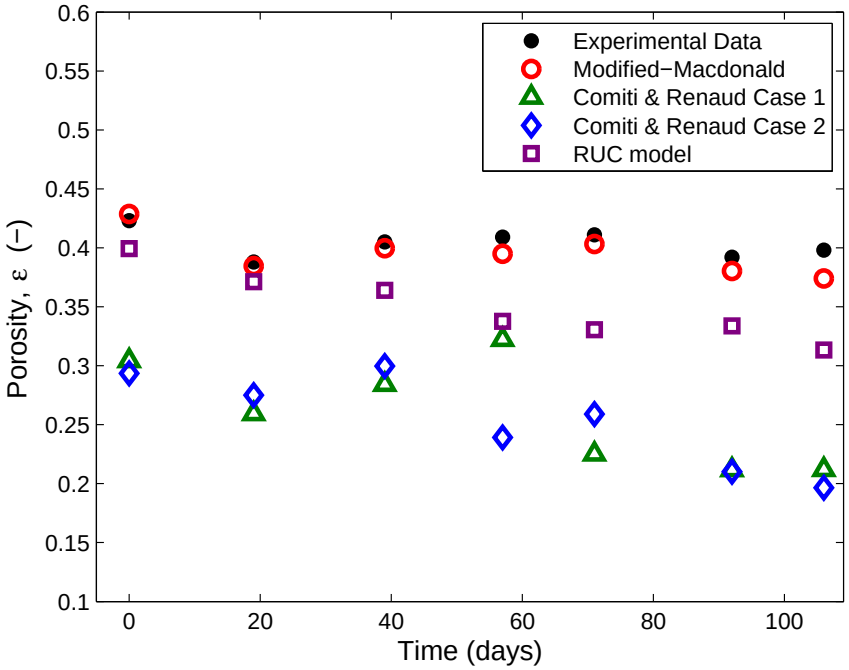

Figure 6.6. Comparison between optimized porosity values for Biofilter 1.

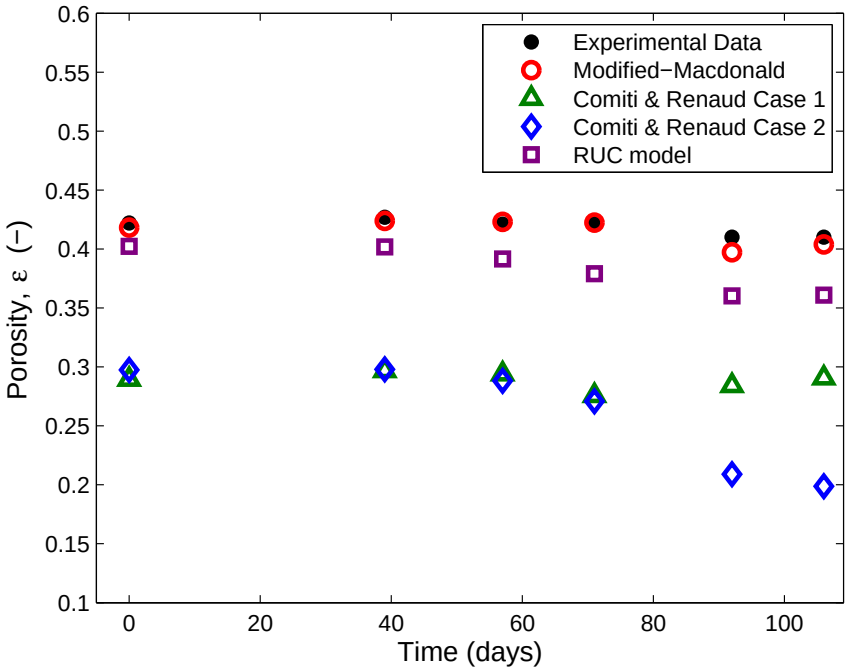

Figure 6.7. Comparison between optimized porosity values for Biofilter 2.

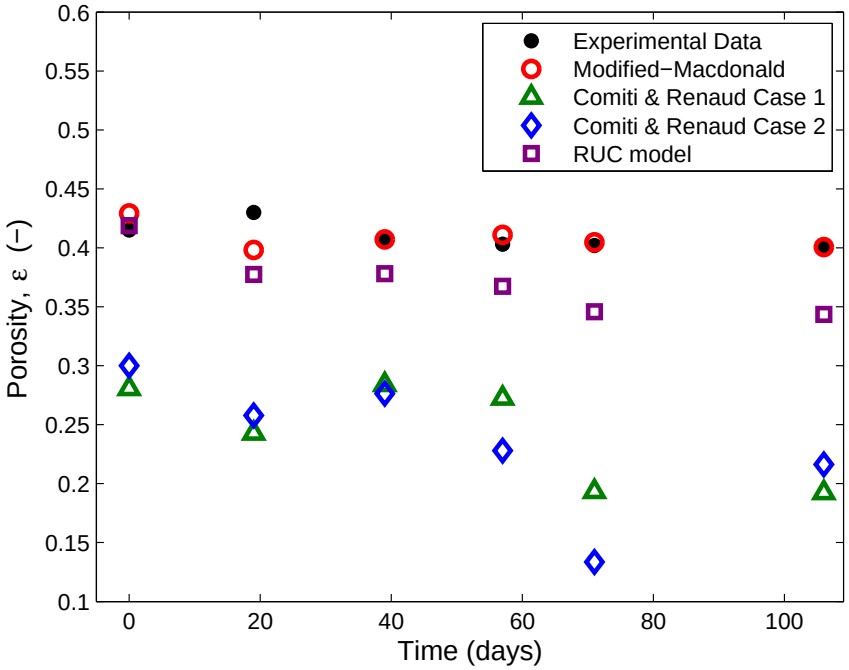

Figure 6.8. Comparison between optimized porosity values for Biofilter 3.

relatively small. The RUC model somewhat underestimates the porosity values for all three biofilters. The Modified-Macdonald equation appears to give remarkable results when compared to the experimental values. This is true for all three biofilters throughout the entire experiment, except for Biofilter 1 on day 106 and Biofilter 3 on day 19. The most probable reason for this is due to the fact that the Modified-Macdonald equation was used in Excel® to optimize the value of ϕ.

After comparing the porosity values determined by the three models, with the porosity values obtained with the experimental procedure, Dumont et al. [4] found that the model of Comiti and Renaud cannot be used to predict the porosity of a packed bed, based on its inaccuracy as is evident in Figures 6.6 to 6.8. The probable cause is due to the fact that this model requires three unknown variables that need to be optimized at once.

The percentage differences, PD, between the results obtained from Case 1 and 2 in the Comiti and Renaud model were determined as follows:

$$\mathrm{PD} = \frac{x_1 - x_2}{x_1} \times 100, \tag{6.3}$$

where x_1 and x_2 denote the values obtained for the variable under consideration from Case 1 and 2, respectively. The results from equation (6.3) for the porosity are shown in Table 6.4.

Table 6.4. Percentage difference in ε between Case 1 and Case 2 considered in the Comiti and Renaud model.

Day	Biofilter 1	Biofilter 2	Biofilter 3
0	3.46%	−2.79%	−6.90%
19	−6.09%		−6.16%
39	−5.47%	−0.41%	2.67%
57	25.79%	1.98%	16.38%
71	−15.07%	1.77%	30.94%
92	0.76%	26.45%	
106	7.23%	31.59%	−12.55%

The values given in Table 6.4 show that when considering Biofilter 1 together with the Comiti and Renaud model, there are greater differences in values on days 57 and 71. In Biofilter 2 on days 92 and 106 the differences in values are significantly greater than earlier in the experiment whereas in Biofilter 3 the PD are considerably larger from day 57 onwards.

6.3 Optimized Roughness Coefficient Results

The differences between the optimized values for B in the Modified-Macdonald equation are graphically represented in Figures 6.9 to 6.11. The roughness coefficient, B, does not maintain a constant value throughout the course of the experiment. This is a possible result of increasing biofilm growth on the surface of the packing material and non-uniformity violating the assumption of homogeneous biofilm growth [4]. Although the range of roughness ($1.8 \leq B \leq 4.0$) was chosen in the study of Macdonald et al. [21] (discussed in Section 3.2), it is important to recall that a different packing material was used in the present study than that used by Macdonald et al [21]. In this study, the values of the particle roughness coefficient, B, ranged from 1.62 to 4.95 for all three biofilters. The latter values correspond to the values used in the literature (Morgan-Sagastume et al. [26]) and tends to increase as the biofilm growth inside the packed beds develop over time. Since the change in B-values can be related to the increase in biofilm growth, it can therefore be related to the increase in the pressure drop over time. Since the biofilm growth continuously affects the surface roughness of the packed bed, no universal constant value can be strictly assigned to B. Even so, Dumont et al. [4] concluded that the use of the Modified-Macdonald equation is the

best way to predict the change in porosity in a biofilter over time.

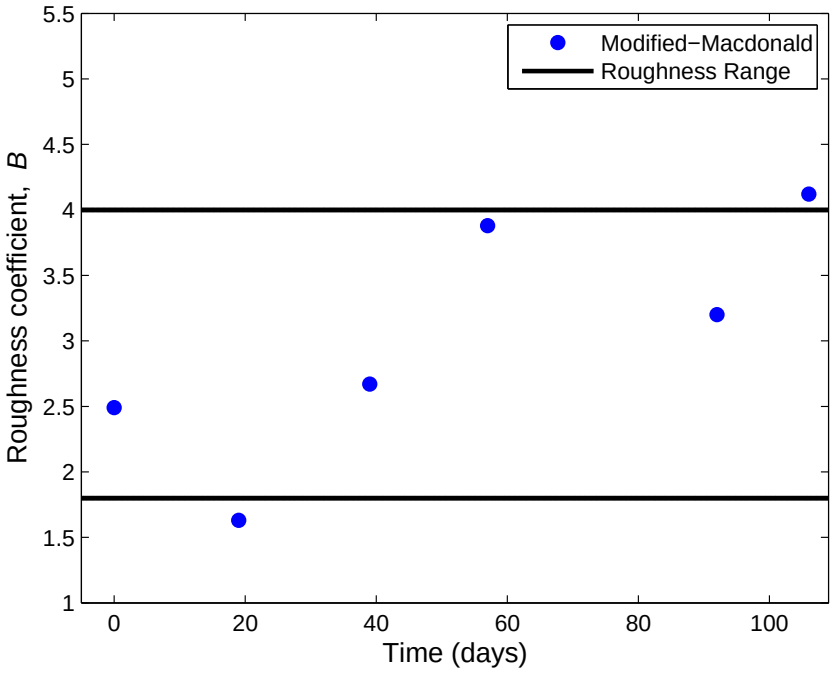

Figure 6.9. Comparison between optimized roughness coefficient values for Biofilter 1.

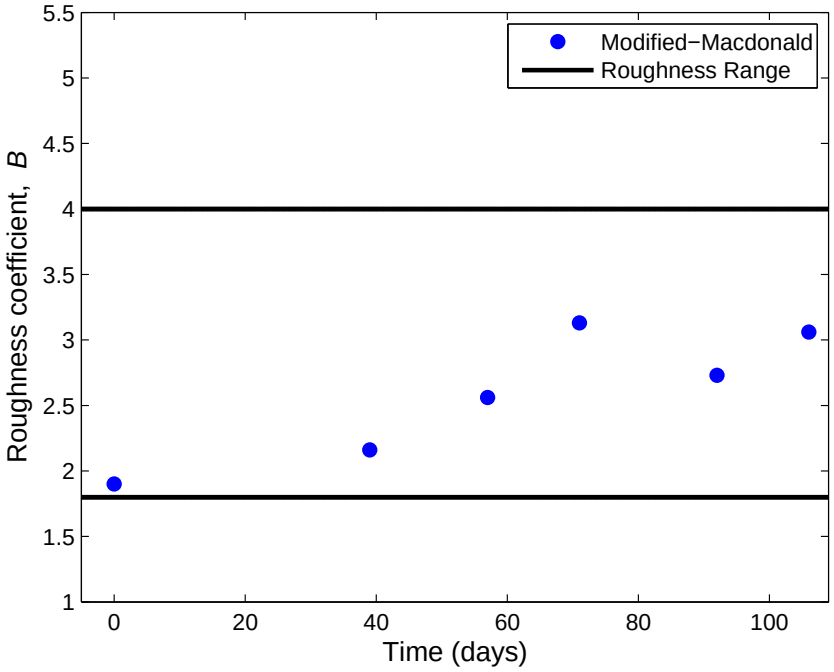

Figure 6.10. Comparison between optimized roughness coefficient values for Biofilter 2.

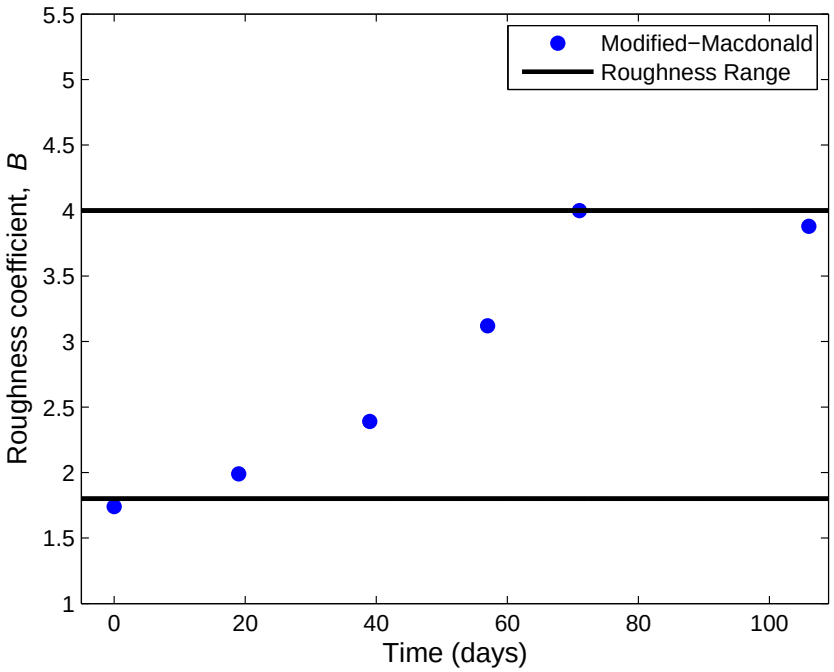

Figure 6.11. Comparison between optimized roughness coefficient values for Biofilter 3.

6.4 Optimized Tortuosity Results

The differences between the optimized values for τ obtained from the three models and the effect of the different initial guessed values in the case of the Comiti and Renaud model are shown in Figures 6.12 to 6.14. Note that the experimental tortuosity values were determined with equation (5.1) by making use of the experimentally measured porosity values. In comparison with the other models, the Modified-Macdonald equation proved to be the most accurate model when compared to the experimental tortuosity data, regardless of the biofilter being considered. In all three biofilters the RUC model under-predicts the tortuosity data with equation (5.4). Note that the porosity values optimized with the Modified-Macdonald equation and the RUC model were used in equations (5.1) and (5.4), respectively, which were then plotted in Figures 6.12 to 6.14. In the case of the Comiti and Renaud model, the optimized τ-values obtained by the application of this model are shown.

According to Dumont et al. [4], since the tortuosity remained more or less constant, the changes over time in pressure drops cannot be related to the significant change in the free cross-sectional area of the packed bed, but rather to the changes over time in particle roughness as a result of

the biofilm development.

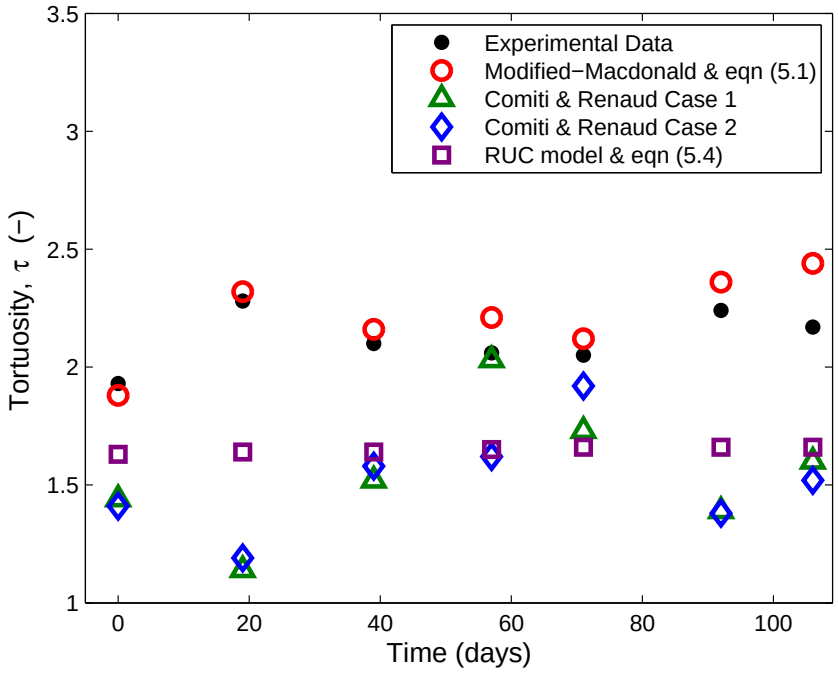

Figure 6.12. Comparison between optimized tortuosity values for Biofilter 1.

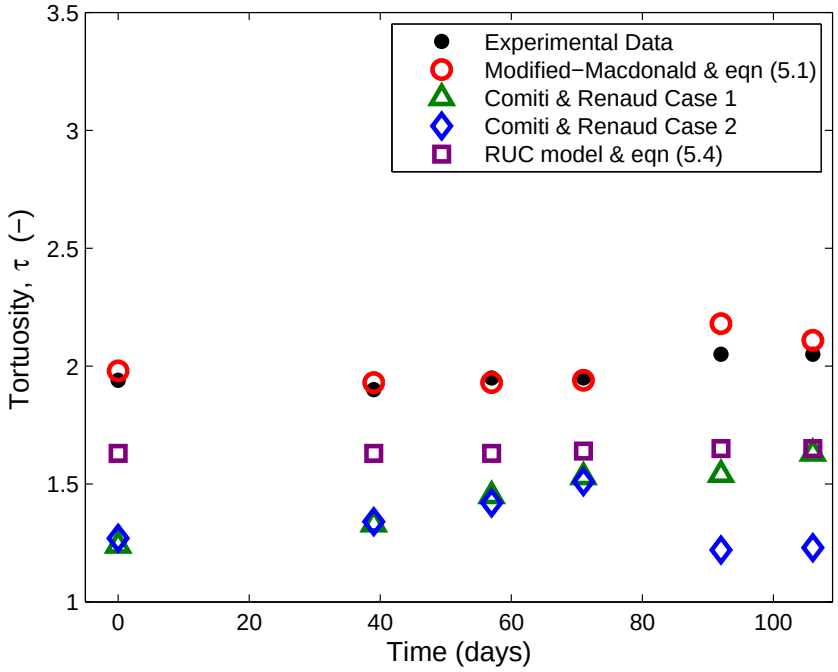

Figure 6.13. Comparison between optimized tortuosity values for Biofilter 2.

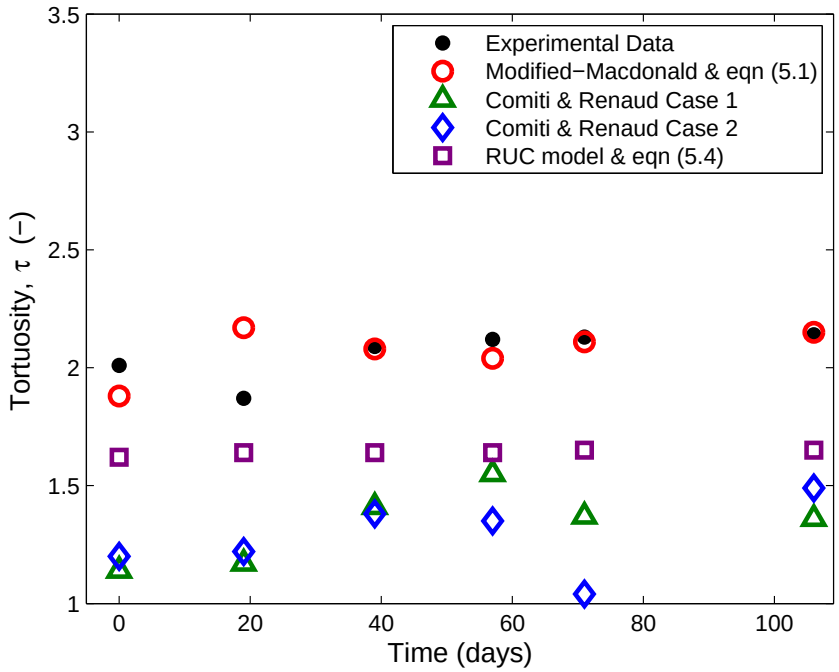

Figure 6.14. Comparison between optimized tortuosity values for Biofilter 3.

The percentage differences between the results obtained from Case 1 and 2 with the Comiti and Renaud model, also determined with equation (6.3), can be seen in Table 6.5. The highest percentage values in Table 6.5 are obtained for the same days and biofilters as in Table 6.4.

Table 6.5. Percentage difference in τ between Case 1 and Case 2 considered in the Comiti and Renaud model.

Day	Biofilter 1	Biofilter 2	Biofilter 3
0	2.61%	−2.08%	−5.13%
19	−4.53%		−4.62%
39	−4.09%	−0.31%	2.01%
57	20.05%	1.47%	12.51%
71	−11.01%	1.32%	24.28%
92	0.56%	20.59%	
106	5.42%	24.78%	−9.28%

6.5 Optimized Biofilm Thickness Results

Alonso et al. [5] developed a model for determining the biofilm affected porosity, based on the assumption that the biomass growth on the surface of the particles is consistent over the entire biofilter, i.e.,

$$\varepsilon_f = 1 - (1 - \varepsilon_o)\left[\left(1 + 2\frac{L_f}{D_p}\right)^3 - \frac{n}{4}\left(2\frac{L_f}{D_p}\right)^2\left(4\frac{L_f}{D_p} + 3\right)\right] \tag{6.4}$$

Equation (6.4) expresses the relationship between D_p, the biofilm thickness, L_f, the number of packing spheres a given sphere is in contact with (or coordination number), n, and the initial porosity of the bed prior to containing biofilm, ε_o [4]. According to Dullien et al. [27] the coordination number for a close, random type of packing is related to ε_o as follows:

$$\varepsilon_o = 1.072 - 0.1193n + 0.004312n^2. \tag{6.5}$$

Morgan-Sagastume et al. [26] solved equation (6.5) by setting ε_o equal to their experimentally determined initial porosity, $\varepsilon_o = 0.520$. The results were $n_1 = 22$ and $n_2 = 6$. Since $6 \leq n \leq 12$ for various types of solid structures (refer to Table 6.6), $n_2 = 6$ was used.

Table 6.6. Coordination number, n, and porosity, ε, for different types of structures [6].

Type of structure	**Coordination number**	**Porosity**
Simple Cubic	6	0.477
Orthorhombic	8	0.395
Tetragonal-sphenoidal	10	0.302
Rhombohedral	12	0.260

Figure 6.15 shows the porosity values given in Table 6.6 as a function of the coordination number (also given in Table 6.6). Figure 6.15 shows, in addition, a curve fitted through the data by means of the least squares method as well as equation (6.5). The latter two curves show satisfactory correspondence, except for $6 < n < 8$ where deviations occur.

Despite the deviations, equation (6.5) was still used in the present study to determine the value of n, with measured ε_o-values of 0.423, 0.422 and 0.415 for Biofilter 1, 2 and 3, respectively. Values of 7.4 and 7.5 were obtained which were then rounded to 7. Morgan-Sagastume et al. [26] similarly obtained a value of 5.7 for n which was rounded to 6.

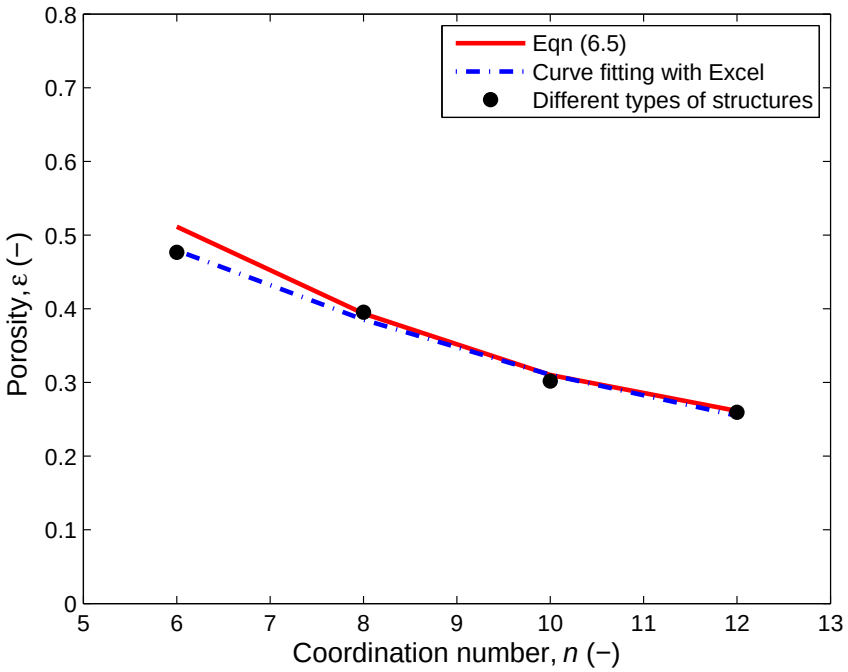

Figure 6.15. Porosity as a function of the coordination number.

By making use of the optimized porosity values determined with the Modified-Macdonald equation and taking the sphericity of the packing material into consideration, Dumont et al. [4] calculated the biofilm thickness by solving the following equation:

$$\varepsilon_f = 1 - (1 - \varepsilon_o)\left[\left(1 + 2\frac{L_f}{\phi D_p}\right)^3 - \frac{n}{4}\left(2\frac{L_f}{\phi D_p}\right)^2\left(4\frac{L_f}{\phi D_p} + 3\right)\right]. \tag{6.6}$$

The values that were used throughout the entire analyses were $\phi = 0.85$, $D_p = 0.01$ m and $n = 7$. The results from using equation (6.6) to determine the biofilm thickness, L_f, are shown in Figures 6.16 to 6.18. Note that the experimental biofilm thickness values were also determined with equation (6.6) by using the experimental porosity values. For the RUC model, its own optimized porosity values were used in equation (6.6) to determine the biofilm thickness. The Comiti and Renaud model has been excluded from predicting the biofilm thickness values due to its inability to accurately predict the biofilm affected porosity values.

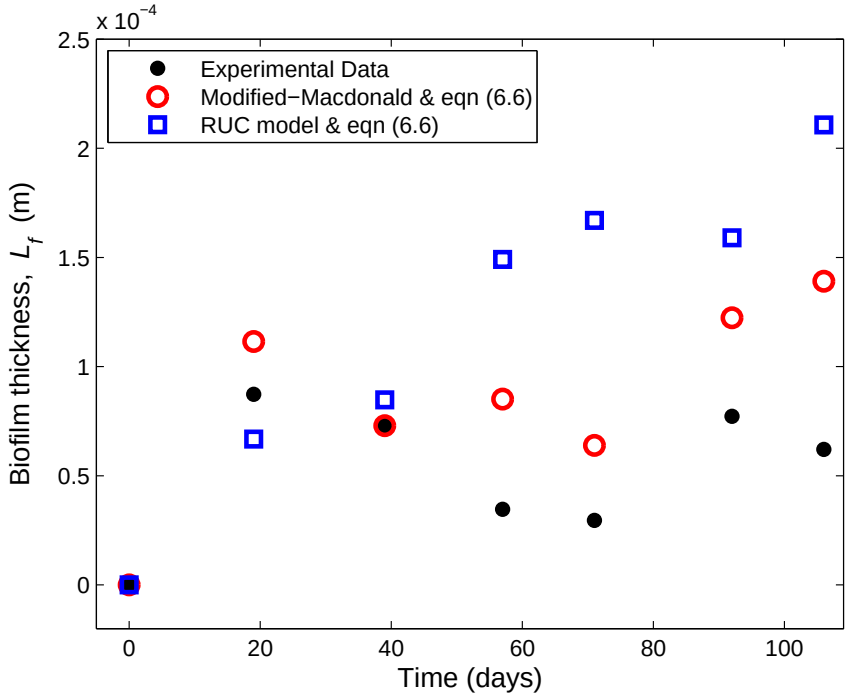

Figure 6.16. Comparison between optimized biofilm thickness values for Biofilter 1.

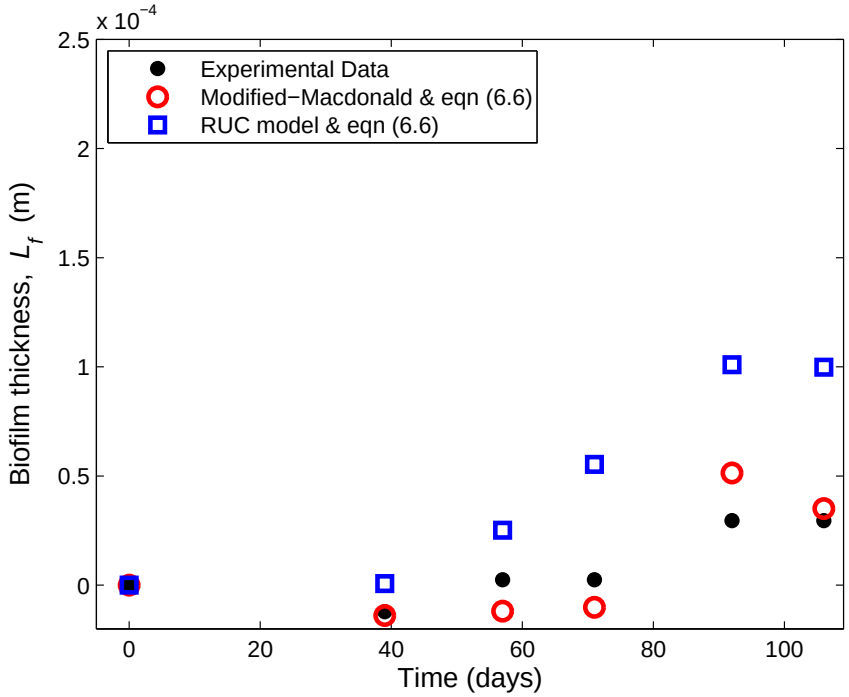

Figure 6.17. Comparison between optimized biofilm thickness values for Biofilter 2.

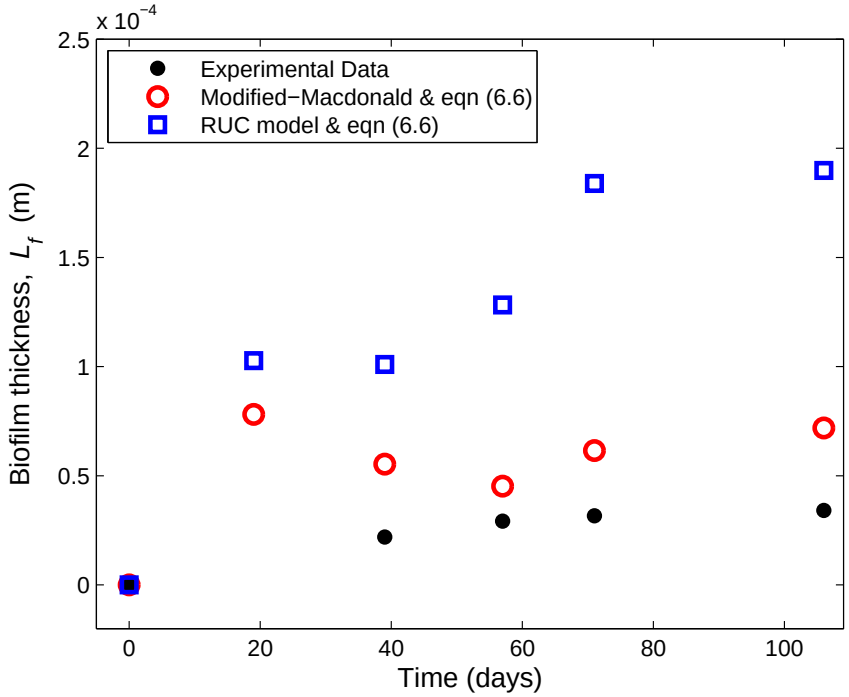

Figure 6.18. Comparison between optimized biofilm thickness values for Biofilter 3.

From Figures 6.16 to 6.18 it is clear that both the Modified-Macdonald and RUC models mostly over-predict the L_f-values, when compared to the experimental results. When compared to each other, however, the more accurate results were obtained from the Modified-Macdonald equation. A probable cause for this may be the fact that the Modified-Macdonald equation was used twice in the optimization process, whereas the RUC model was used only once. This is because the Modified-Macdonald equation was used to additionally optimize the value of ϕ.

6.6 Optimized Specific Surface Area Results

Taking into consideration the sphericity of the packing material, the following equations were proposed by Alonso et al. [5]:

$$a_o = \frac{6(1-\varepsilon_o)}{\phi D_p}, \tag{6.7}$$

$$a_f = \frac{a_o}{2}\left[\left(1+\frac{2L_f}{\phi D_p}\right)\left((2-n)\frac{2L_f}{\phi D_p}+2\right)\right]. \tag{6.8}$$

Equations (6.7) and (6.8) represent the initial SSA without biofilm, a_o, and the SSA in the presence of biofilm, a_f. Equations (6.6) to (6.8) were used by Morgan-Sagastume et al. [26] to successfully

characterize the effects of biofilm growth on pressure drops in biofilters.

As discussed in Section 4.1, the schist particles used have an average SSA, a_s, equal to 600 1/m. This value was calculated by assuming that the schist particles are spherical i.e.,

$$a_s = \frac{4\pi R^2}{\frac{4}{3}\pi R^3} = \frac{3}{R} = \frac{3}{\frac{0.01}{2}} = 600 \text{ 1/m}.$$

The latter, however, holds for one single sphere. Substituting the known values for ε_o, ϕ and D_p into equation (6.7), the average SSA without the presence of biofilm (day 0) for the entire packed bed is shown in Table 6.7.

Table 6.7. The a_o-values for the three respective biofilters (day 0).

Biofilter	a_o **with** $\phi = 1$	a_o **with** $\phi = 0.85$
1	346	407
2	346	408
3	351	413

Table 6.7 shows that when the average sphericity deviates from a sphere ($\phi = 1$), the initial SSA increases.

The a_f-values determined with equations (6.7) and (6.8) are graphically represented in Figures 6.19 to 6.21 together with the a_{vd}-values obtained through optimization with the model of Comiti and Renaud. Note that the experimental SSA values were also determined with equations (6.7) and (6.8) by using the experimental porosity values. Both the Modified-Macdonald and RUC models give accurate results, since the SSA values correspond closely to that of the experimental data.

In Biofilters 1 and 3 the Comiti and Renaud model over-predicts the experimental SSA values for days 0 to 57 and under-predicts the data thereafter. In Biofilter 2 the model over-predicts the experimental SSA values for days 0 to 57 after which it fluctuates about the experimental values depending on the initial guessed values used (i.e. in Case 1 and 2). Considering the sensitivity of the Comiti and Renaud model, the percentage differences between the SSA values for Case 1 and 2 (from equation (6.3)) are shown in Table 6.8.

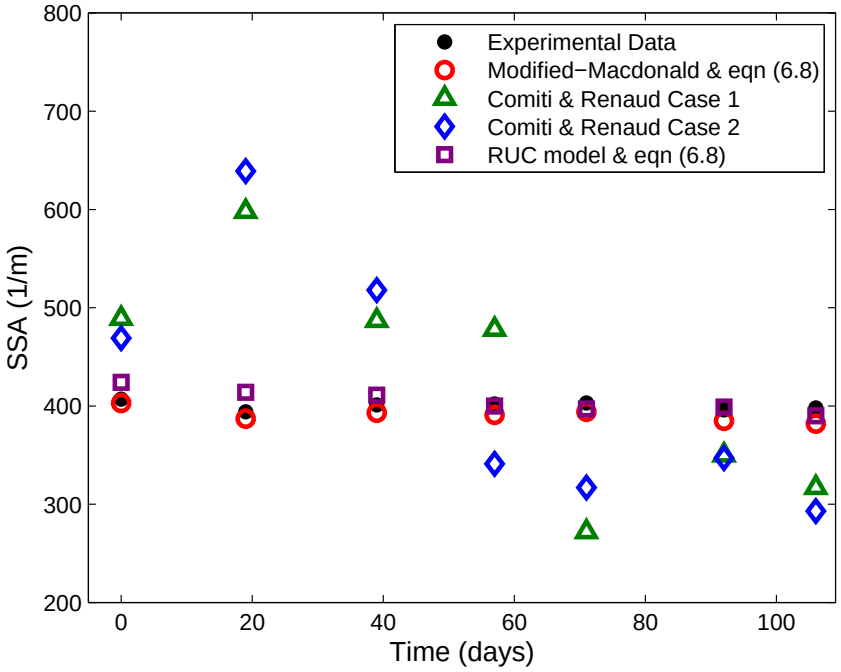

Figure 6.19. Comparison between optimized SSA values in Biofilter 1.

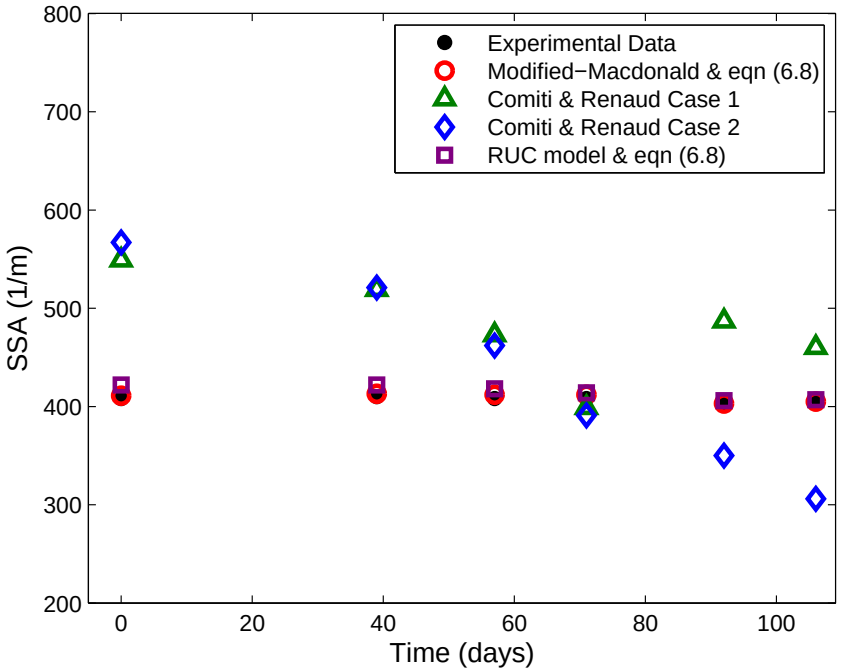

Figure 6.20. Comparison between optimized SSA values in Biofilter 2.

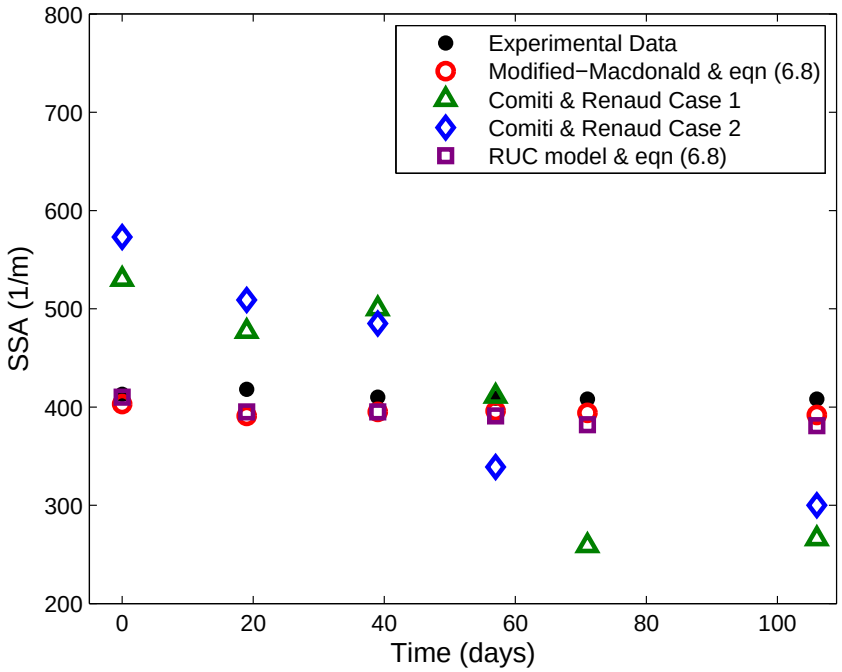

Figure 6.21. Comparison between optimized SSA values in Biofilter 3.

Table 6.8. Percentage difference in a_{vd} between Case 1 and Case 2 considered in the Comiti and Renaud model.

Day	Biofilter 1	Biofilter 2	Biofilter 3
0	4.06%	−3.28%	−8.04%
19	−6.80%		−6.64%
39	−6.35%	−0.48%	3.03%
57	28.77%	2.32%	17.68%
71	−16.38%	2.02%	29.38%
92	0.78%	28.11%	
106	7.37%	33.41%	−12.62%

After running Excel® Solver multiple times for each biofilter and experimenting with the initial guessed values, it was found that Excel® Solver is not only slightly sensitive to the initial guessed values, but also does not necessarily give an optimal solution when requested to adjust multiple (> 2) unknown variables. Therefore, Solver is not especially ideal when considering the Comiti and Renaud model. Research shows that when using Solver in a smooth nonlinear case, it only focuses on the local minimum or maximum instead of the global minimum or maximum [32, 33]. Therefore, when inserting an initial guessed value, it will result in Solver finding the closest

optimum value in that specific case, whereas inserting a different initial guessed value can result in finding another optimum value. This does not necessarily mean that either of these values is the global minimum. If Solver has to optimize one variable, for instance ε, there is not much room for adjustment, whereas when there are two variables to be optimized, the range of optimum values becomes wider. In the case of more than two variables, such as with the model of Comiti and Renaud, there might be too many options of minimum values for the SSR and therefore the local minimum becomes a larger uncertainty factor in the results.

In reference to Tables 6.4, 6.5 and 6.8, the rather significant PD-values appear on the same days of biofilter operation for all three biofilters, i.e. for Biofilter 1 on days 57 and 71, Biofilter 2 on days 92 and 106 and for Biofilter 3 on day 57 onward. No correlation could however be found between the PD-values and the SSR value for a specific day and biofilter. In order to obtain an explanation for this phenomenon one will have to study the GRG nonlinear algorithm used by Excel®, which falls beyond the scope of this study.

Recall that Biofilters 1 and 3 were inoculated with activated sludge. Compared to the experimental a_o-values, the biofilm development slightly decreased the SSA, i.e. from 407 to 394 in Biofilter 1, from 408 to 404 in Biofilter 2 and from 413 to 408 in Biofilter 3 over the 110 days. Biofilter 2, however, was not inoculated with activated sludge. The biofilm development only appeared some time around day 80 of the experiment and may therefore be responsible for the even smaller decrease in SSA. The tap water, used for irrigation, might have been the cause of the biofilm development.

6.7 Sensitivity Analysis: Sphericity

Model performance of the Modified-Macdonald equation compared to the RUC model may be different should the RUC model be used to optimize the sphericity value in the empirical modelling approach, instead of the Modified-Macdonald equation. Therefore, the effect of optimizing the sphericity with the RUC model was investigated and the results are discussed in this section.

The optimization steps followed in Excel® in order to optimize ϕ with the RUC model is identical to the procedure outlined in Section 6.1, in which the Modified-Macdonald equation was used to optimize ϕ. After running Solver, it was found that the average sphericity in Biofilters 1, 2 and 3 are 0.58, 0.66 and 0.65, respectively (the average ϕ-values determined by Dumont et al. [4] for the respective biofilters were not given, only the overall average value was presented). This yields

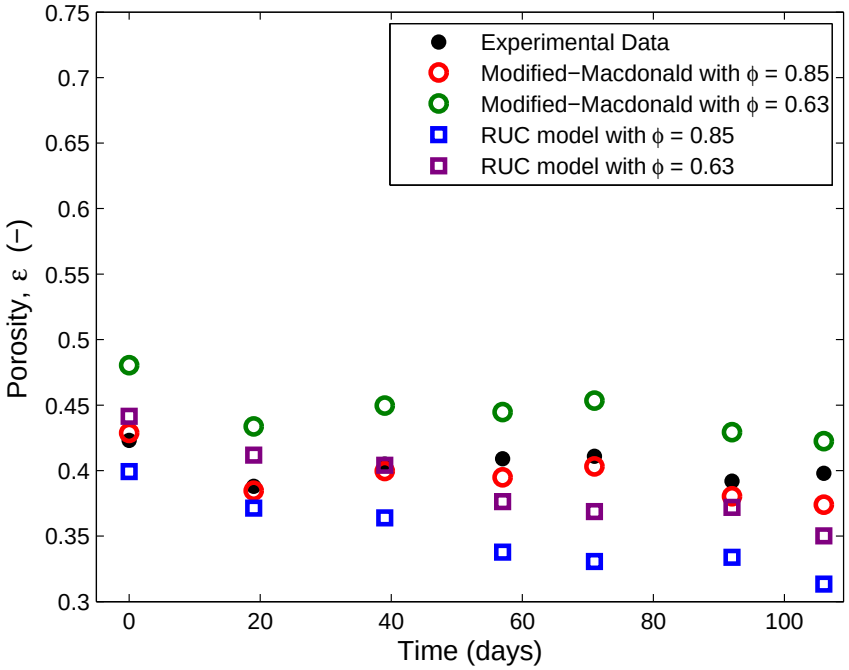

Figure 6.22. Biofilter 1: Comparison between optimized porosity values for $\phi = 0.85$ and $\phi = 0.63$.

an overall average sphericity of 0.63 for the RUC model. The ϕ-value was therefore changed from $\phi = 0.85$ to $\phi = 0.63$ and the optimization steps were followed once again in order to optimize ε and B with the Modified-Macdonald equation and ε in the case of the RUC model. Since Dumont et al. [4] came to the conclusion that the Comiti and Renaud model cannot be used to predict the porosity of a packed bed, the model was not taken into consideration in the sensitivity analysis.

The differences between the optimized porosity values obtained by setting the value of ϕ equal to 0.85 and 0.63 are graphically represented in Figure 6.22 for Biofilter 1. Figures B1 and B2 for Biofilters 2 and 3, respectively, are given in Appendix B.

From Figures 6.22, B1 and B2 it is clear that when ϕ was optimized with the RUC model, i.e. when $\phi = 0.63$, the results obtained from the Modified-Macdonald equation over-predicts the experimental data. The predictions of the RUC model, however, are more accurate when $\phi = 0.63$ than when $\phi = 0.85$, as expected. The results from the RUC model with $\phi = 0.63$ are, however, still not as satisfactory as the results obtained from the Modified-Macdonald equation with $\phi = 0.85$. The reason for the overall better performance from the Modified-Macdonald equation may be that two values have to be optimized. This increases the chances of obtaining

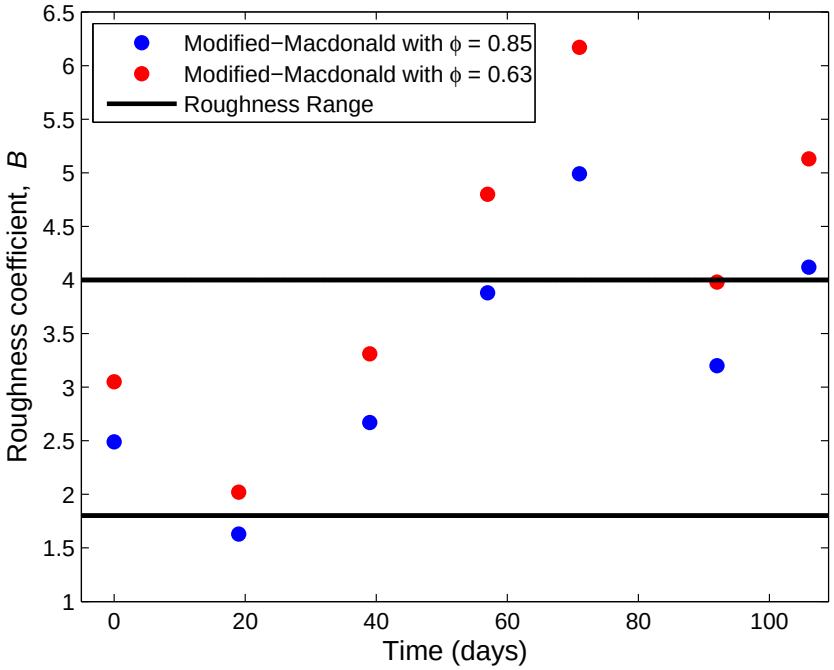

Figure 6.23. Biofilter 1: Comparison between optimized B-values for $\phi = 0.85$ and $\phi = 0.63$.

more accurate results when compared to a model with one variable to be optimized. This study thus reveals that Solver affects the outcome either positively or negatively, depending on the number of variables to be optimized. The positive outcome is when two variables have to be optimized, resulting in a more satisfactory performance. The negative outcome is when three variables need to be optimized and when the initial guessed values influence the results, such as with the model of Comiti and Renaud.

A comparison between the optimized B-values obtained from the Modified-Macdonald equation by setting the value of ϕ equal to 0.85 and 0.63 is graphically represented in Figures 6.23, B3 and B4 for Biofilters 1, 2 and 3, respectively. From Figures 6.23, B3 and B4 it is clear that all the values of B are higher when $\phi = 0.63$ than when $\phi = 0.85$ in all three Biofilters. The average relative PD obtained with $\phi = 0.63$ and $\phi = 0.85$ is 23% for Biofilters 1, 2 and 3.

Figures 6.24, B5 and B6 graphically represent the differences between the tortuosity values obtained from the Modified-Macdonald equation and the RUC model with $\phi = 0.85$ and $\phi = 0.63$ for Biofilters 1, 2 and 3, respectively. Considering the Modified-Macdonald equation, the τ-values obtained from equation (5.1) are satisfactory when $\phi = 0.85$, but over-predicts the experimental data when $\phi = 0.63$ which is due to ϕ appearing in the denominator of equation (5.1) and also

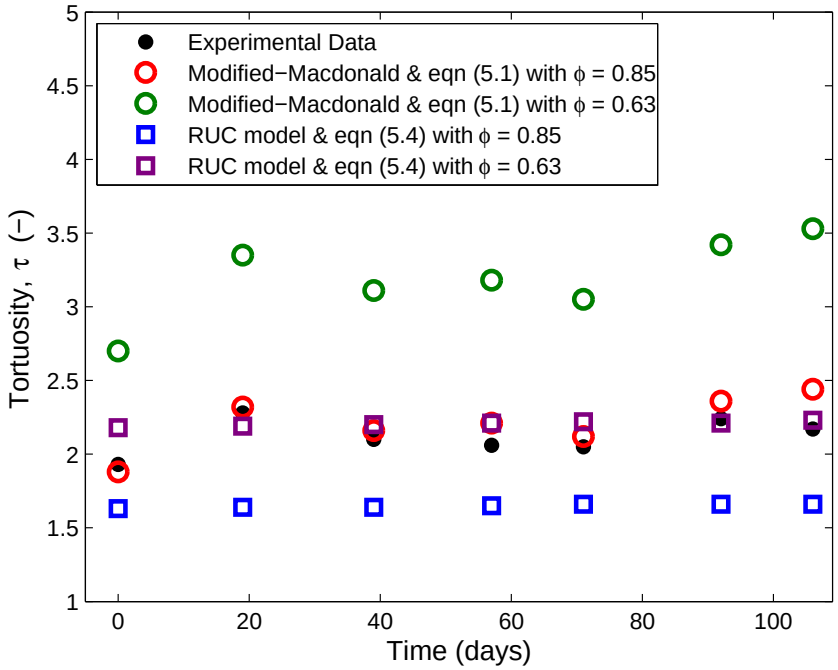

Figure 6.24. Biofilter 1: Comparison between optimized τ-values for $\phi = 0.85$ and $\phi = 0.63$.

being squared. The RUC model gives satisfactory results with $\phi = 0.63$, whereas it under-predicts the data when $\phi = 0.85$. The latter under-prediction in τ-values is a result of an increasing ϕ-value in the denominator of equation (5.4).

A comparison between the optimized L_f-values obtained is graphically presented in Figures 6.25, B7 and B8 for Biofilters 1, 2 and 3, respectively.

Considering Biofilter 1, both the Modified-Macdonald equation and the RUC model perform better when $\phi = 0.63$ than when $\phi = 0.85$. Unstable (i.e. negative) L_f-values obtained from the Modified-Macdonald equation with $\phi = 0.85$ for Biofilter 2 on days 39, 57 and 71 and from the Modified-Macdonald equation with $\phi = 0.63$ for Biofilter 3 on days 19, 39 and 57, might be a result of Excel® Solver not always obtaining the optimal solution (discussed in Section 6.6), which in this case is a negative value. It follows that a conclusion cannot be made on which sphericity value results in a better performance for Biofilters 2 and 3.

The differences between the optimized SSA values are graphically represented in Figure 6.26 for Biofilter 1. Figures B9 and B10 for Biofilters 2 and 3, respectively, are once again given in Appendix B.

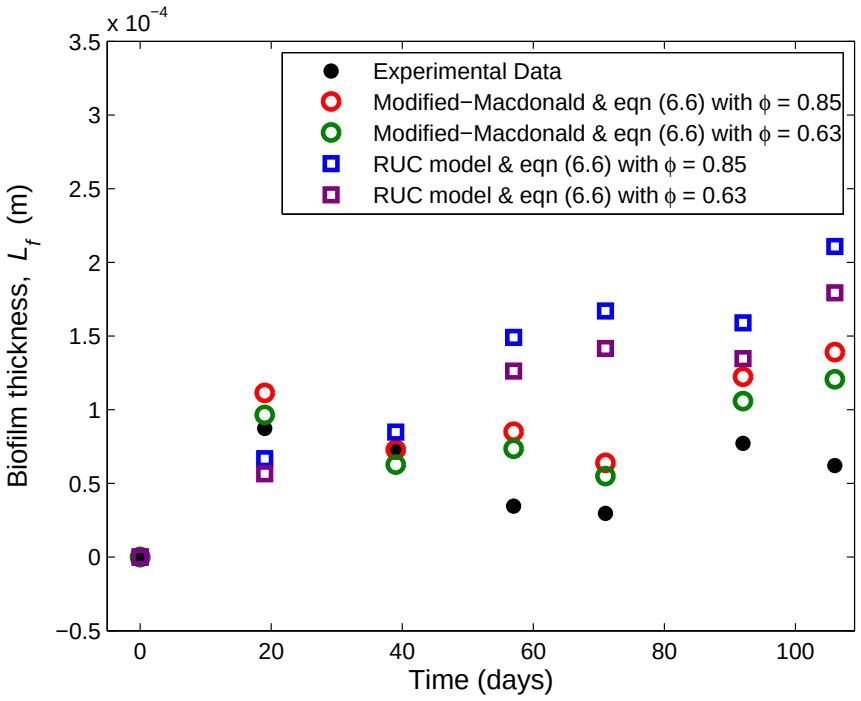

Figure 6.25. Biofilter 1: Comparison between optimized L_f-values for $\phi = 0.85$ and $\phi = 0.63$.

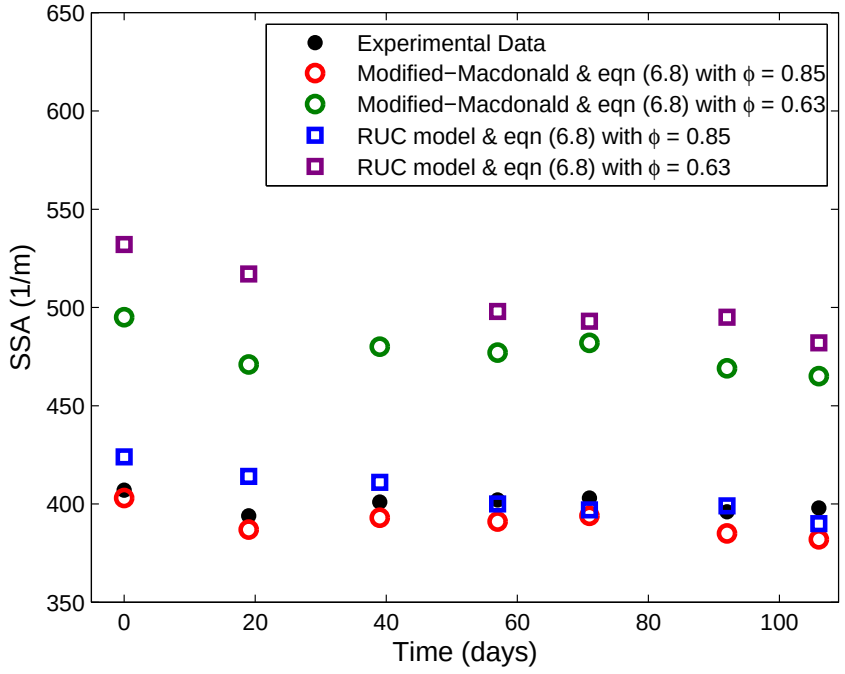

Figure 6.26. Biofilter 1: Comparison between optimized SSA values for $\phi = 0.85$ and $\phi = 0.63$.

From Figures 6.26, B9 and B10 it is clear that when the sphericity was optimized with the RUC model, the SSA results obtained from both the Modified-Macdonald equation and the RUC model over-predict the experimental data. The latter phenomenon is a result of the decreasing ϕ-value in the denominator of the terms in which it appear in equation (6.8) which leads to an increase in SSA.

Taking the overall performance into account, the Modified-Macdonald equation with $\phi = 0.85$ yields the most accurate results when considering ε_f, a_f and τ in all three biofilters. When $\phi = 0.63$, the more accurate L_f-results for Biofilter 1 were obtained with the Modified-Macdonald equation. Considering the RUC model, the ε_f- and τ-results were more accurate for all three biofilters when $\phi = 0.63$ than when $\phi = 0.85$. The same holds for the L_f-results for Biofilters 1 and 3. When referring to the a_f-values obtained with the RUC model, the results were more accurate for all three biofilters when $\phi = 0.85$ than when $\phi = 0.63$. According to equations (6.6) and (6.8), when the ϕ-value decreases, a_f increases and L_f decreases. Considering, for example, the L_f-values shown by Figures 6.25 and B8, the observation was made that the experimental L_f results were over-predicted with the RUC model when $\phi = 0.85$. Therefore, decreasing the value of ϕ will result in more accurate L_f-values, when compared to the experimental data. However, from Figures 6.26, B9 and B10, the results obtained from the RUC model with $\phi = 0.85$ are acceptable. Therefore, decreasing the value of ϕ will result in the RUC model obtaining less accurate a_f-values that will over-predict the experimental data in Biofilters 1 and 2. The most probable cause of the overall results of the sensitivity analysis being in favour of the Modified-Macdonald equation (despite which model is used to optimize ϕ), may be due to the fact that Solver obtains more accurate results when two variables (rather than one or three) are optimized at once, as mentioned in Section 6.1. Even though the results obtained from the RUC model are less accurate (even when $\phi = 0.63$) than those obtained from the Modified-Macdonald equation, a major advantage of using the RUC model is the fact that it is justifiable from a physical point of view, and can be used to predict the pressure drop and SSA in a biofilter over time without the necessity to follow an empirical approach [34]. The latter phenomenon will be discussed in the following chapter.

Chapter 7

Analytical Modelling Approach

Woudberg et al. [35] used an analytical modelling approach based on the RUC model. The first step in the analytical procedure is to predict the biofilm thickness. Thereafter the SSA will be determined in order to calculate the pressure drop over the three biofilters. Similar to the study by Van Jaarsveld and Woudberg [34], a comparison will be made between the results obtained from the empirical modelling approach (discussed in Chapter 6) with that obtained from the analytical modelling approach. Thereafter, an alternative approach for predicting the SSA will be introduced, followed by a sensitivity analysis.

7.1 Predicting the Biofilm Thickness

According to Alonso et al. [5], the packing solids that were in contact prior to the presence of biofilm growth, will remain in contact during the entire course of biofilter operation. Therefore, the biofilm growth will take place in the remaining empty spaces between the solids.

A schematic representation of the packing material covered in biofilm growth is shown in Figure 7.1. The variable, A_L, is defined as the biofilm surface area lost with each point of contact and U_L the biofilm volume lost with each point of contact. Both A_L and U_L can be expressed in terms of the particle radius, R, and the biofilm thickness, L_f.

The first step towards deriving equation (6.4), which was used to calculate the biofilm thickness, is to express the biofilm affected porosity in terms of the total bed volume, U_o, and the volume

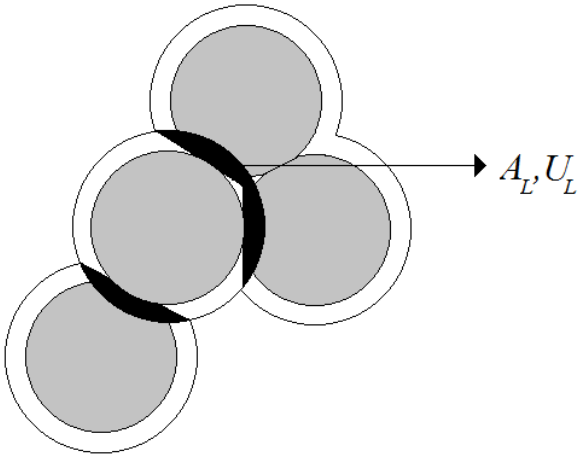

Figure 7.1. Schematic representation of the packing material covered in biofilm [5].

of the solids covered in biofilm, $(U_s)_b$, i.e.,

$$\begin{aligned} \varepsilon_f &= \frac{(U_o) - (U_s)_b}{U_o} \\ &= 1 - \frac{(U_s)_b}{U_o}, \end{aligned} \tag{7.1}$$

which can be written in terms of R, L_f and U_L, i.e.,

$$\begin{aligned} \varepsilon_f &= 1 - \frac{\frac{4}{3}\pi(R+L_f)^3 - nU_L}{U_o} \\ &= 1 - \frac{\frac{4}{3}\pi(R+L_f)^3 - nU_L}{U_o}\frac{(U_s)_o}{(U_s)_o}, \end{aligned} \tag{7.2}$$

where $(U_s)_o$ is the total volume of solids without biofilm. Subsequently, ε_f can be written as

$$\begin{aligned} \varepsilon_f &= 1 - \frac{\frac{4}{3}\pi(R+L_f)^3 - nU_L}{(U_s)_o}(1-\varepsilon_o) \\ &= 1 - \frac{\frac{4}{3}\pi(R+L_f)^3 - nU_L}{\frac{4}{3}\pi R^3}(1-\varepsilon_o) \\ &= 1 - (1-\varepsilon_o)\left[\left(1+\frac{L_f}{R}\right)^3 - \frac{nU_L}{\frac{4}{3}\pi R^3}\right]. \end{aligned} \tag{7.3}$$

In order to determine U_L one has to integrate over the section of the solid (assumed to be a sphere) covered in biofilm, which is shown in Figures 7.2 and 7.3. This section lies between the radius, r, of the solid including the biofilm and the height (not covered in biofilm), $r-h$. From

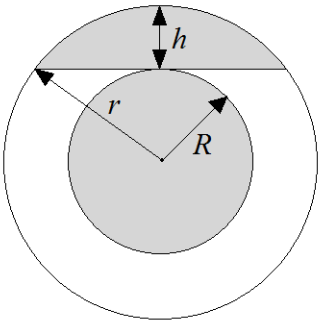

Figure 7.2. Schematic 2D representation of the solid covered in biofilm.

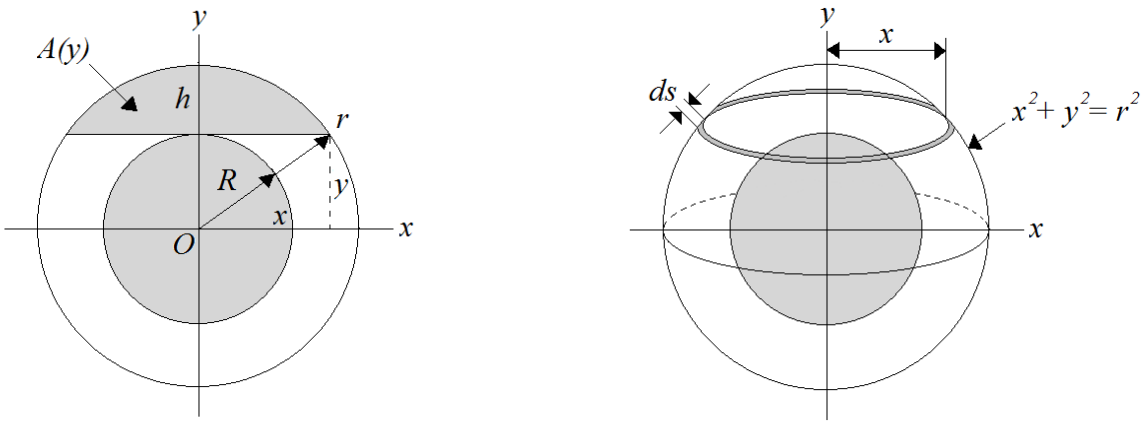

(a) (b)

Figure 7.3. 2D and 3D representation of the solid containing biofilm.

Figure 7.3 if follows that $A = \pi x^2$. Since $r^2 = x^2 + y^2$, $A(y) = \pi(r^2 - y^2)$. Recall that the solid with biofilm is still assumed to be a sphere of radius r, therefore $r - h \leq y \leq r$. The next step is to integrate over the boundaries of the spherical cap $r - h$ and r, i.e.,

$$\begin{aligned} U_L &= \int_{r-h}^{r} \pi(r^2 - y^2)dy \\ &= \pi \left[r^2 y - \frac{1}{3} y^3 \right]_{r-h}^{r} \\ &= \pi h^2 \left(r - \frac{h}{3} \right). \end{aligned} \tag{7.4}$$

Let $r = R + L_f$ and $h = L_f$, then U_L can be written as follows:

$$\begin{aligned} U_L &= \pi L_f^2 \left(R + L_f - \frac{1}{3} L_f \right) \\ &= \pi L_f^2 \left(R + \frac{2}{3} L_f \right). \end{aligned} \tag{7.5}$$

After substituting equation (7.5) into equation (7.3), ε_f can be rewritten and expressed as

$$\begin{aligned} \varepsilon_f &= 1 - (1 - \varepsilon_o) \left[\left(1 + \frac{L_f}{R} \right)^3 - \frac{n \phi L_f^2 \left(R + \frac{2}{3} L_f \right)}{\frac{4}{3} \pi R^3} \right] \\ &= 1 - (1 - \varepsilon_o) \left[\left(1 + \frac{L_f}{R} \right)^3 - \frac{n}{4} \left(\frac{L_f}{R} \right)^2 \left(3 + \frac{2 L_f}{R} \right) \right], \end{aligned} \tag{7.6}$$

which, after introducing ϕ into the $\frac{L_f}{R}$-ratio, yields equation (6.6) (given in Chapter 6) with $D_p = 2R$, i.e.,

$$\varepsilon_f = 1 - (1 - \varepsilon_o) \left[\left(1 + \frac{L_f}{\phi R} \right)^3 - \frac{n}{4} \left(\frac{L_f}{\phi R} \right)^2 \left(2 \frac{L_f}{\phi R} + 3 \right) \right]. \tag{7.7}$$

The first step in order to predict the biofilm thickness, is to solve for $x = \frac{L_f}{\phi R}$, by writing equation (7.7) as a third degree polynomial in x:

$$\begin{aligned} \varepsilon_f &= 1 - (1 - \varepsilon_o) \left[(1 + x)^3 - \frac{n}{4} x^2 (2x + 3) \right] \\ &= 1 - (1 - \varepsilon_o) \left[\left(1 - \frac{n}{2} \right) x^3 + \left(3 - \frac{3n}{4} \right) x^2 + 3x + 1 \right]. \end{aligned} \tag{7.8}$$

Rearranging the terms of equation (7.8) leads to

$$(1 - \varepsilon_o) \left[\left(1 - \frac{n}{2} \right) x^3 + \left(3 - \frac{3n}{4} \right) x^2 + 3x + 1 \right] = 1 - \varepsilon_f. \tag{7.9}$$

Equation (7.9) can then be expressed as the following polynomial:

$$a x^3 + b x^2 + c x + d = 0,$$

with

$$a = (1 - \varepsilon_o) \left(1 - \frac{n}{2} \right); \; b = (1 - \varepsilon_o) \left(3 - \frac{3n}{4} \right); \; c = 3(1 - \varepsilon_o) \text{ and } d = \varepsilon_f - \varepsilon_o.$$

Recall from Section 6.5 that the value of n needs to be determined with equation (6.5). Subsequently, a value of 7 was obtained by making use of the measured values of ε_o for Biofilters 1, 2 and 3.

In order to compare the present analytical modelling approach with the empirical modelling approach presented in Chapter 6, the value to be used for ϕ will be 0.85. The calculated values for $L_f = \phi Rx$ with $R = D_p/2$, $D_p = 0.01$ and $\phi = 0.85$ are given in Tables 7.1, 7.2 and 7.3 for Biofilters 1, 2 and 3, respectively. Recall that data is missing for Biofilter 2 on day 19 and for Biofilter 3 on day 92, as discussed in Chapter 6. The optimized L_f-values obtained from the empirical approach are also shown in Tables 7.1 to 7.3.

Table 7.1. Biofilter 1: L_f-values for each of the 7 days with $\phi = 0.85$.

Day	$\boldsymbol{L_f}$**(m) from analytical approach**	$\boldsymbol{L_f}$**(m) from empirical approach [4]**
0	0.00	0.00
19	8.73×10^{-5}	1.12×10^{-4}
39	4.45×10^{-5}	7.30×10^{-5}
57	3.46×10^{-5}	8.20×10^{-5}
71	2.96×10^{-5}	6.40×10^{-5}
92	7.72×10^{-5}	1.22×10^{-4}
106	6.21×10^{-5}	1.39×10^{-4}

Table 7.2. Biofilter 2: L_f-values for each of the 7 days with $\phi = 0.85$.

Day	$\boldsymbol{L_f}$**(m) from analytical approach**	$\boldsymbol{L_f}$**(m) from empirical approach [4]**
0	0.00	0.00
39	3.13×10^{-3}	-1.38×10^{-5}
57	2.45×10^{-6}	-1.17×10^{-5}
71	3.12×10^{-3}	-1.00×10^{-5}
92	2.96×10^{-5}	5.15×10^{-5}
106	2.71×10^{-5}	3.52×10^{-5}

Table 7.3. Biofilter 3: L_f-values for each of the 7 days with $\phi = 0.85$.

Day	$\boldsymbol{L_f}$**(m) from analytical approach**	$\boldsymbol{L_f}$**(m) from empirical approach [4]**
0	0.00	0.00
19	3.15×10^{-3}	7.81×10^{-5}
39	2.19×10^{-5}	5.52×10^{-5}
57	2.92×10^{-5}	4.52×10^{-5}
71	3.17×10^{-5}	6.15×10^{-5}
106	3.41×10^{-5}	7.19×10^{-5}

Figures 7.4 to 7.6 show the calculated L_f-values (given in Tables 7.1 to 7.3) versus ε_{exp}-values.

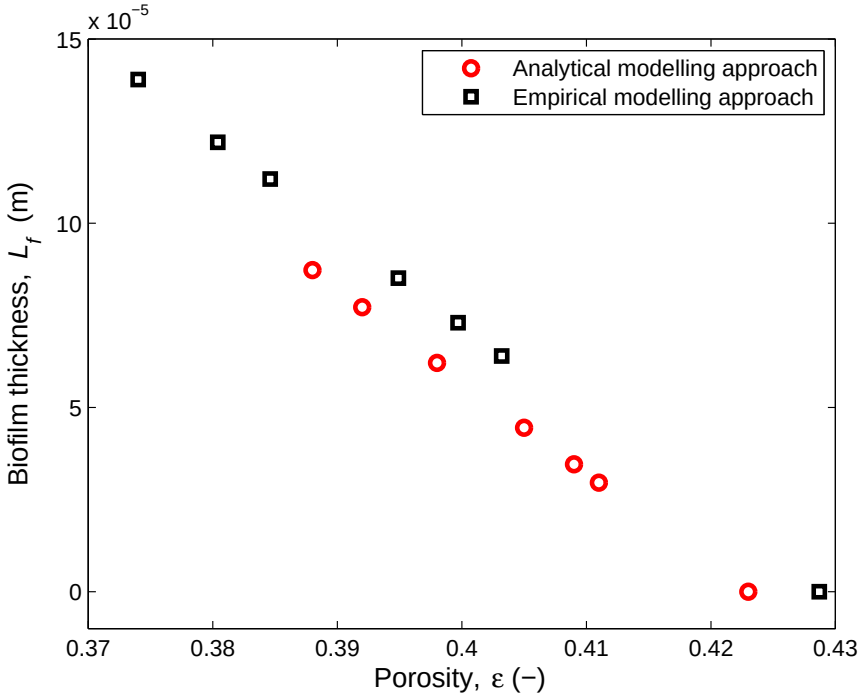

Figure 7.4. Biofilter 1: Biofilm thickness as a function of porosity.

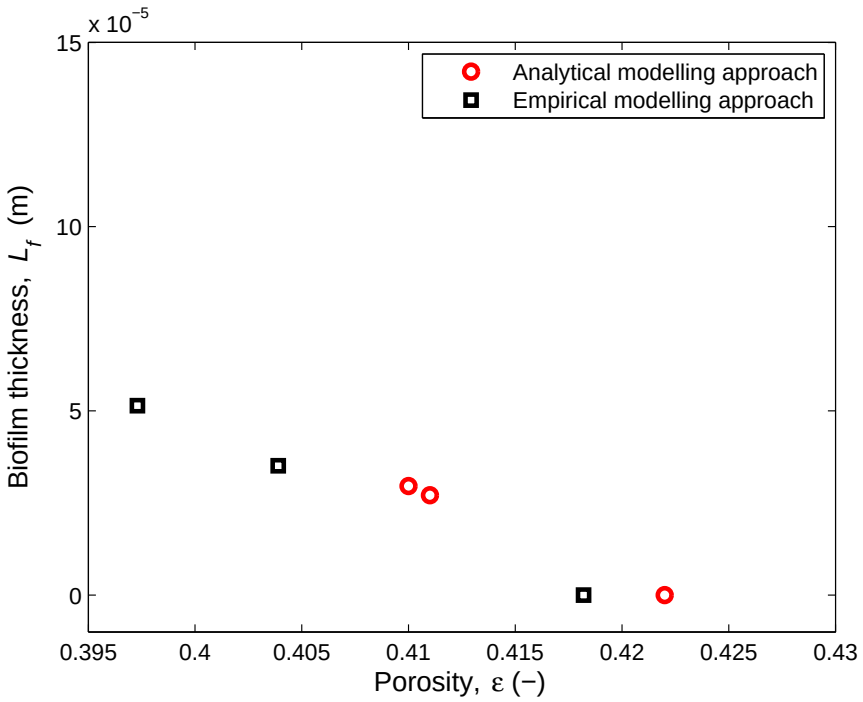

Figure 7.5. Biofilter 2: Biofilm thickness as a function of porosity.

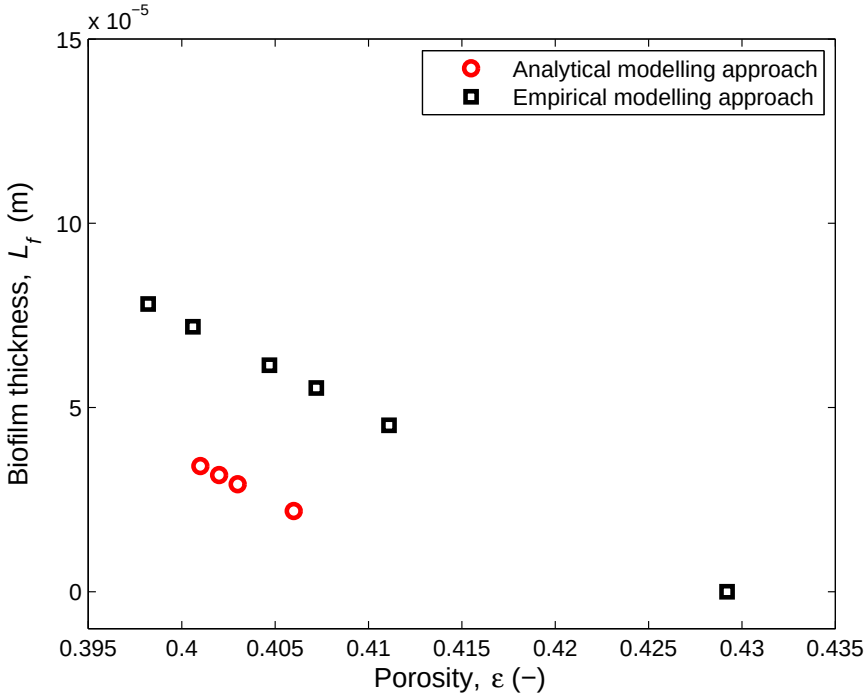

Figure 7.6. Biofilter 3: Biofilm thickness as a function of porosity.

The optimized L_f-values (also given in Tables 7.1, 7.2 and 7.3) versus the optimized ε-values, obtained by Dumont et al. [4] in the empirical approach, are also shown. The L_f-values obtained from both the analytical and empirical approach increase with decrease in porosity.

Unstable (i.e. negative) L_f-values obtained from Dumont et al. [4] for Biofilter 2 on days 39, 57 and 71, as shown in Table 7.2, have been omitted from Figure 7.5, since the biofilm thickness cannot be negative. As discussed in Section 6.6, this might be a result of Excel® Solver not always obtaining the optimal solution. The outlier L_f-value for Biofilter 3 on day 19 at $\varepsilon_f = 0.430$, obtained from equation (7.7) by the analytical method, has been omitted from Figure 7.6 in order to graphically represent the behaviour of the other L_f-values more clearly.

Knowing the biofilm thickness values (obtained from the empirical approach [4]) for the 7 days of the experiment on which data was recorded, equation (7.7) was used in order to determine the biofilm affected porosity which, in turn, was used to calculate the tortuosity on the respective days. The results can be seen in Figures 7.7, 7.8 and 7.9. The latter figures are duplicates of Figures 5.4, 5.5 and 5.6, but with equation (5.4) in which ε is replaced with ε_f, given by equation (7.7), added for the RUC model. Note that the results for $\phi = 1$ serve as a reference for the case in which the sphericity is not included. The value of $\phi = 1$ corresponds to particles that are spheres.

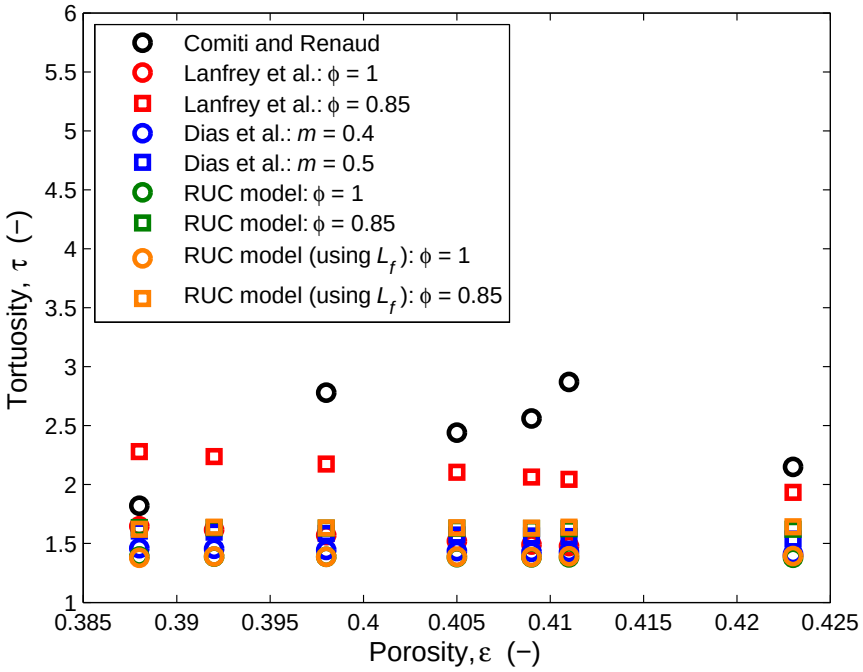

Figure 7.7. Biofilter 1: Tortuosity as a function of porosity.

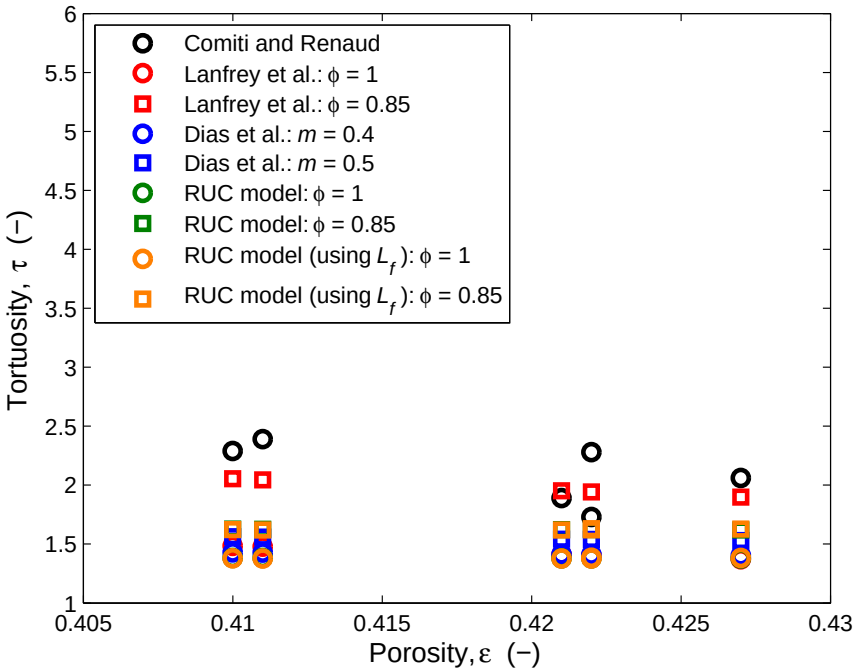

Figure 7.8. Biofilter 2: Tortuosity as a function of porosity.

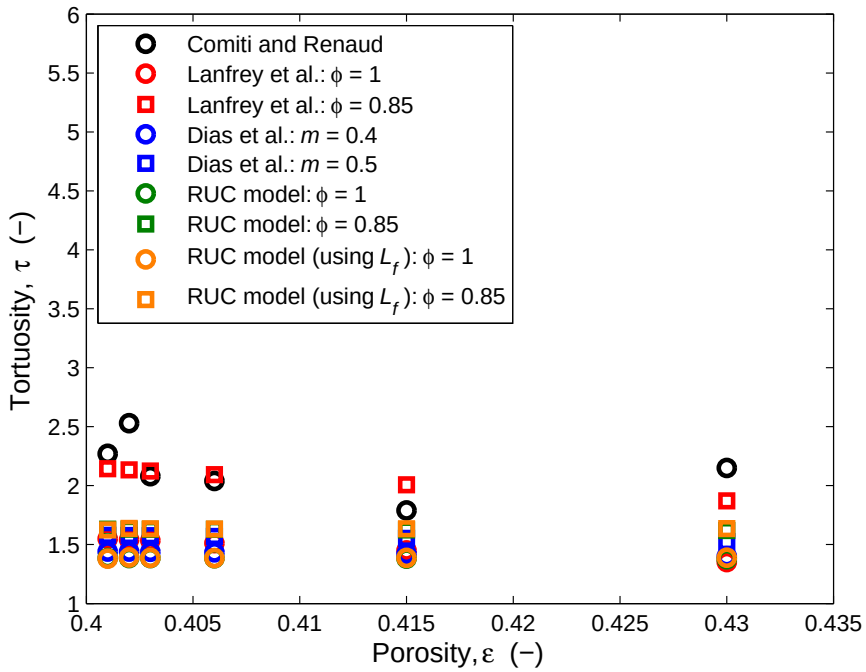

Figure 7.9. Biofilter 3: Tortuosity as a function of porosity.

Figures 7.7, 7.8 and 7.9 show that in both cases ($\phi = 1$ and $\phi = 0.85$) the corresponding value sets obtained from the RUC model are similar, regardless of whether the experimental porosity values or calculated porosity values, using the biofilm thickness, were used to calculate the tortuosity. This is satisfactory, since an alternative manner is presented in which to predict the tortuosity values by making use of the biofilm thickness, should the measured porosity values on each day not be available.

In Section 7.2 the SSA, a_f, will be predicted and compared to the values obtained with the empirical modelling approach.

7.2 Predicting the Specific Surface Area

In order to formulate the equation for a_f (equation (6.8)), one has to find an expression for the biofilm surface area lost, indicated by A_L in Figure 7.1. From Figure 7.3 it follows that

$$A_L = \int dA = 2\pi x ds. \tag{7.10}$$

Recall that $x^2 + y^2 = r^2$, thus $x = (r^2 - y^2)^{1/2}$. Therefore,

$$\frac{dx}{dy} = \frac{1}{2}(r^2 - y^2)^{-1/2}(-2y) = \frac{-y}{\sqrt{r^2 - y^2}} = -\frac{y}{x}. \tag{7.11}$$

The next step is to determine ds. From Figure 7.3(b) it follows that $ds^2 = dx^2 + dy^2$, therefore,

$$\begin{aligned} ds &= \sqrt{dx^2 + dy^2} \\ &= \sqrt{\frac{dy^2}{dy^2}(dx^2 + dy^2)} \\ &= dy\sqrt{1 + \left(\frac{dx}{dy}\right)^2}. \end{aligned} \tag{7.12}$$

From equation (7.11),

$$\begin{aligned} ds &= dy\sqrt{1 + \left(-\frac{y}{x}\right)^2} \\ &= dy\sqrt{\frac{x^2 + y^2}{x^2}} \\ &= \frac{r}{x}dy. \end{aligned} \tag{7.13}$$

The final step in determining an expression for A_L, in terms of L_f, is to integrate between the boundaries, $r - h$ and r, i.e.,

$$\begin{aligned} A_L &= \int_{r-h}^{r} 2\pi x ds \\ &= \int_{r-h}^{r} 2\pi x \left(\frac{r}{x}\right) dy \\ &= 2\pi \Big[ry\Big]_{r-h}^{r} \\ &= 2\pi r h. \end{aligned} \tag{7.14}$$

Recall from Section 7.1 that $r = R + L_f$ and $h = L_f$, i.e.,

$$A_L = 2\pi L_f (R + L_f). \tag{7.15}$$

The biofilm affected SSA can be expressed in terms of the fluid-solid interface covered in biofilm,

$(A_{fs})_b$, and the total bed volume, i.e.,

$$a_f = \frac{(A_{fs})_b}{U_o}. \tag{7.16}$$

The latter equation can be written in terms of R, L_f and A_L i.e.,

$$\begin{aligned} a_f &= \frac{4\pi(R+L_f)^2 - nA_L}{U_o} \\ &= \frac{4\pi(R+L_f)^2 - nA_L}{U_o}\frac{(U_s)_o}{(U_s)_o} \\ &= \frac{4\pi(R+L_f)^2 - nA_L}{\frac{4}{3}\pi R^3}(1-\varepsilon_o) \\ &= 3(1-\varepsilon_o)\left[\frac{4\pi(R^2+2RL_f+L_f^2) - nA_L}{4\pi R^3}\right] \\ &= \frac{3(1-\varepsilon_o)}{2R}\left[2 + 4\frac{L_f}{R} + 2\frac{L_f^2}{R^2} - \frac{nA_L}{2\pi R^2}\right]. \end{aligned} \tag{7.17}$$

After substituting equation (7.15) into equation (7.17), it follows that

$$\begin{aligned} a_f &= \frac{3(1-\varepsilon_o)}{2R}\left[2 + 4\frac{L_f}{R} + 2\frac{L_f^2}{R^2} - \frac{2n\pi L_f(R+L_f)}{2\pi R^2}\right] \\ &= \frac{3(1-\varepsilon_o)}{2R}\left[2 + 4\frac{L_f}{R} + 2\frac{L_f^2}{R^2} - \frac{nL_f}{R} - \frac{nL_f^2}{R^2}\right] \\ &= \frac{3(1-\varepsilon_o)}{2R}\left[2 + \frac{L_f}{R}(4-n) + \frac{L_f^2}{R^2}(2-n)\right] \\ &= \frac{3(1-\varepsilon_o)}{2R}\left[\frac{L_f}{R}\left(2 + \frac{L_f}{R}(2-n)\right) + \left(2 + \frac{L_f}{R}(2-n)\right)\right]. \end{aligned} \tag{7.18}$$

The sphericity can be introduced into the $\frac{L_f}{R}$-ratio which leads to equation (6.8), presented in Chapter 6, i.e.,

$$a_f = \frac{a_o}{2}\left(1 + \frac{2L_f}{\phi D_p}\right)\left(\frac{2L_f}{\phi D_p}(2-n) + 2\right). \tag{7.19}$$

Subsequently, the biofilm affected SSA for each day of the experiment can be calculated, as presented in Tables 7.4 to 7.6, using equation (7.19), since the corresponding L_f-values are known.

In Tables 7.4, 7.5 and 7.6 the SSA values are presented. The SSA for day 0, a_o, was calculated with equation (6.7) (also shown in Table 6.7) and the remaining values for the other days, using

Table 7.4. Biofilter 1: SSA values for each of the 7 days with $\phi = 0.85$.

Day	$a_f(\mathrm{m}^{-1})$ **from analytical approach**	$a_f(\mathrm{m}^{-1})$ **from empirical approach [4]**
0	407	403
19	394	387
39	401	393
57	402	391
71	403	394
92	396	385
106	398	382

Table 7.5. Biofilter 2: SSA values for each of the 7 days with $\phi = 0.85$.

Day	$a_f(\mathrm{m}^{-1})$ **from analytical approach**	$a_f(\mathrm{m}^{-1})$ **from empirical approach [4]**
0	408	411
39	–	413
57	408	412
71	–	412
92	404	403
106	404	405

Table 7.6. Biofilter 3: SSA values for each of the 7 days with $\phi = 0.85$.

Day	$a_f(\mathrm{m}^{-1})$ **from analytical approach**	$a_f(\mathrm{m}^{-1})$ **from empirical approach [4]**
0	413	403
19	–	391
39	410	395
57	409	396
71	408	394
106	408	392

the analytical approach together with the ε_{exp}- and L_f-values (shown in Tables 7.1, 7.2 and 7.3), were calculated with equation (7.19). It is important to note that when the ε_f-value for a specific day on which data was recorded is higher than ε_o, in the analytical approach, the results obtained were unrealistic negative values for a_f and were therefore disregarded. This was the case for days 39 and 71 for Biofilter 2 and day 19 in the case of Biofilter 3. Also shown in Tables 7.4 to 7.6 are the a_f-values obtained from the empirical approach in which equation (7.19) was also used together with the optimized ε- and L_f-values, resulting from the Modified-Macdonald equation.

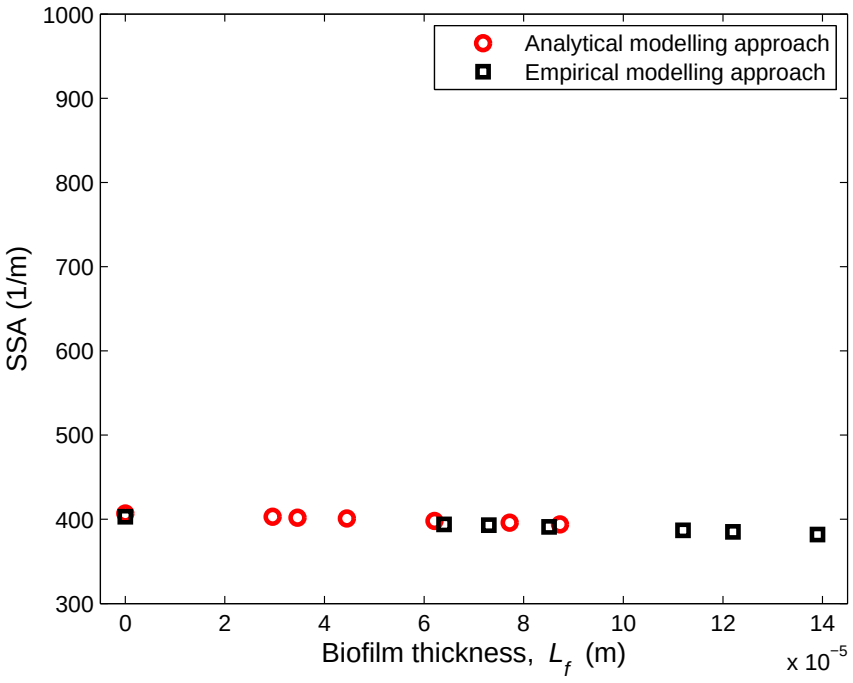

Figure 7.10. Biofilter 1: SSA as a function of biofilm thickness.

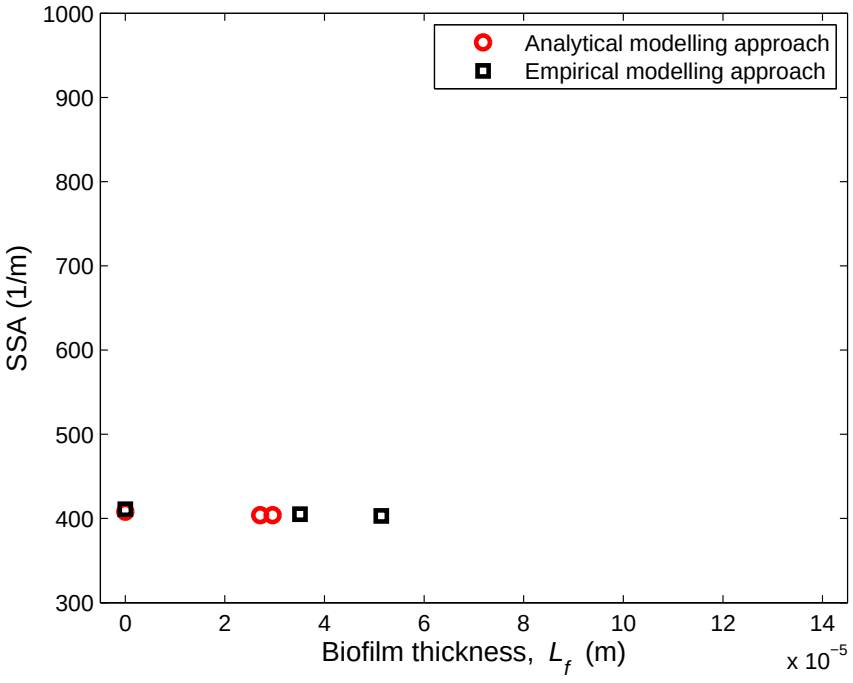

Figure 7.11. Biofilter 2: SSA as a function of biofilm thickness.

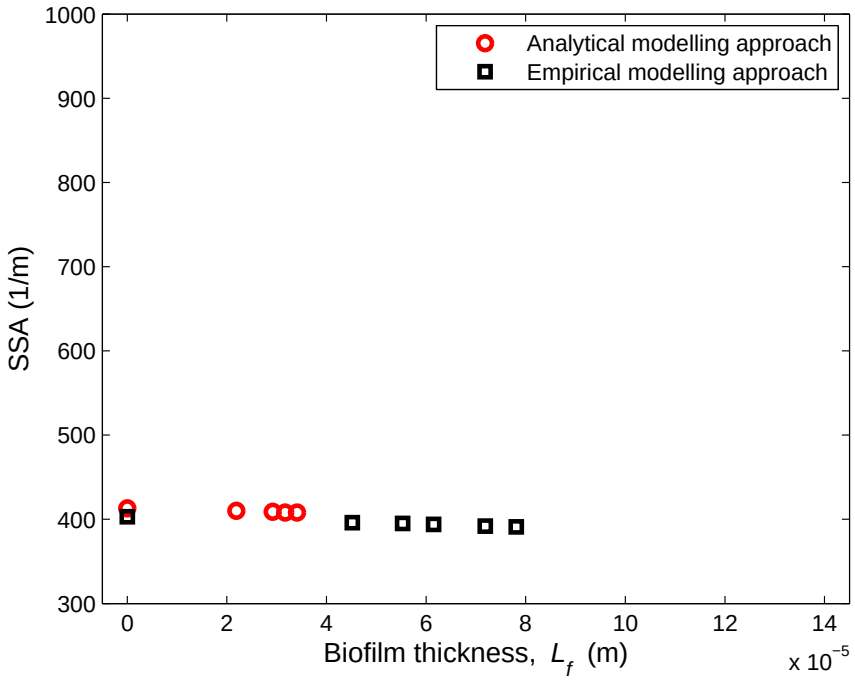

Figure 7.12. Biofilter 3: SSA as a function of biofilm thickness.

Considering the SSA values obtained from equation (7.19), Figures 7.10, 7.11 and 7.12 show that the biofilm affected SSA remains more or less constant with an increase in biofilm thickness (refer to Tables 7.4, 7.5 and 7.6). The same holds for the values obtained from the empirical modelling approach. This is due to the large order of magnitude difference between the terms containing L_f in equation (7.19), as well as the terms excluding L_f. Note that unstable L_f-values obtained from Dumont et al. [4] for Biofilter 2 on days 39, 57 and 71, as shown in Table 7.2, have been omitted from Figure 7.11, since the biofilm thickness cannot be negative.

In the following section the biofilm affected SSA, a_f, and the adapted RUC model will be used in order to predict the pressure gradient.

7.3 Pressure Drop Prediction

Replacing D_p with d_s in equation (6.7) and replacing ϕd_s with $\frac{6}{a_o}(1-\varepsilon_o)$ in the RUC model (equation (3.23)), as well as ε with ε_f, yields

$$-\frac{1}{q}\frac{dp}{dx} = \frac{25.4(1-\varepsilon_f)^{4/3}\mu a_o^2}{(36(1-\varepsilon_o)^2(1-(1-\varepsilon_f)^{1/3})(1-(1-\varepsilon_f)^{2/3})^2} + \frac{\beta(1-\varepsilon_f)c_d\rho q a_o}{12\varepsilon_f(1-\varepsilon_o)(1-(1-\varepsilon_f)^{2/3})^2}. \tag{7.20}$$

In order to calculate the pressure drop over a period of 110 days, the known a_f-values, calculated with the analytical approach (refer to Tables 7.4, 7.5 and 7.6), will be used. The initial SSA can be expressed in terms of a_f by making use of equation (7.19), yielding

$$a_o = \frac{2a_f}{\left(1+\frac{L_f}{\phi R}\right)\left((2-n)\frac{L_f}{\phi R}+2\right)}. \tag{7.21}$$

Therefore, equation (7.20) can now be written as

$$\begin{aligned} -\frac{1}{q}\frac{dp}{dx} &= \frac{25.4(1-\varepsilon_f)^{4/3}\mu a_f^2}{(9(1-\varepsilon_o)^2(1-(1-\varepsilon_f)^{1/3})(1-(1-\varepsilon_f)^{2/3})^2}\left[\left(1+\frac{L_f}{\phi R}\right)\left((2-n)\frac{L_f}{\phi R}+2\right)\right]^{-2} \\ &+ \frac{\beta(1-\varepsilon_f)c_d\rho q a_f}{6\varepsilon_f(1-\varepsilon_o)(1-(1-\varepsilon_f)^{2/3})^2}\left[\left(1+\frac{L_f}{\phi R}\right)\left((2-n)\frac{L_f}{\phi R}+2\right)\right]^{-1}, \end{aligned} \tag{7.22}$$

and will henceforth be known as the adapted RUC model.

From Figures 4.4 to 4.6 it is clear that the pressure drop increases over time as a result of biofilm growth. However, compared to the average radius of a schist particle, the average biofilm thickness is significantly small, i.e. 0.96%, 0.30% and 0.47% for Biofilters 1, 2 and 3, respectively. The ε-values fall in the range $0.388-0.423$ for Biofilter 1, $0.410-0.427$ for Biofilter 2 and $0.401-0.430$ for Biofilter 3, which is a considerably small change. The change in SSA values is also small and falls in the respective ranges $394-407$, $404-408$ and $408-418$ 1/m for Biofilters 1, 2 and 3. In addition, the tortuosity values also remained more or less constant over the entire time of biofilter operation. According to an assumption made by Dumont et al. [4], the changes over time in pressure drops are therefore related to the changes over time in particle roughness as a result of the biofilm development. The adjustment and optimizing of the roughness coefficient, B, is what made the Modified-Macdonald equation to predict the pressure gradient so satisfactory. The RUC model, however, under-predicted the pressure gradient over the entire experiment. In the case of the RUC model the significant change in pressure drop will be attributed to the change in the ϕ-value over time as a result of biofilm developing and covering more than one particle (as illustrated in Figure 7.1 for four particles), instead of only one spherical particle, as assumed by

Dumont et al. [4]. It is therefore important to analytically determine the sphericity as a function of L_f in order to confirm whether or not it will be able to compensate for the under-prediction of the RUC model, as observed in Chapter 5.

7.4 Calculating the Sphericity of a Cluster of Spheres

According to equation (2.8) the sphericity is a function of U_p and S_p. Also note that $n = 7$ means that there are 7 spheres in contact with a single sphere. In this section, the sphericity of such a cluster (consisting of 8 spheres, including biofilm) with volume, U_p, and outer surface area, S_p, will be calculated.

Recall from Section 7.1 that $r = R + L_f$. The first step is to calculate the volume of the cluster of spheres (including biofilm), U_p, i.e.,

$$U_p = \frac{4}{3}\pi\left(R + L_f\right)^3 + \frac{4}{3}\pi n(R + L_f)^3 - 2\pi n L_f^2\left(R + \frac{2}{3}L_f\right), \tag{7.23}$$

which, after rewriting and rearranging the terms, can be expressed as

$$U_p = \frac{4}{3}\pi\left(R + L_f\right)^3 + \frac{4}{3}\pi n R^3 + 4\pi n L_f R^2 + 2\pi n L_f^2 R. \tag{7.24}$$

Secondly, the outer surface area of the cluster of spheres, S_p, can also be expressed in terms of R and L_f, i.e.,

$$S_p = 4\pi\left(R + L_f\right)^2 + 4\pi n\left(R + L_f\right)^2 - 2n\left(R + L_f\right)2\pi L_f, \tag{7.25}$$

and after rewriting and rearranging the terms of the latter equation, S_p can finally be written as

$$S_p = 4\pi\left(R + L_f\right)^2 + 4\pi n R^2 + 4\pi n L_f R. \tag{7.26}$$

The next step in finding the average ϕ-value is to substitute equations (7.24) and (7.26) into equation (2.8), which yields

$$\phi = \frac{\pi^{1/3}\left(8\pi\left(R + L_f\right)^3 + 8\pi n R^3 + 24\pi n L_f R^2 + 12\pi n L_f^2 R\right)^{2/3}}{4\pi\left(R + L_f\right)^2 + 4\pi n R^2 + 4\pi n L_f R}. \tag{7.27}$$

Due to the small variation in ε_f-values in equation (6.6) the L_f-values vary little over time. Therefore, there is also little variation in the analytically determined ϕ-values. Thus, the decision was made to calculate an average sphericity value, rather than different ϕ-values for the respective

days of biofilter operation. However, if the RUC model were to be applied to data with a greater variation in ε_f-values, resulting in a greater variation in L_f-values, a value of ϕ, applicable to each respective day of biofilter operation may be preferable to work with, rather than an average value. After taking the averages of the L_f-values (given in Tables 7.1, 7.2 and 7.3) obtained from the empirical approach for the three respective biofilters and substituting the known values for n and R into equation (7.27), it was found that the average sphericity values for Biofilters 1, 2 and 3 are 0.50, 0.57 and 0.53, respectively. The objective of this study (given the experimental data provided) is to use the analytically determined average ϕ-value as a lower limit and the empirically determined ϕ-value, i.e. $\phi = 0.85$, as an upper limit in order to indicate the significance of the effect of this variable on the predictions. Since the analytically determined average ϕ-values are lower than the $\phi = 0.63$ value determined through optimization with the RUC model (refer to Section 6.7), the former was used as a lower limit. In order to avoid using the sphericity as a fitting parameter, such as in the empirical modelling approach, the idea in the analytical approach is not to calculate ϕ-values in order for the RUC model to accurately fit the experimental pressure drop data. Even though this will result in predictions that satisfactorily correspond with the experimental data, the aim is for the RUC model to remain purely analytical and to only investigate the influence of the two limiting ϕ-values on the pressure drop prediction.

7.5 Results for Calculating the Pressure Gradient

The pressure gradient predicted for day 39 for all three biofilters with the Modified-Macdonald equation (equation (3.5)) and the adapted RUC model (equation (7.22)) including the two ϕ-

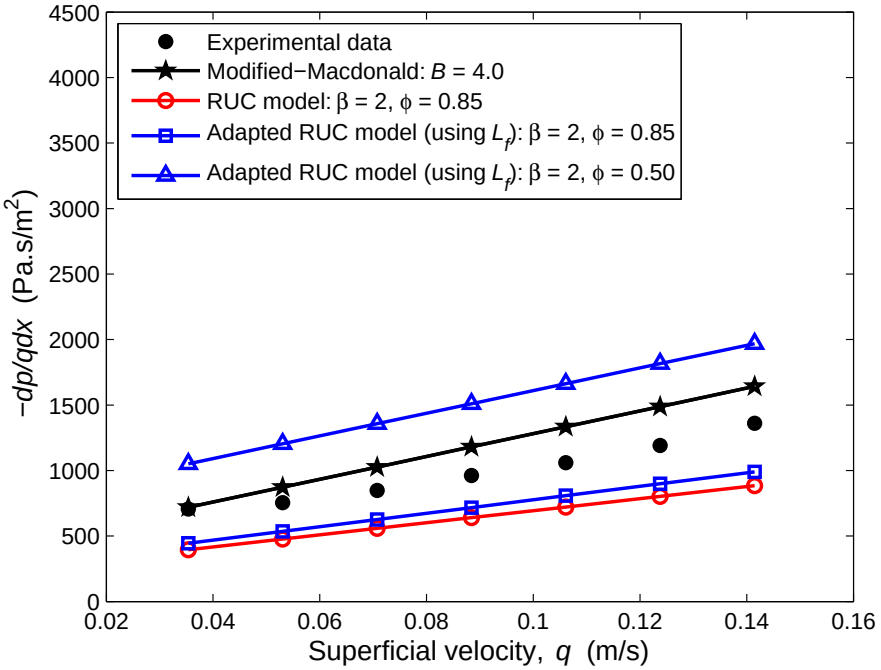

Figure 7.13. Biofilter 1: Adapted RUC vs Modified-Macdonald equation for day 39.

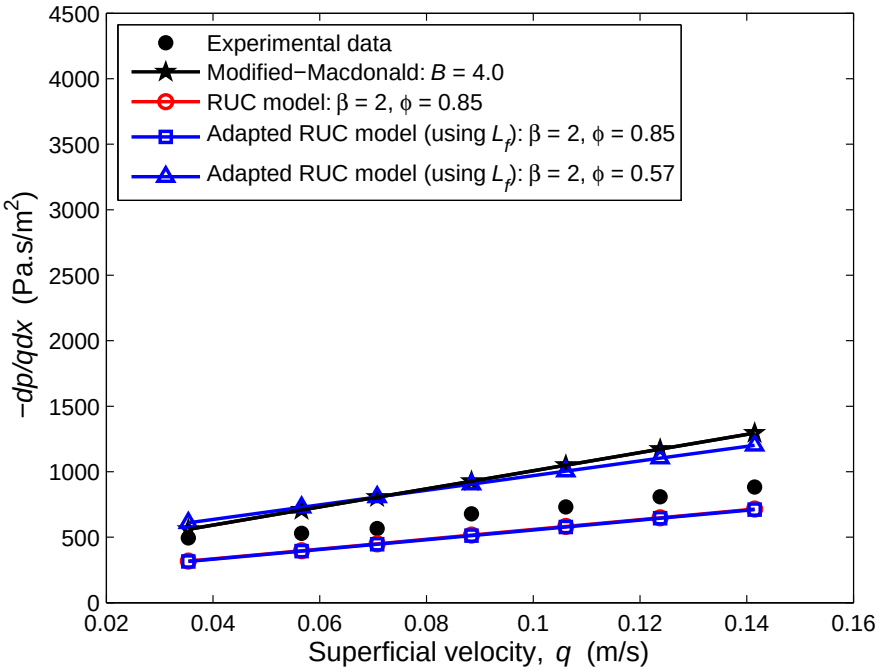

Figure 7.14. Biofilter 2: Adapted RUC vs Modified-Macdonald equation for day 39.

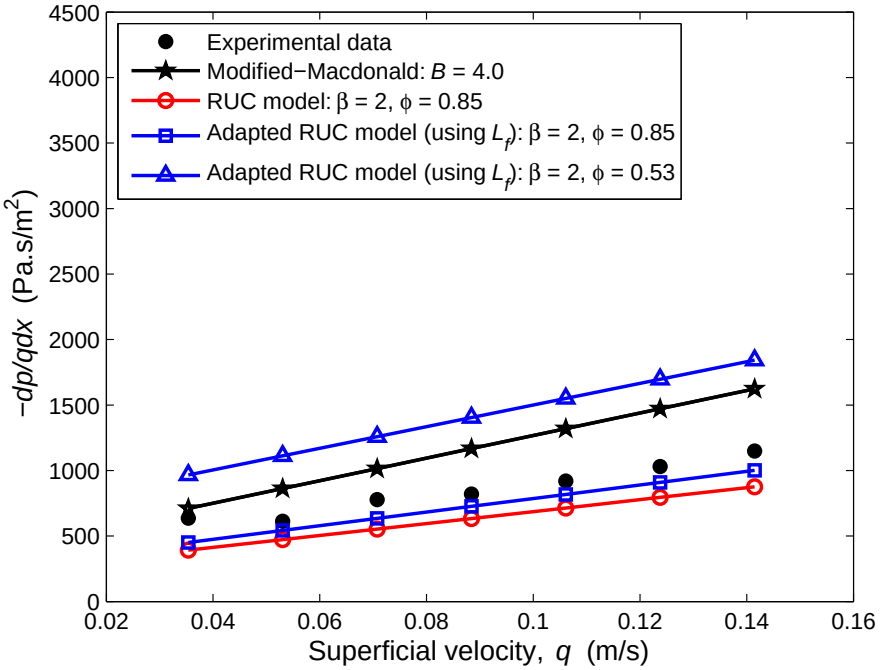

Figure 7.15. Biofilter 3: Adapted RUC vs Modified-Macdonald equation for day 39.

values, are compared to the experimental pressure drop data in Figures 7.13, 7.14 and 7.15 (results for days 19, 57, 71, 92 and 106 are presented in Appendix C).

The Modified-Macdonald equation (with $B = 4.0$) generally provides accurate predictions. The adapted RUC model using L_f and the two ϕ-values capture the experimental data in between which is a desired result. The over- and under-prediction of the adapted RUC model, when using the two different ϕ-values, illustrates the significant effect of the value used for ϕ in the model predictions. Due to the relatively small variation in biofilm growth, the RUC model (without the use of L_f-values) and the adapted RUC model (with the use of L_f-values) obtain relatively similar results throughout the entire period of biofilter operation (when the same ϕ-value of 0.85 is used).

In Section 7.6 an alternative approach is presented for predicting the SSA values, should the experimental pressure gradient and superficial velocity values be available.

7.6 Alternative Approach for Predicting the Specific Surface Area

In order to be able to use the alternative approach for calculating the SSA, the experimental pressure gradient and superficial velocity values should be known.

Rewriting equation (7.22) by setting the sum of all the terms equal to zero, leads to

$$f a_f^2 + g a_f + h = 0, \tag{7.28}$$

where

$$\begin{aligned} f &= \frac{25.4(1-\varepsilon_f)^{4/3}\mu}{(9(1-\varepsilon_o)^2(1-(1-\varepsilon_f)^{1/3})(1-(1-\varepsilon_f)^{2/3})^2}\left[\left(1+\frac{L_f}{\phi R}\right)\left((2-n)\frac{L_f}{\phi R}+2\right)\right]^{-2}, \\ g &= \frac{\beta(1-\varepsilon_f)c_d\rho q}{6\varepsilon_f(1-\varepsilon_o)(1-(1-\varepsilon_f)^{2/3})^2}\left[\left(1+\frac{L_f}{\phi R}\right)\left((2-n)\frac{L_f}{\phi R}+2\right)\right]^{-1}, \end{aligned} \tag{7.29}$$

and

$$h = -\left(-\frac{1}{q}\frac{dp}{dx}\right). \tag{7.30}$$

After solving the roots of equation (7.28) in Matlab®, only the positive values are retained for a_f. The latter values, corresponding to the seven different superficial velocity values and accompanying pressure drop values measured for each day are presented in Tables 7.7, 7.8 and 7.9.

Table 7.7. Biofilter 1: SSA values calculated with the RUC model.

Day	$\boldsymbol{a_f}(\mathrm{m^{-1}})$						
19	519	478	457	440	451	447	427
39	575	544	538	540	536	544	563
57	626	665	670	674	701	712	705
71	634	694	639	744	758	766	767
92	640	604	601	572	613	632	657
106	695	717	735	767	757	781	807

Table 7.8. Biofilter 2: SSA values calculated with the RUC model.

Day	a_f(m^{-1})						
39	1212	1406	1551	1791	1983	2194	2405
57	520	505	520	508	510	509	500
71	1242	1444	1624	1867	2091	2281	2494
92	632	533	576	585	595	589	594
106	601	558	580	579	599	587	605

Table 7.9. Biofilter 3: SSA values calculated with the RUC model.

Day	a_f(m^{-1})						
19	1393	1588	1758	1986	2189	2419	2642
39	555	490	522	497	498	503	510
57	506	547	541	531	548	533	538
71	575	606	609	623	632	640	645
106	571	602	631	638	650	634	645

Tables 7.10 to 7.12 give the average a_f-values calculated for each day. For direct comparison with the results from the empirical approach the value of ϕ used in equations (7.28) to (7.30) is 0.85. After comparing the corresponding values obtained with the analytical approach, presented in Tables 7.4 to 7.6, it is found that both methods for calculating the SSA are adequate, especially since the value sets are of the same order of magnitude and corresponds well to the values obtained from the empirical approach. Recall from Section 7.2 that when the ε_f-value for a specific day on which data was recorded is higher than ε_o, the results obtained are negative and therefore disregarded. These results can be seen in Tables 7.10, 7.11 and 7.12 where values are omitted.

Table 7.10. Biofilter 1: Comparison of SSA values for each day with $\phi = 0.85$.

Day	**Porosity,** ε_{exp}	L_f(m)	a_f(m^{-1}) (**from** L_f)	a_f(m^{-1})(from $-\frac{1}{q}\frac{dp}{dx}$)
0	0.423	0.00	407	407
19	0.388	8.73×10^{-5}	394	460
39	0.405	4.45×10^{-5}	401	548
57	0.409	3.46×10^{-5}	402	679
71	0.411	2.96×10^{-5}	403	722
92	0.392	7.72×10^{-5}	396	617
106	0.398	6.21×10^{-5}	398	751

Table 7.11. Biofilter 2: Comparison of SSA values for each day with $\phi = 0.85$.

Day	**Porosity,** ε_{exp}	L_f(m)	a_f(m^{-1}) (**from** L_f)	a_f(m^{-1})(from $-\frac{1}{q}\frac{dp}{dx}$)
0	0.422	0.00	408	408
39	0.427	3.13×10^{-3}	–	1791
57	0.421	2.45×10^{-6}	408	510
71	0.422	3.12×10^{-3}	–	1863
92	0.410	2.96×10^{-5}	404	586
106	0.411	2.71×10^{-5}	404	587

Table 7.12. Biofilter 3: Comparison of SSA values for each day with $\phi = 0.85$.

Day	**Porosity,** ε_{exp}	L_f(m)	a_f(m^{-1}) (**from** L_f)	a_f(m^{-1})(from $-\frac{1}{q}\frac{dp}{dx}$)
0	0.415	0.00	413	413
19	0.430	3.15×10^{-3}	–	1996
39	0.406	2.19×10^{-5}	410	511
57	0.403	2.92×10^{-5}	409	535
71	0.402	3.17×10^{-5}	408	618
106	0.401	3.41×10^{-5}	408	624

Figures 7.16, 7.17 and 7.18 show a comparison between the analytical and empirical modelling approaches for the biofilm affected SSA as a function of biofilm thickness for Biofilters 1, 2 and 3, respectively. Each data point of the analytical model prediction represents the average of the SSA values obtained from the seven different pressure drop measurements (given in the last columns of Tables 7.10 to 7.12).

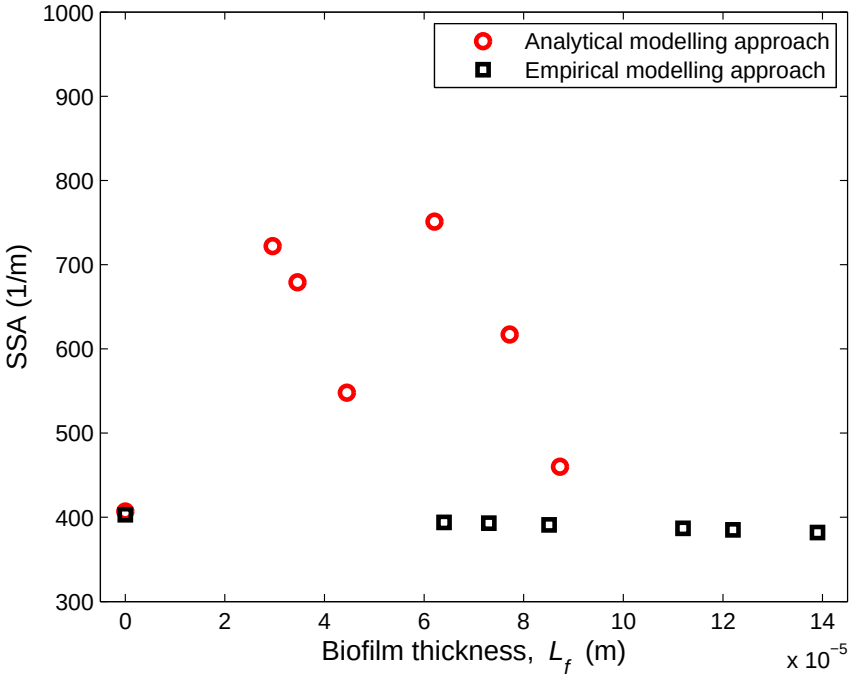

Figure 7.16. Biofilter 1: SSA as a function of biofilm thickness.

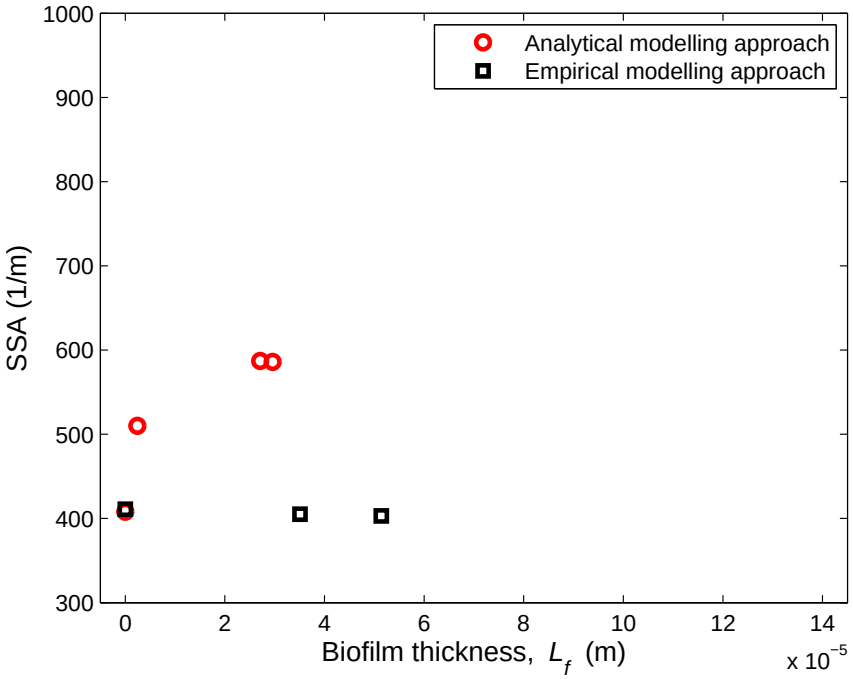

Figure 7.17. Biofilter 2: SSA as a function of biofilm thickness.

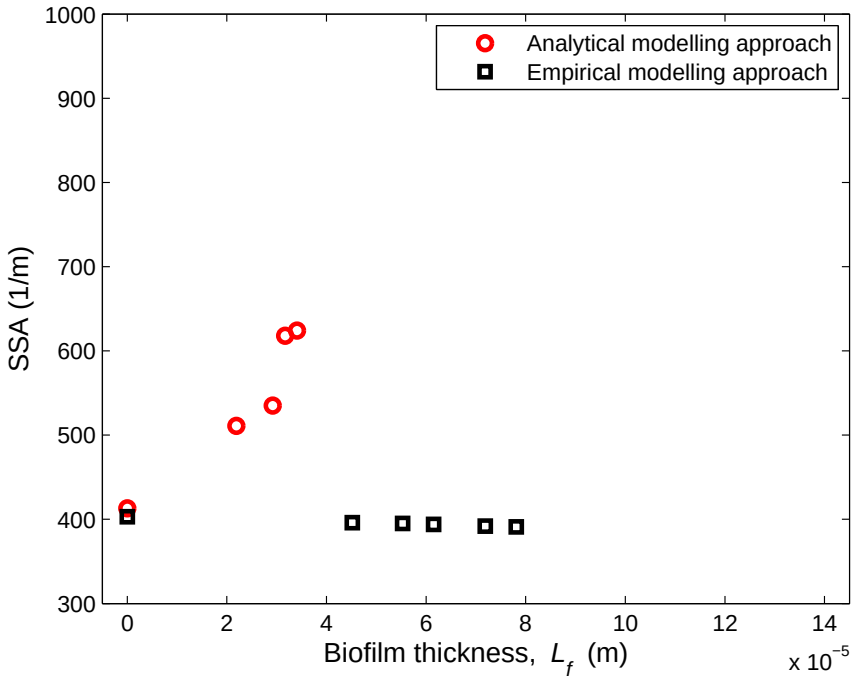

Figure 7.18. Biofilter 3: SSA as a function of biofilm thickness.

The scatter of data provided by the analytical approach in Figures 7.16, 7.17 and 7.18 is a result of the fluctuation in measured pressure drop values as well as the average calculation. The biofilm affected SSA values obtained from the empirical modelling approach remain more or less constant. This is due to the terms in equation (7.19) containing L_f remaining significantly smaller than the term to which it is added.

7.7 Roughness Coefficient

The average porosity values of Biofilters 1, 2 and 3 are 0.404, 0.420 and 0.407, respectively, and fall in the range given by Jian-Chao et al. [22] (refer to Section 2.7) for which the effect of surface roughness is not negligible. The roughness factor, χ, will therefore be calculated in this section and compared to the findings of Jian-Chao et al. [22].

The results obtained for a_f, obtained from the analytical approach, given in Tables 7.10 to 7.12 in Section 7.6, were substituted into equation (2.10) for which $a_o = S^*_{v,s}$ and $a_f = S^*_v$ for each biofilter on each day of the experiment on which data was recorded. The results are given in Table 7.13.

Table 7.13. Corresponding SSA and χ-values.

	Biofilter 1		**Biofilter 2**		**Biofilter 3**	
Day	a_f	χ	a_f	χ	a_f	χ
0	407	1.0	408	1.0	413	1.0
19	460	1.1			1996	4.8
39	548	1.3	1791	4.4	411	1.2
57	679	1.7	510	1.3	535	1.3
71	722	1.8	1863	4.6	618	1.5
92	617	1.5	586	1.4		
106	751	1.8	587	1.4	624	1.5
Average		1.5		2.3		1.9

It was found that the average values of χ are 1.5, 2.3 and 1.9 for Biofilters 1, 2 and 3, respectively. This yields an average roughness factor of 1.9. The results are shown in Figures 7.19 to 7.21.

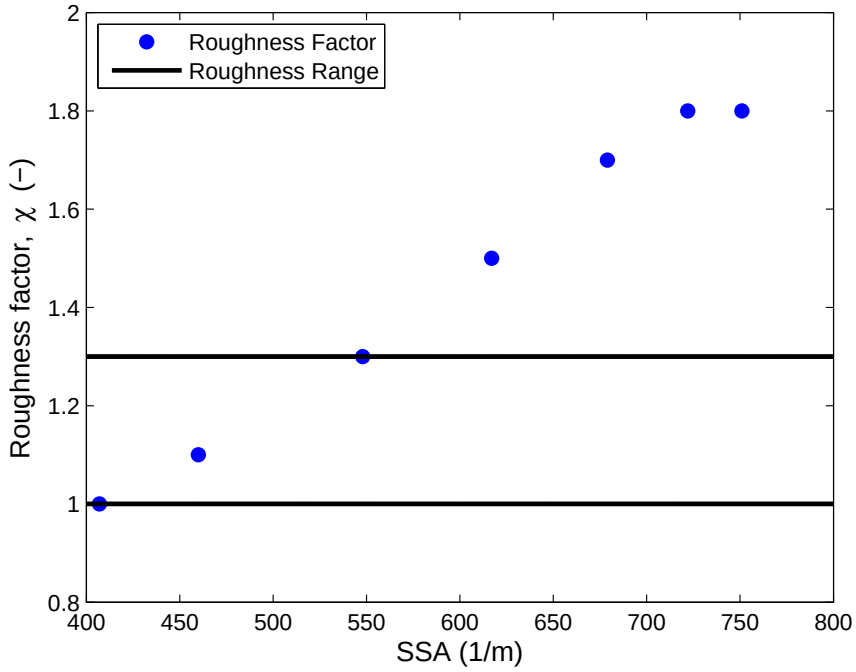

Figure 7.19. Biofilter 1: Corresponding SSA and χ-values.

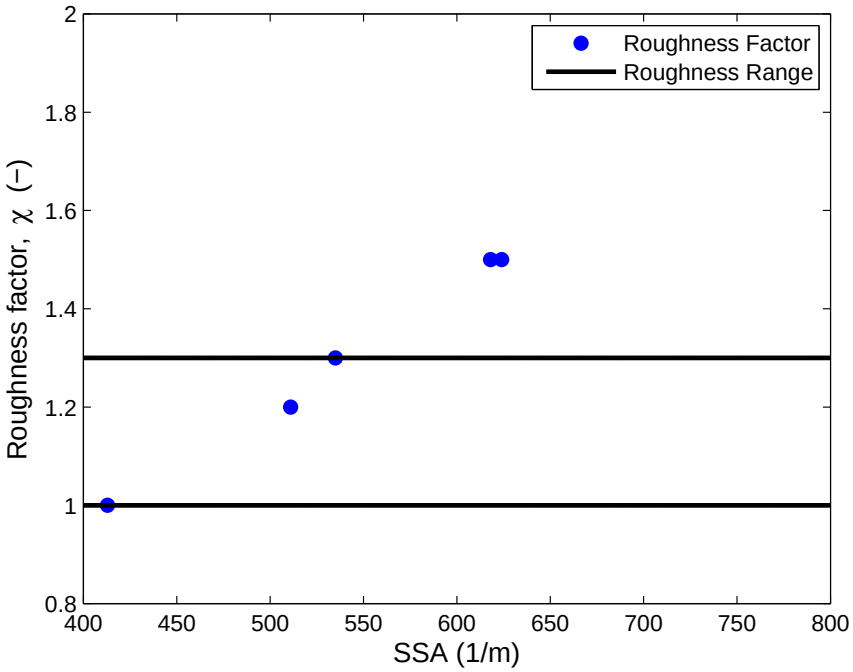

Figure 7.21. Biofilter 3: Corresponding SSA and χ-values.

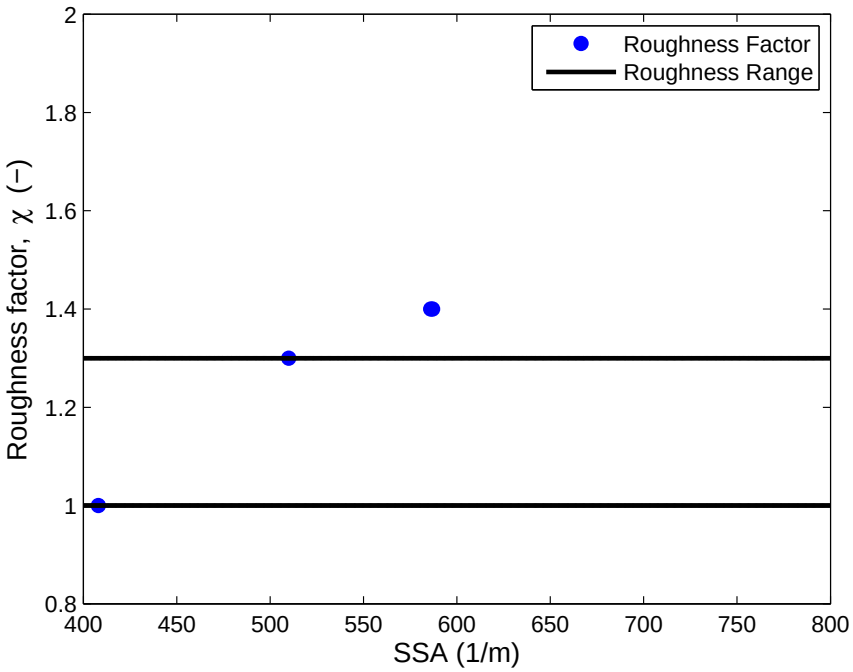

Figure 7.20. Biofilter 2: Corresponding SSA and χ-values.

From Figures 7.19 to 7.21 it is clear that the value of χ increases with an increase in a_f, as expected, according to equation (2.10). The outlier χ-values for Biofilter 2 on days 39 and 71 and for Biofilter 3 on day 19 have been omitted from Figures 7.20 and 7.21 in order to show the behaviour of the other χ-values more clearly. Recall that Jian-Chao et al. [22] obtained χ-values in the range 1.0 to 1.33 which is roughly half the average value obtained for the particles used in this experiment. It is important to recall that Jian-Chao et al. [22] based their study on fractal analysis rather than actual data and also not on expanded schist particles, such as in the present study. Nevertheless, the overall result is satisfactory, since the average χ-value obtained from the results in the present study is consistent with the value used in the RUC model, i.e. $\beta = 2.0$. However, if the outlier χ-values for Biofilter 2 on days 39 and 71 and for Biofilter 3 on day 19 (refer to Table 7.13) were to be excluded from the calculations, the new average χ-values would be 1.5 and 1.3, respectively. This yields an overall average of 1.4 which is in close correspondence to the range of values reported by Jian-Chao et al. [22].

7.8 Sensitivity Analysis

In this section the absolute relative percentage differences in biofilm thickness and SSA will be presented for a 1 and 2% error in ε_o in all three biofilters. Thereafter the differences between the results obtained from the Modified-Macdonald equation and the RUC model when $n = 8$, instead of $n = 7$, are investigated.

7.8.1 Initial porosity

Determining L_f with equation (7.7), n with equation (6.5) and a_f with equation (7.19) cannot be done without ε_o. According to Dumont et al. [3], the measured ε_o-values are subject to an experimental error of 1%. Since a 3% error leads to a negative a_f-value on day 71 in Biofilter 1, the decision was made to only investigate the effects of a 1 and 2% error in ε_o. The results of the investigation concerning L_f for Biofilters 1, 2 and 3 are graphically represented in Figures 7.22 to 7.24, respectively.

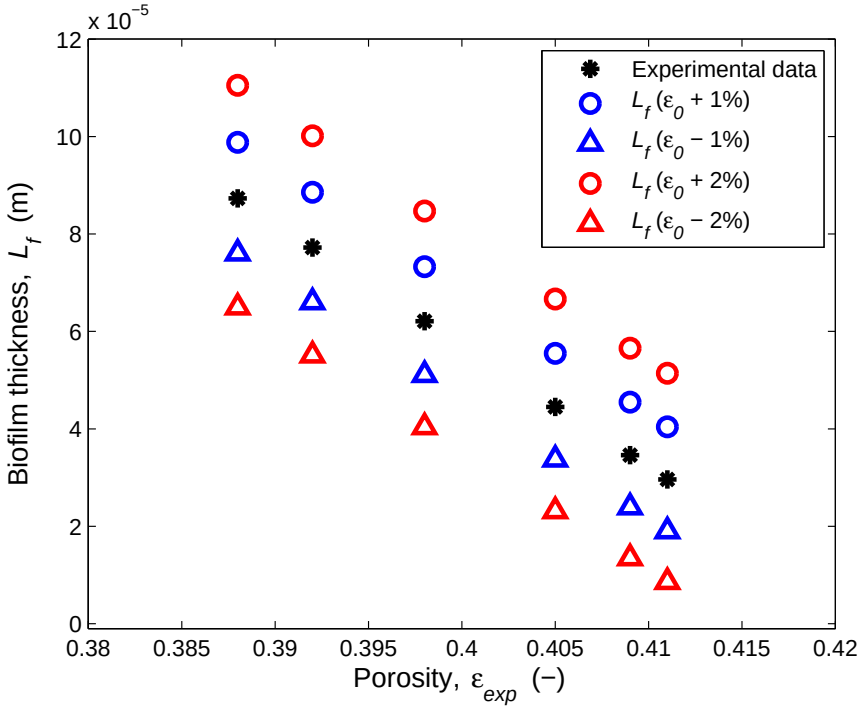

Figure 7.22. Biofilter 1: The effect of a 1 and 2% error in ε_o on the biofilm thickness.

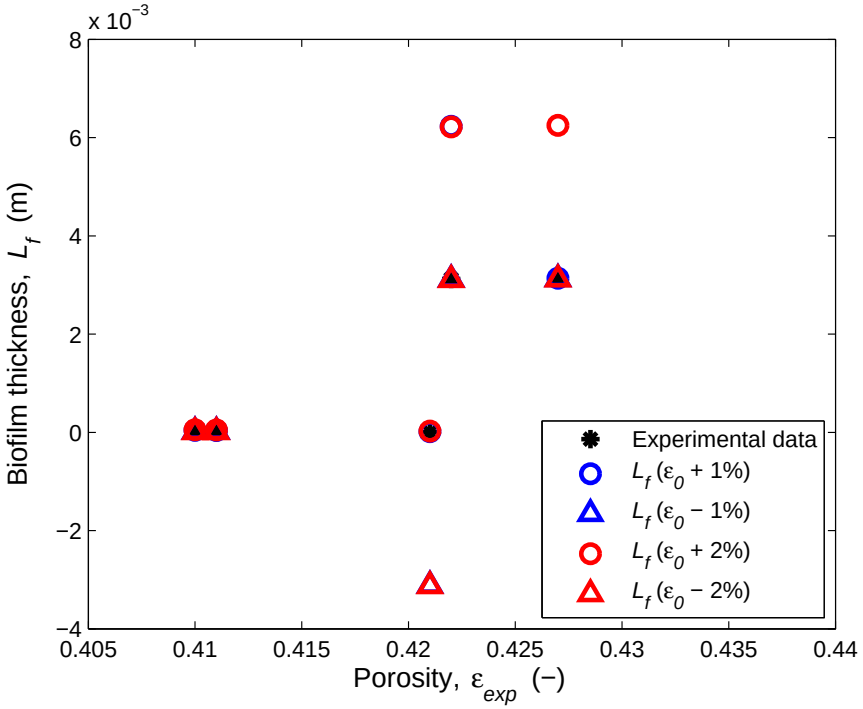

Figure 7.23. Biofilter 2: The effect of a 1 and 2% error in ε_o on the biofilm thickness.

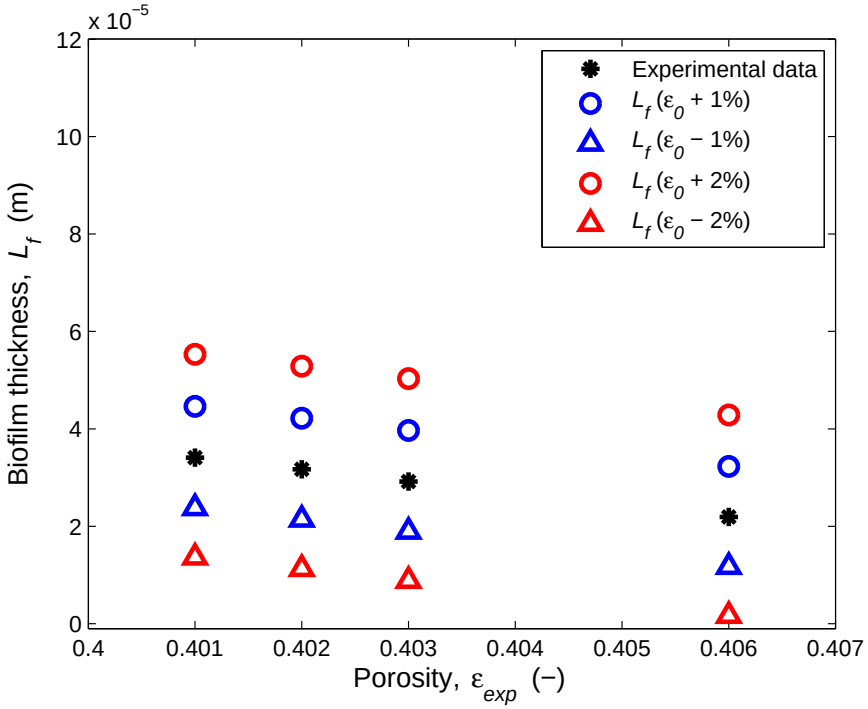

Figure 7.24. Biofilter 3: The effect of a 1 and 2% error in ε_o on the biofilm thickness.

It is evident that each 1% error in ε_o leads to a difference of a factor of approximately 1.0×10^{-5} in the value of L_f and each 2% error leads to a difference of a factor of approximately 2.0×10^{-5}. In Biofilters 1, 2 and 3 the absolute relative percentage difference falls in the ranges $12 - 37\%$, $0 - 100\%$ and $0 - 48\%$ for a 1% error, respectively.

For a 2% error, the absolute relative percentage differences respectively range between $25 - 74\%$, $0 - 100\%$ and $0 - 96\%$ for Biofilters 1, 2 and 3. The outlier L_f-values for Biofilter 2 on days 39 and 71, corresponding to $\varepsilon_{exp} = 0.429$ and $\varepsilon_{exp} = 0.422$, respectively, and for Biofilter 3 on day 19, corresponding to $\varepsilon_{exp} = 0.430$, are a result of the considerably larger L_f-values shown in Tables 7.2 and 7.3, respectively. The outlier L_f-values for Biofilter 2, corresponding to $\varepsilon_{exp} = 0.421$, is a result of the considerably smaller L_f-value on day 57, shown in Table 7.2. Note that a 1 and 2% error in the initial porosity only results in a 1 and 2% error in n, respectively. Since the effect is negligibly small it will not be shown graphically.

The comparison between the experimental data and the effect of the percentage differences can be seen in Figures 7.25 to 7.27 for Biofilters 1, 2 and 3, respectively.

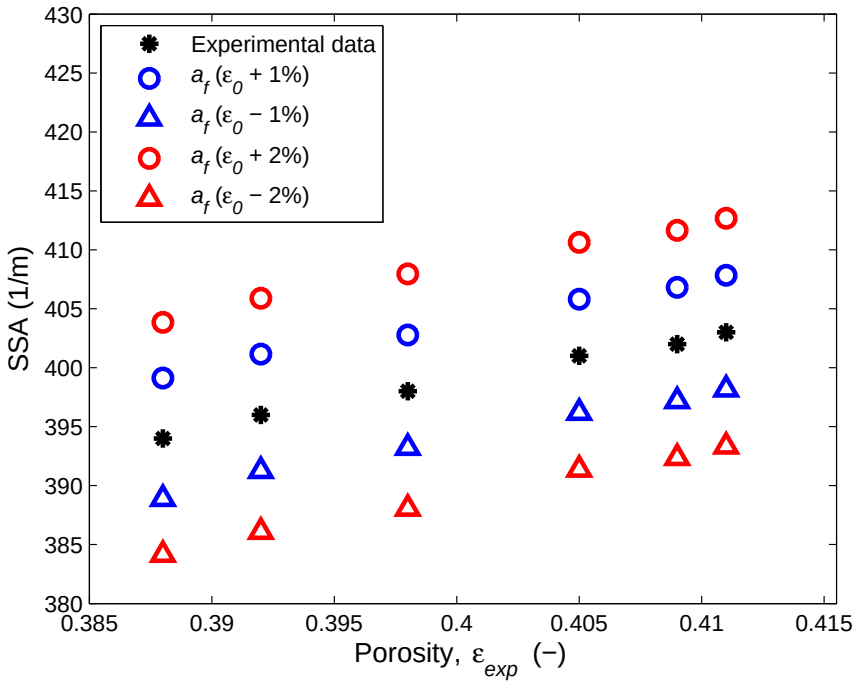

Figure 7.25. Biofilter 1: The effect of a 1 and 2% error in ε_o on the SSA.

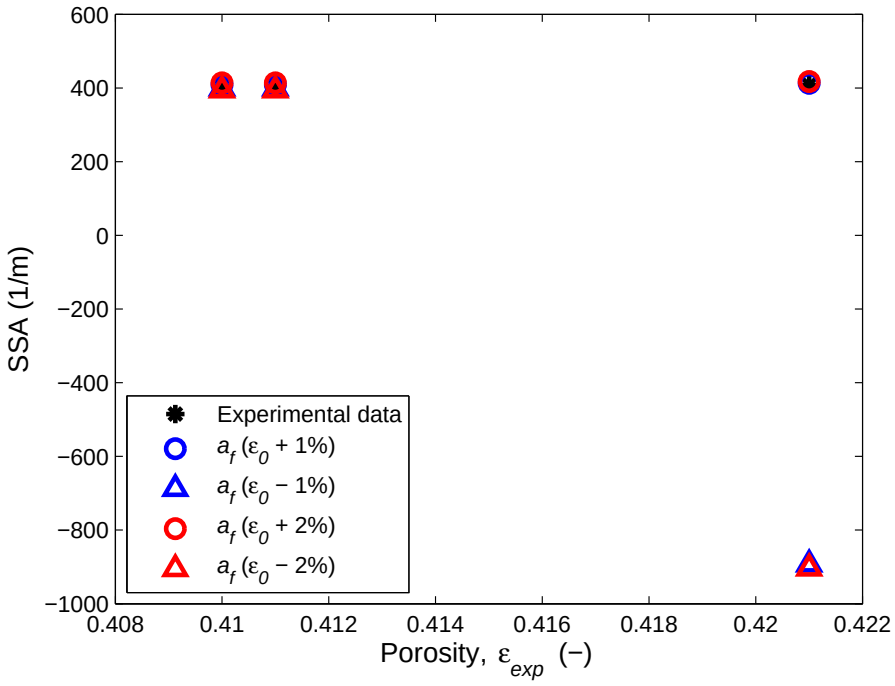

Figure 7.26. Biofilter 2: The effect of a 1 and 2% error in ε_o on the SSA.

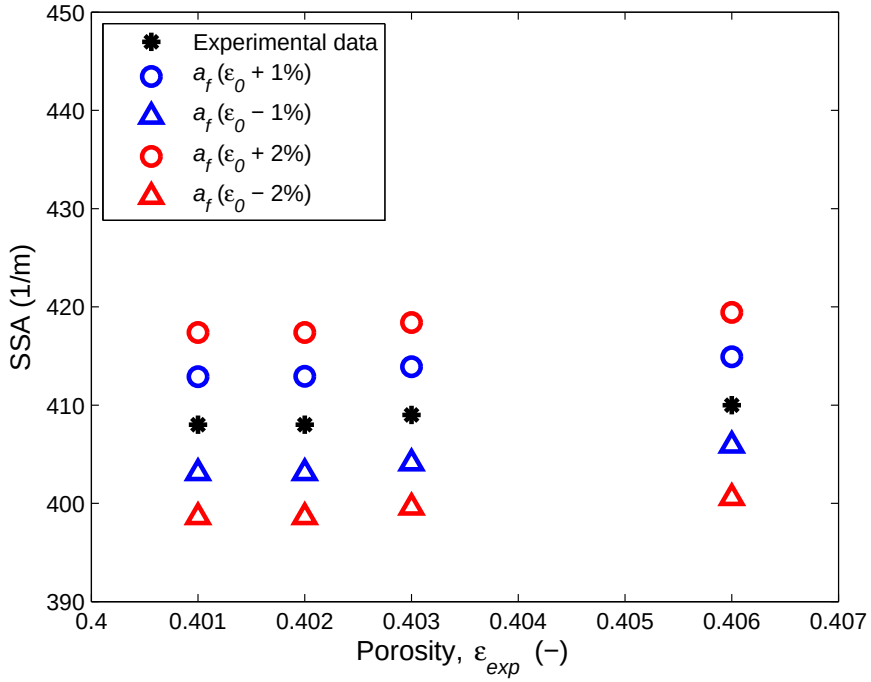

Figure 7.27. Biofilter 3: The effect of a 1 and 2% error in ε_o on the SSA.

A 1% error in ε_o leads to an approximate relative percentage error of 1% in the SSA, whereas a 2% error in ε_o leads to a relative percentage error in the range 2 to 3%. The outlier a_f-values for Biofilter 2, corresponding to $\varepsilon_{exp} = 0.421$, are a result of the considerably smaller L_f-value on day 57, shown in Table 7.5. Recall from Section 7.2 that the SSA values obtained for Biofilter 2 on days 39 and 71 and for Biofilter 3 on day 19 were unrealistic (i.e. negative). These specific SSA results, shown in Tables 7.5 and 7.6, were therefore emitted from the plots.

The sensitivity analysis showed that the L_f- and a_f-predictions made by the RUC model are sensitive to the initial porosity, based on the large absolute relative percentage differences reported for the L_f-values, which is consequently incorporated into the a_f-values. Since the experimentally determined ε_o affects the predictions for the biofilm thickness, SSA and as a result the pressure drop prediction, it is important that it should be measured accurately. The accuracy of the model predictions therefore depends on the accuracy of the ε_o measurement used as input parameter to the model.

7.8.2 Coordination number

In order to analyze the effect of the coordination number on the results obtained from the analytical modelling approach, the value of n has been changed. Instead of rounding the value of n to 7, such as in Section 7.1, it was rounded to 8. Results from the investigation are graphically represented in Figures 7.28, B11 and B12 for Biofilters 1, 2 and 3, respectively.

It is clear that the effect of changing the value of n is negligibly small, since the data points from the sensitivity analysis are hidden behind the results obtained from the analytical approach with $n = 8$. The average relative percentage differences are 0.34%, 6.39% and 3.27% for Biofilters 1, 2 and 3, respectively. Also, taking the magnitude of the biofilm thickness values into consideration, the effect of changing the value of n is relatively small.

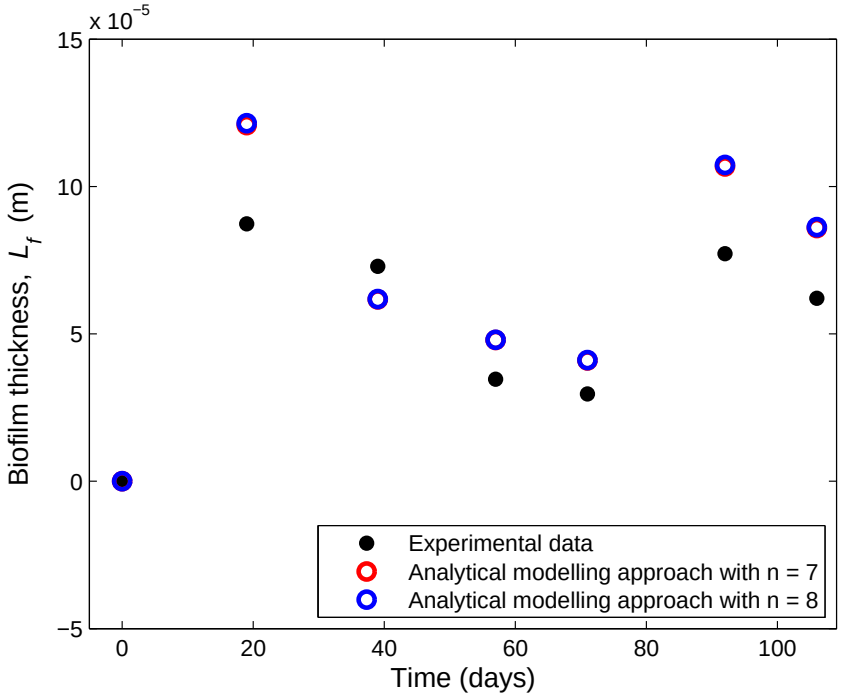

Figure 7.28. Biofilter 1: Comparison between L_f-values for $n = 7$ and $n = 8$.

A comparison between the SSA values obtained from equation (7.19) with $n = 7$ and $n = 8$ is graphically represented in Figures 7.29, B13 and B14 for Biofilters 1, 2 and 3, respectively. Note that the results for Biofilter 2 on days 39 and 71 and for Biofilter 3 on day 19 have been emitted from the plots, since the values are negative. The initial SSA does not depend on the value of the coordination number, therefore, the values on day 0 based on $n = 7$ and $n = 8$ are equal.

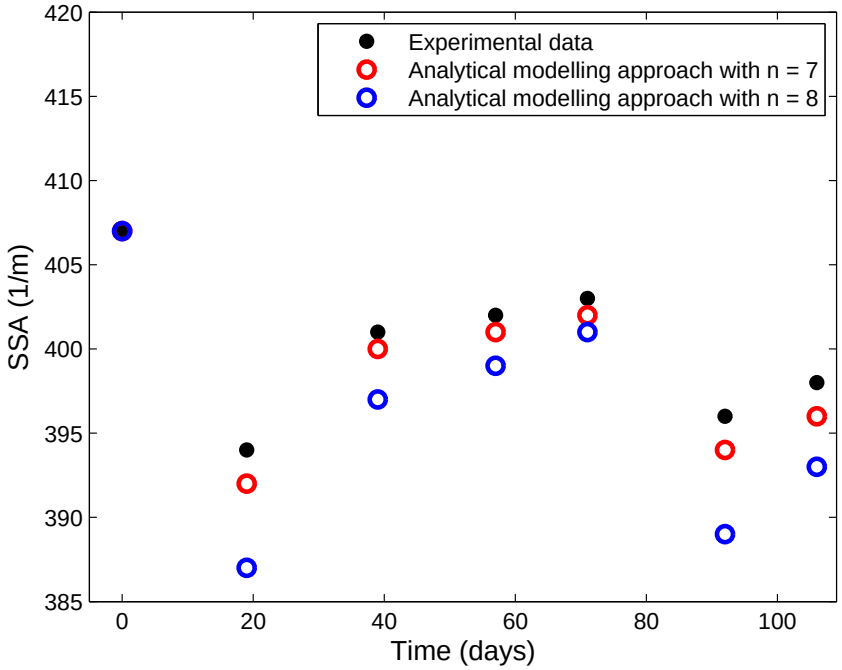

Figure 7.29. Biofilter 1: Comparison between a_f-values for $n = 7$ and $n = 8$.

After changing the value of n in equation (7.19), the average relative percentage differences were found to be 0.71%, 1.99% and 1.15% for Biofilters 1, 2 and 3, respectively, which is once again negligibly small. Therefore, regardless of the variable in question (i.e. L_f or SSA), rounding up or rounding down the value of the coordination number may depend on personal preference.

Chapter 8

Conclusions

In order to obtain more knowledge about biofilm growth and the effect it has on the operation of a biofilter, different porous media models were used to predict the pressure drop over three different biofilters. According to the author of this thesis, only empirical models are available in the literature for modelling pressure drop over a biofilter. These models include the Ergun equation, the Macdonald equation and the Modified-Macdonald equation. The analytical RUC model, based on an adaptation of the model used by Du Plessis and Woudberg [2], is introduced in order to avoid the use of empirical curve fitting parameters. The aim was to investigate the effects that the various parameters have on the pressure drop, and to find physical reasoning behind possible deviations, rather than introducing coefficients in order for the results to fit the experimental data satisfactorily. The Ergun and Macdonald equations were excluded from pressure drop predictions, since the results obtained under-predicted the experimental pressure drop data throughout the entire experiment. However, the Modified-Macdonald equation performed remarkably, which is an indication that the changes made to the Macdonald equation by Morgan-Sagastume et al. [26] are applicable to a wide variety of porosities and packing materials. Dumont et al. [4] made use of an empirical approach, together with the Modified-Macdonald equation and the RUC model, as well as the Comiti and Renaud model, in order to fit the experimental pressure drop measurements and subsequently determine the changes in packed bed characteristics. After using an optimization method, together with Excel® Solver, it was found that the Comiti and Renaud model cannot be used to predict the porosity of a packed bed, based on its inaccuracy. The probable cause is due to the fact that this model requires three unknown variables that needed to be optimized. Also, Excel® Solver appears to be slightly sensitive to initial guessed values. Considering the optimized porosity, tortuosity and biofilm thickness values, the RUC model gave less accurate results when compared to the Modified-Macdonald equation. Both models gave accurate results concerning

the optimized SSA values, since the latter correspond closely to that of the experimental data. A probable cause for the overall remarkable performance of the Modified-Macdonald equation may be the fact that the model was used twice in the optimization process, whereas the RUC model was used only once. This is because the Modified-Macdonald equation was used to additionally optimize the value of the sphericity. After using the RUC model to obtain the sphericity value in the empirical modelling approach, instead of the Modified-Macdonald equation, a sensitivity analysis was performed on the effect of the value of the sphericity on the optimization results. As a result, the RUC model obtained more accurate results, however, the overall results were, once again, in favour of the Modified-Macdonald equation. The most probable cause, despite which model is used to optimize the sphericity, may be due to the fact that Solver obtains more accurate results when two variables, rather than one or three, are optimized at once. In the analytical approach, the biofilm thickness was determined in order to subsequently determine the SSA with a method based on an approach used in the literature. An alternative approach involved using the RUC model in order to express the pressure drop in terms of the biofilm affected SSA. Both methods were found to be adequate, since the SSA values obtained are of the same order of magnitude. The changes in the packed bed characteristics were found to be relatively small. Consequently, the assumption was made by Dumont et al. [4] that the significant increase in pressure drop can be attributed to the change in surface roughness, as a result of biofilm development. Therefore, the remarkable performance of the Modified-Macdonald equation was attributed to the optimized surface roughness values. The RUC model initially under-predicted the experimental pressure drop values. Consequently, the assumption was made in the analytical approach that the significant increase in pressure drop can be attributed to changes in the sphericity value as a result of biofilm developing and covering a cluster of particles of which the number of particles is determined by the coordination number. Therefore, it is important to incorporate the analytically determined sphericity as a function of the biofilm thickness and the coordination number, into the adapted RUC model. The pressure drop results obtained from the adapted RUC model with the empirically and analytically determined sphericity values as limits, captured the experimental data in between. The resulting over- and under-prediction of the adapted RUC model illustrates the significant effect of the value used for the sphericity in the model predictions. The biofilm affected SSA values, obtained by the RUC model in the analytical approach, was used to determine the roughness coefficient. Not only do the results justify the β-value used in the RUC model, but it also corresponds with the values obtained by Jian-Chao et al. [22]. After performing a sensitivity analysis on the analytical approach, it was found that the experimentally determined initial porosity value should be measured accurately in order to obtain accurate model predictions. Also, regardless of the variable in question, the

rounding of the coordination number may depend on personal preference. Despite the fact that the results obtained from the adapted RUC model in the analytical approach are less accurate than those obtained from the Modified-Macdonald equation in the empirical approach, a major advantage of using the adapted RUC model is the fact that it is justifiable from a physical point of view, and can be used to predict the pressure drop and SSA in a biofilter over time, without the necessity to use empirical curve fitting parameters. The results and conclusions obtained in this study are solely based on the experimental data available to the author. Further validation of the proposed analytical model is recommended on experimental biofilter data that at least provide less fluctuation and a wider range of porosity values associated with the different days of biofilter operation.

Bibliography

[1] A. Courtois, Y. Andres, and E. Dumont. H_2S biofiltration using expanded schist as packing material: Influence of packed bed configurations at constant EBRT. *Journal of Chemical Technology and Biotechnology*, 90:50–56, 2015.

[2] J.P. Du Plessis and S. Woudberg. Pore-scale derivation of the Ergun equation to enhance its adaptability and generalization. *Chemical Engineering Science*, 63:2576–2586, 2008.

[3] E. Dumont, L.M. Ayala Guzman, M.S. Rodriguez Susa, and Y. Andres. H_2S biofiltration using expanded schist as packing material: Performance evaluation and packed-bed tortuosity assessment. *Journal of Chemical Technology and Biotechnology*, 87:725–731, 2012.

[4] E. Dumont, S. Woudberg, and J. van Jaarsveld. Assessment of biofilm thickness in biofilters using porous media models. *Powder Technology*, 303:76–89, 2016.

[5] C. Alonso, M.T. Suidan, G.A. Sorial, F.L. Smit, P. Biswas, P.J. Smit, and R.C. Brenner. Gas treatment in trickle-bed biofilters: Biomass, how much is enough? *Biotechnology and Bioengineering*, 54(6):583–594, 1997.

[6] B.L. Miranda. *Gradation-Based Framework for Asphalt Mixtures*. Thesis, Royal Institute of Technology (KTH), Stockholm, Sweden, April 2012.

[7] P. Baltrenas and K. Macaitis. Effectiveness of air treatment using a plate-type biofilter with a capillary system for humidification of packing material. *Environmental Engineering and Management Journal*, 13:2063–2072, 2014.

[8] M.-C. Delhoménie and M. Heitz. Biofiltration of air: A review. *Critical Reviews in Biotechnology*, 25:53–72, 2005.

[9] D. Schmidt, L. Jacobson, and R. Nicolai. Manure management and air quality: Biofilter design information, 2004. URL `http://www.extension.umn.edu/agriculture/`

manure-management-and-air-quality/air-quality/biofilter-design-information/. Accessed on: 2016-02-16.

[10] Z.M. Shareefdeen. Hydrogen sulfide (H_2S) removal using schist packings in industrial biofilter applications. *Korean Journal of Chemical Engineering*, 32(1):15–19, 2015.

[11] D.W. Abbood. Effects of biomass growth on pressure drop in submerged aerated bioreactors. *Al-Qadisiya Journal for Engineering Sciences*, 2:1–20, 2009.

[12] S.B. Anit and R.J. Artuz. Biofiltration of air, 2000. URL http://www.rpi.edu/dept/chem-eng/Biotech-Environ/Environmental/biofiltration/biofiltration.htm. Accessed on: 2016-02-16.

[13] H.W. Ryu, K.-S. Cho, and D.J. Chung. Relationships between biomass, pressure drop, and performance in polyurethane biofilter. *Bioresource Technology*, 101:1745–1751, 2010.

[14] Z.M. Shareefdeen. A biofilter design tool for hydrogen sulfide removal calculations. *Clean Technology Policy*, 14:543–549, 2012.

[15] US Department of Labor. Osha fact sheet: Hydrogen sulfide, 2005. URL https://www.osha.gov/OshDoc/data_Hurricane_Facts/hydrogen_sulfide_fact.pdf. Accessed on: 2016-02-16.

[16] F. Gaudin, Y. Andres, and P. Le Cloirec. Odorous emission biofiltration with new synthetic packing materials: Essential nutriment release. *Biotechniques for Air Pollution Control*, 1: 263–271, 2005.

[17] R.G. Holdich. *Fundamentals of Particle Technology*. Midland Information Technology and Publishing, Leicestershire, U.K., 2002. ISBN 0-9543881-0-0.

[18] Z.T. Abdzaid. Investigation of the friction factor-Reynolds number relationship for flow through packed beds. *Iraqi Journal of Civil Engineering*, 6(3):70–79, 2010.

[19] Y. Jia, Y. Li, and D. Hlavka. Flow through packed beds, 2009. URL http://www.me.rochester.edu/courses/ME241.gans/PackedBeds(11).pdf. Accessed on: 2016-03-18.

[20] C.T. Simmons. Henry Darcy (1803-1858): Immortalised by his scientific legacy. *Hydrogeology Journal*, 16:1023–1038, 2008.

[21] I.F. Macdonald, M.S. El-Sayed, and F.A.L. Dullien. Flow through porous media - The Ergun equation revisited. *Industrial and Engineering Chemistry Fundamentals*, 18(3):199–208, 1979.

[22] C.A.I. Jian-Chao, Y.U. Bo-Ming, Z.O.U. Ming-Qing, and M.E.I. Mao-Fei. Fractal analysis of surface roughness of particles in porous media. *Chinese Physics Letters*, 27:024705–1 – 024705–4, 2010.

[23] R.B. Bird, W.E. Stewart, and E.N. Lightfoot. *Transport Phenomena*. John Wiley and Sons, New York, 2002. ISBN 0-470-11539-4.

[24] J. Comiti and M. Renaud. A new model for determining mean structure parameters of fixed beds from pressure drop measurements: Application to beds packed with parallelepipedal particles. *Chemical Engineering Science*, 44(7):1539–1545, 1989.

[25] M.-C. Delhoménie, L. Bibeau, J. Gendron, R. Brzezinski, and M. Heitz. A study of clogging in a biofilter treating toluene vapors. *Chemical Engineering Journal*, 94:211–222, 2003.

[26] F. Morgan-Sagastume, B.E. Sleep, and D.G. Allen. Effects of Biomass Growth on Gas Pressure Drop in Biofilters. *Journal of Environmental Engineering*, 127:388–396, 2001.

[27] F.A.L. Dullien. *Porous Media: Fluid Transport and Pore Structure*. Academic Press, 1979. ISBN 978-0-12-223651-8.

[28] E. Dumont. *Personal Communication*, 2015.

[29] I. Iliuta and F. Larachi. Transient biofilter aerodynamics and clogging for VOC degradation. *Chemical Engineering Science*, 59:3293–3302, 2004.

[30] P.-Y. Lanfrey, Z.V. Kuzeljevic, and M.P. Dudukovic. Tortuosity model for fixed beds randomly packed with identical particles. *Chemical Engineering Science*, 65:1891–1896, 2010.

[31] R. Dias, J.A. Teixeira, M. Mota, and A. Yelshin. Tortuosity variation in a low density binary particulate bed. *Separation and Purification Technology*, 51:180–184, 2006.

[32] Public. Excel Forum, 2013. URL `http://www.excelforum.com/excel-formulas-and-functions/957627-help-with-solver-as-solver-gives-wrong-answer.html`. Accessed on: 2016-06-28.

[33] Public. Mr Excel, 2004. URL `http://www.mrexcel.com/forum/excel-questions/92213-solver-gives-different-solution-depending-start-value.html`. Accessed on: 2016-06-28.

[34] J. van Jaarsveld and S. Woudberg. An empirical versus analytical approach for modelling biofilm growth in biofilters. In *Multiphase Flow IX (Editors: P. Vorobieff and C. A. Brebbia), Proceedings of the 9th International Conference on Computational and Experimental Methods in Multiphase and Complex Flow*, pages 143–152, Tallinn, Estonia, 2017. WIT Press, UK.

[35] S. Woudberg, J. van Jaarsveld, and E. Dumont. Analytical determination of the effect of biofilm growth on the pressure drop over a biofilter. In *Proceedings of the World Congress on Momentum, Heat and Mass Transfer*, pages 105(1)–105(6), Prague, Czech Republic, 2016.

Appendix A

Initial Pressure Drop Predictions

The following graphs contain experimental data, recorded on days 19, 39, 57, 71, 92 and 106 over a period of 110 days for each of the three biofilters.

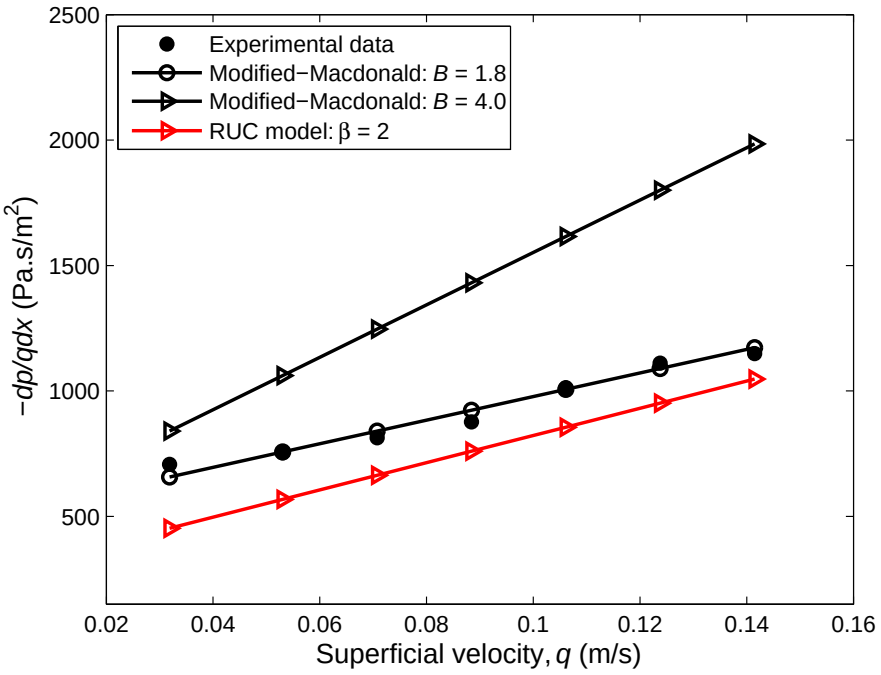

Figure A1. Biofilter 1: Model predictions for day 19.

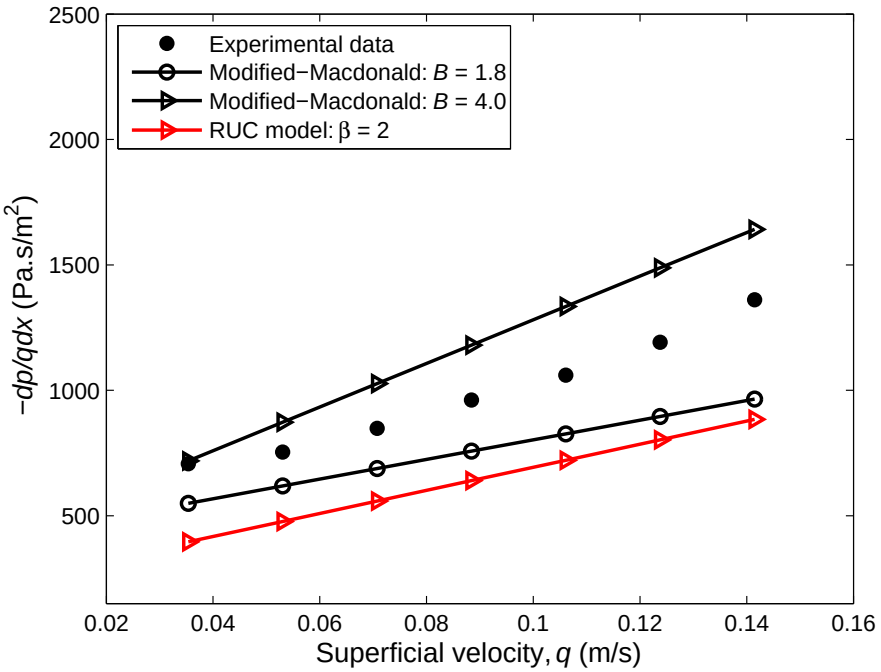

Figure A2. Biofilter 1: Model predictions for day 39.

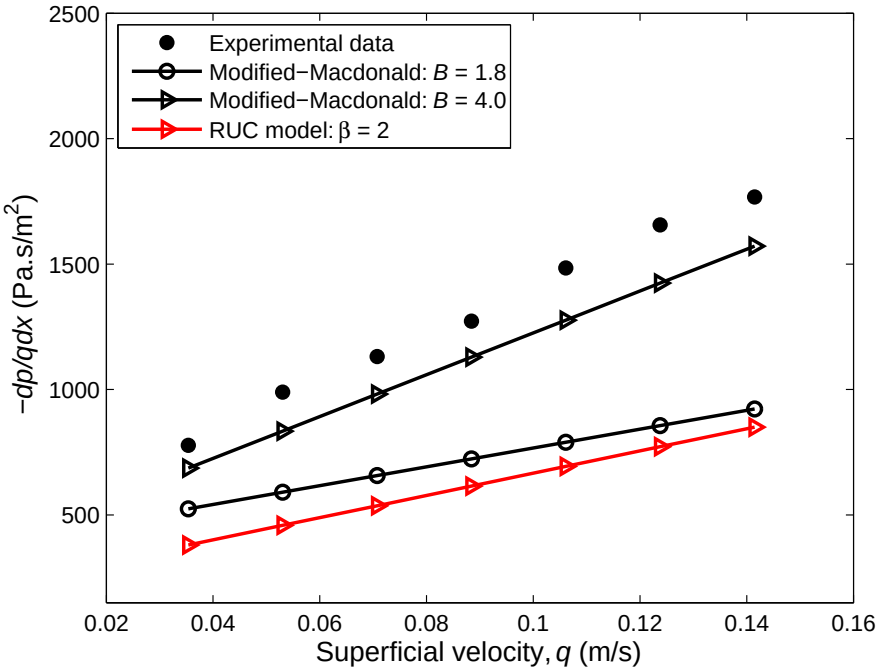

Figure A3. Biofilter 1: Model predictions for day 57.

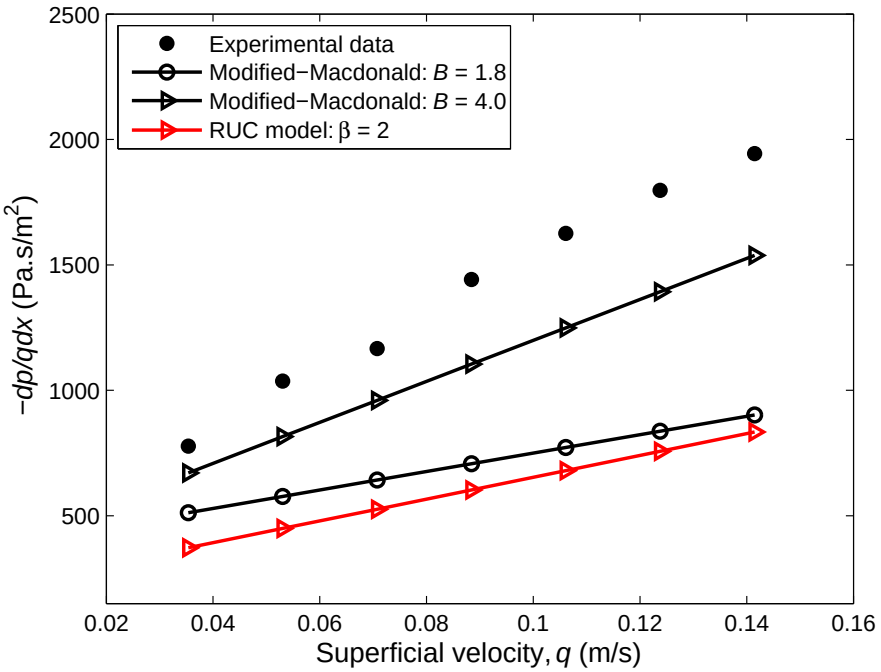

Figure A4. Biofilter 1: Model predictions for day 71.

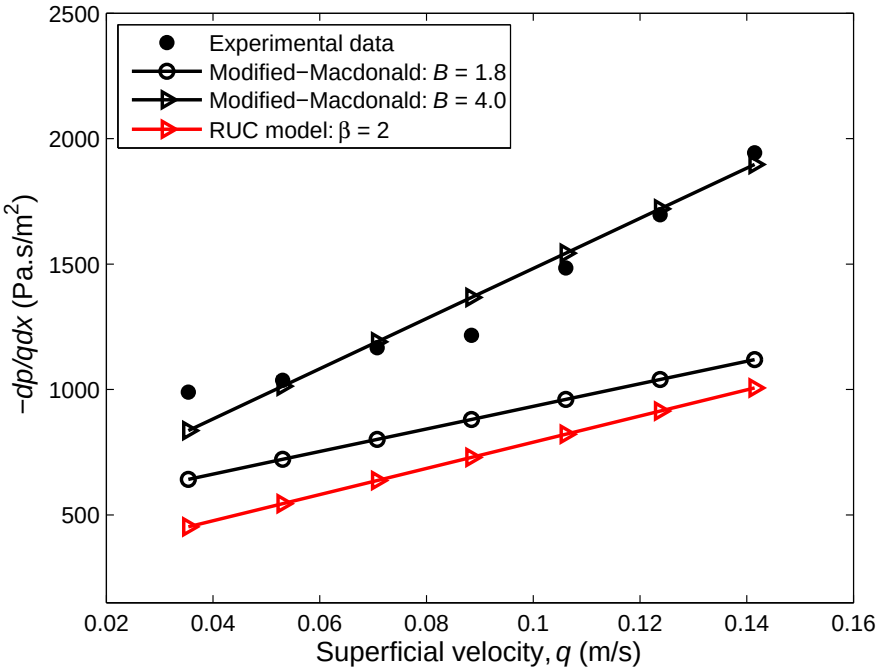

Figure A5. Biofilter 1: Model predictions for day 92.

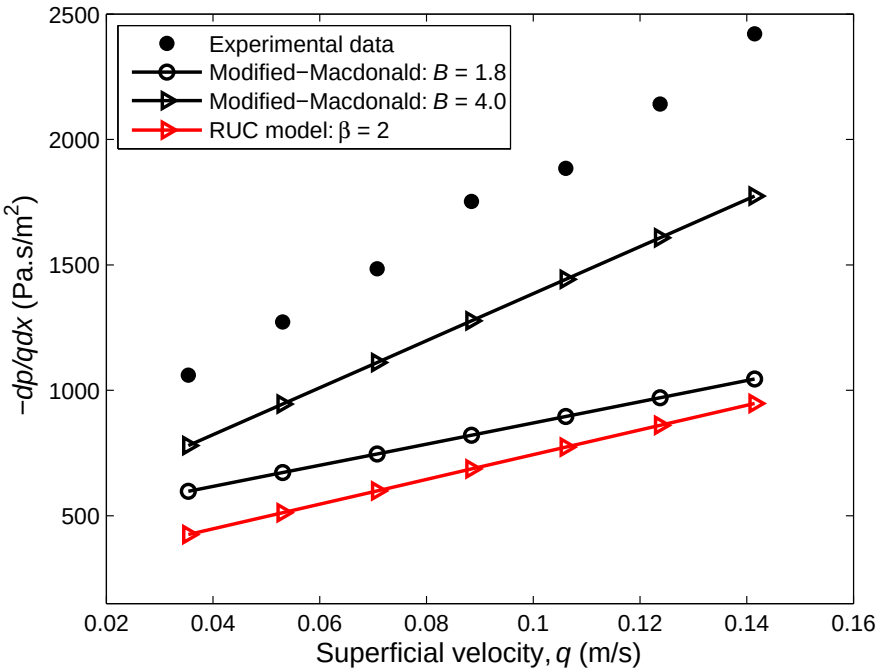

Figure A6. Biofilter 1: Model predictions for day 106.

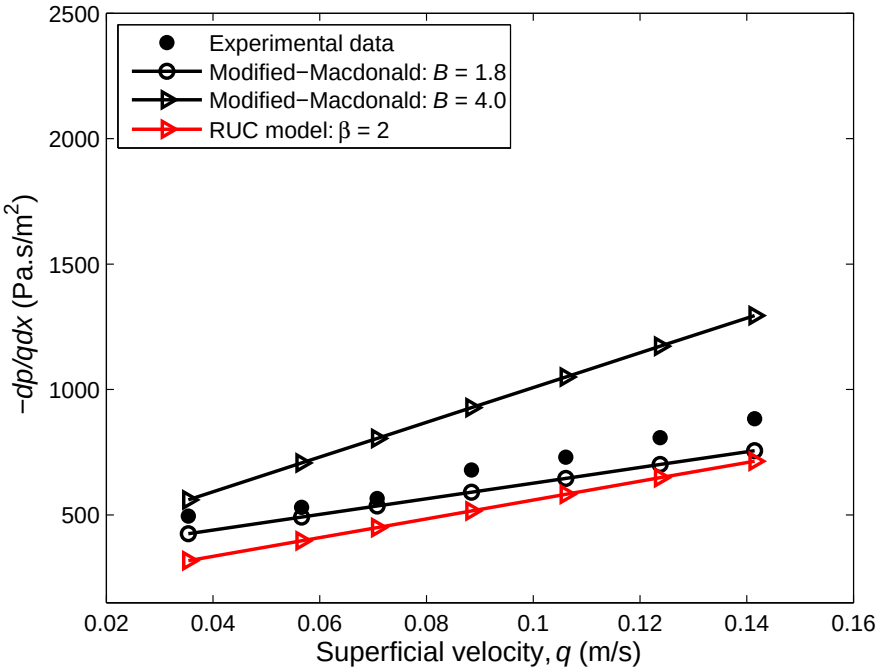

Figure A7. Biofilter 2: Model predictions for day 39.

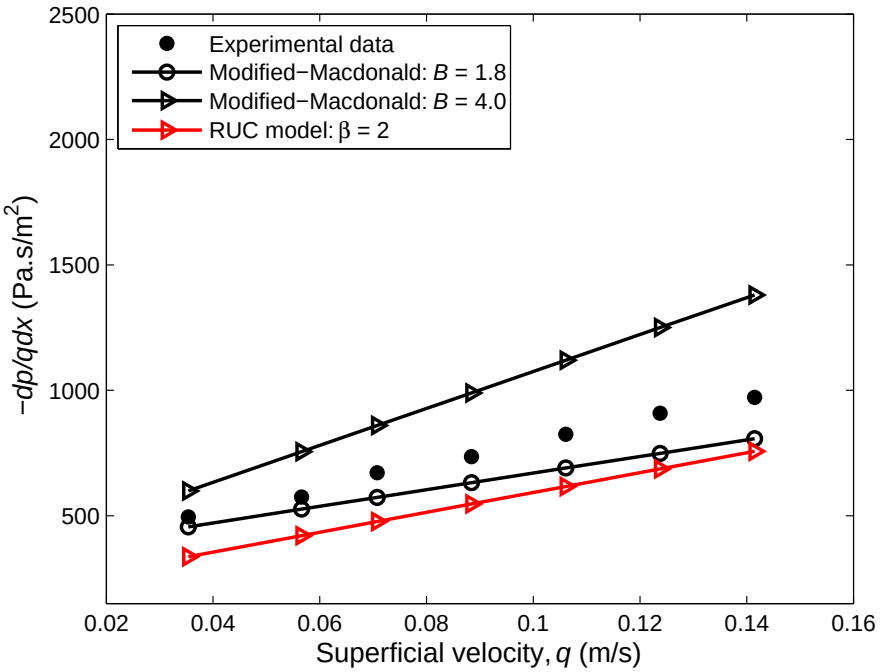

Figure A8. Biofilter 2: Model predictions for day 57.

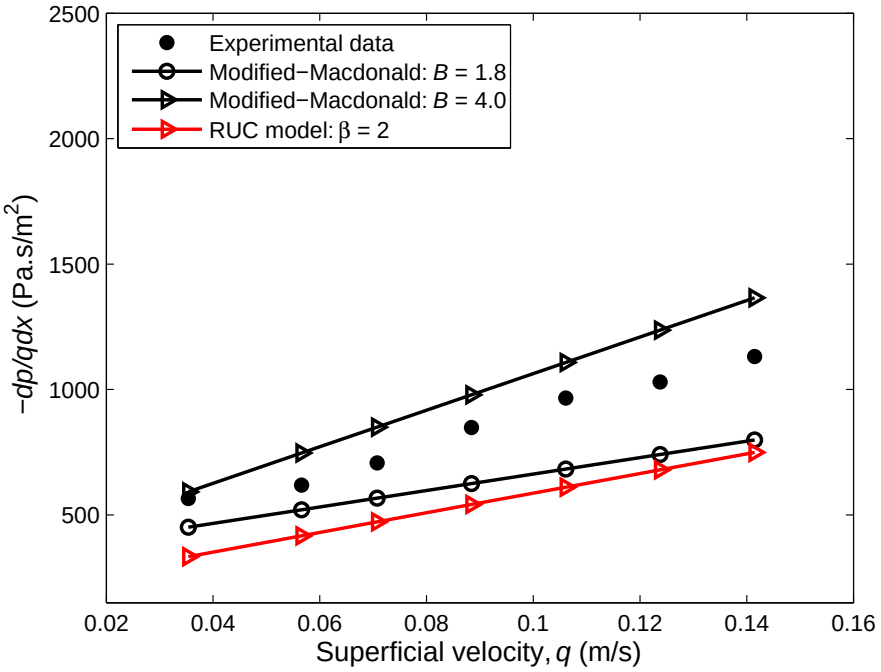

Figure A9. Biofilter 2: Model predictions for day 71.

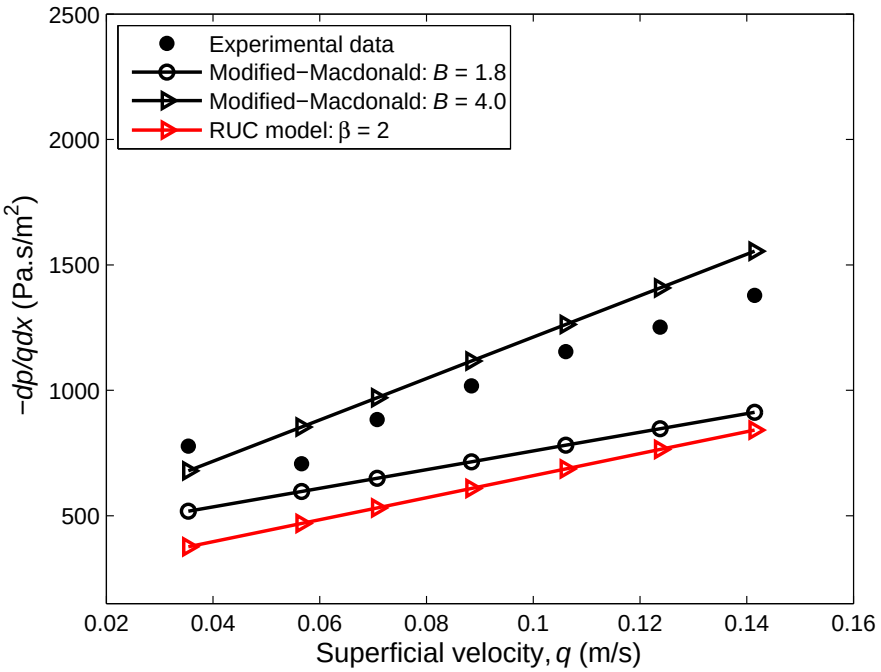

Figure A10. Biofilter 2: Model predictions for day 92.

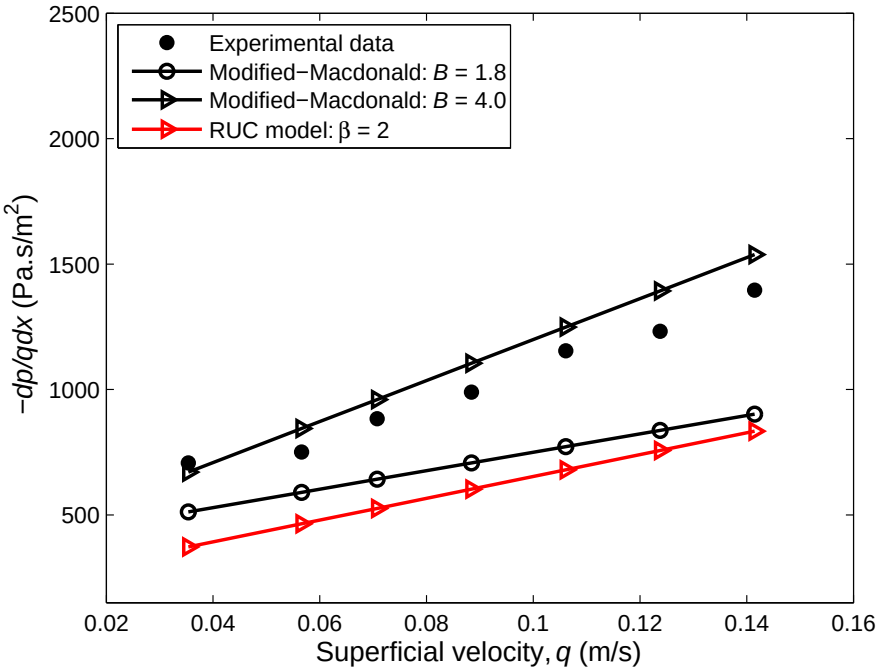

Figure A11. Biofilter 2: Model predictions for day 106.

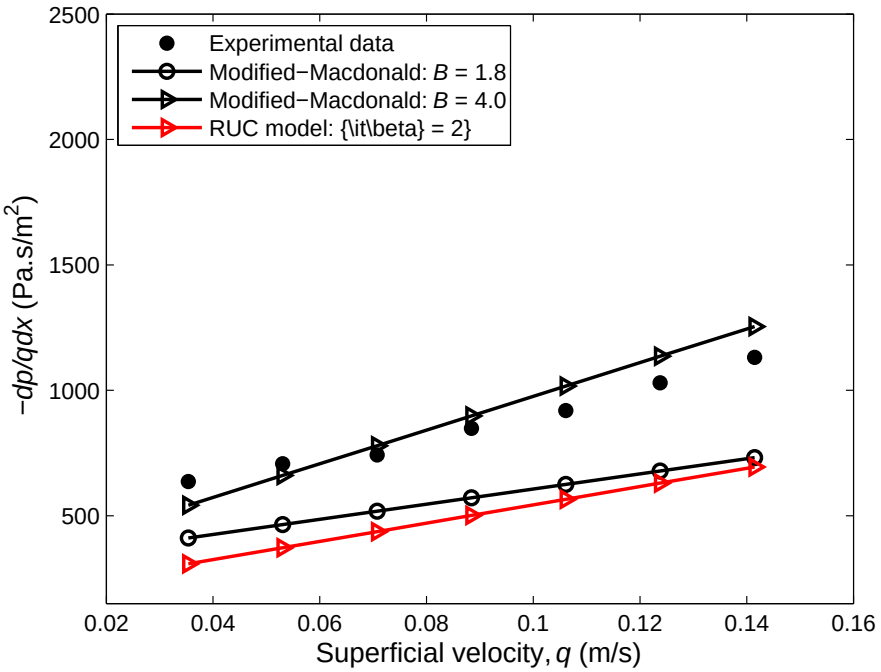

Figure A12. Biofilter 3: Model predictions for day 19.

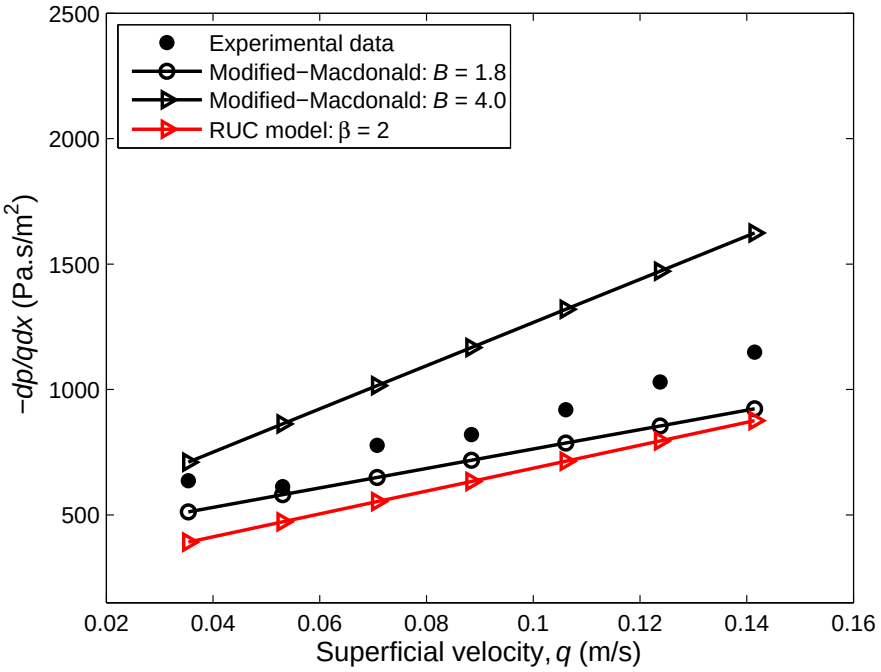

Figure A13. Biofilter 3: Model predictions for day 39.

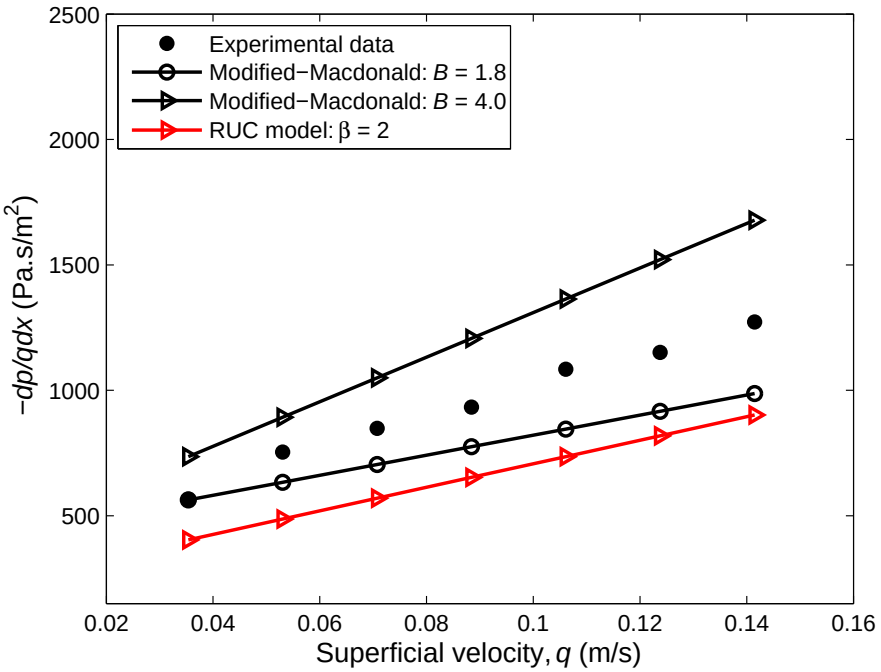

Figure A14. Biofilter 3: Model predictions for day 57.

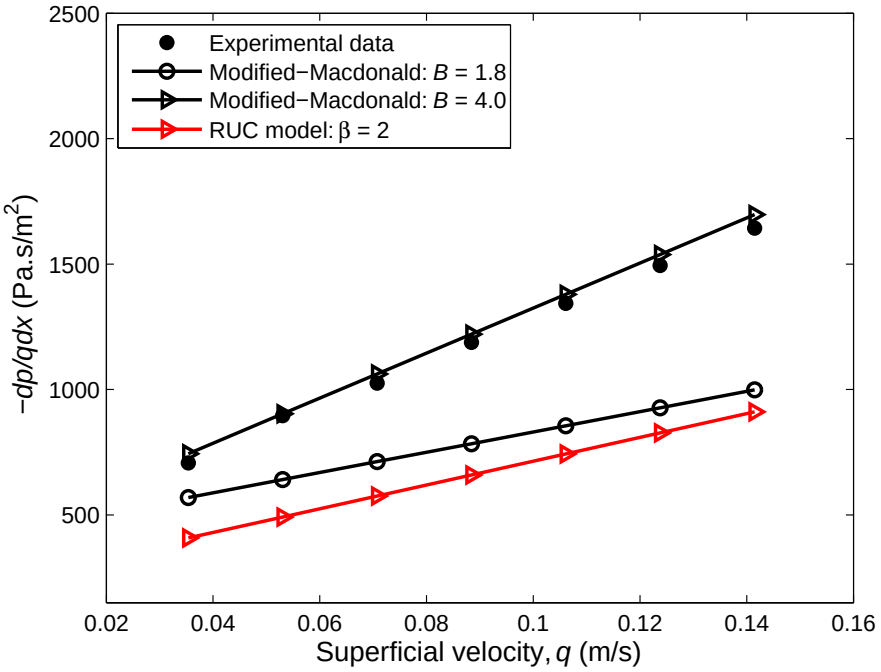

Figure A15. Biofilter 3: Model predictions for day 71.

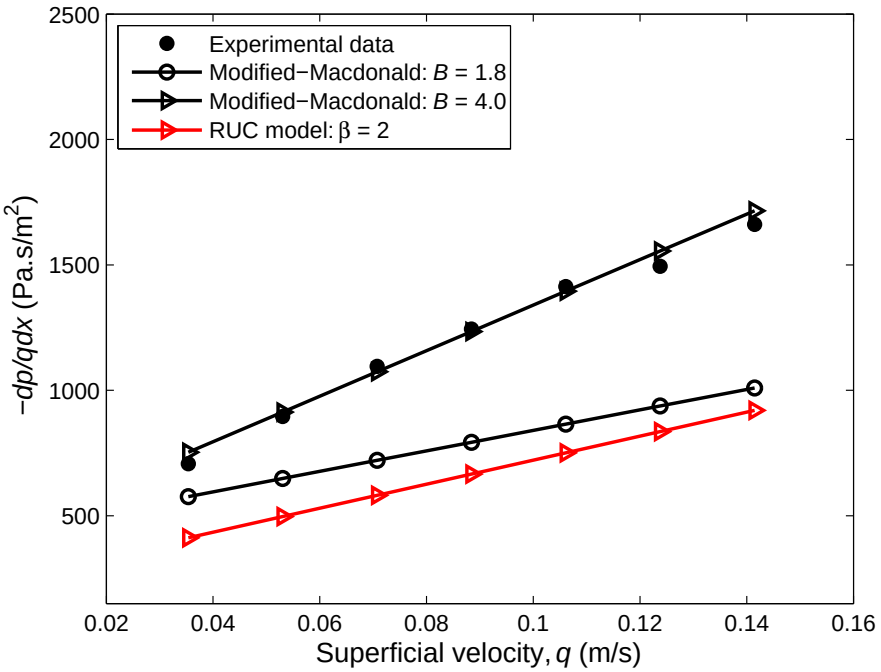

Figure A16. Biofilter 3: Model predictions for day 106.

Appendix B

Sensitivity Analysis

Figures B1 to B10 contain the differences between the results obtained from the Modified-Macdonald equation and the RUC model when $\phi = 0.85$ and $\phi = 0.63$ for Biofilters 2 and 3. Figures B11 to B14 contain the results obtained from the sensitivity analysis on the effect of the coordination number in the analytical approach for Biofilters 2 and 3.

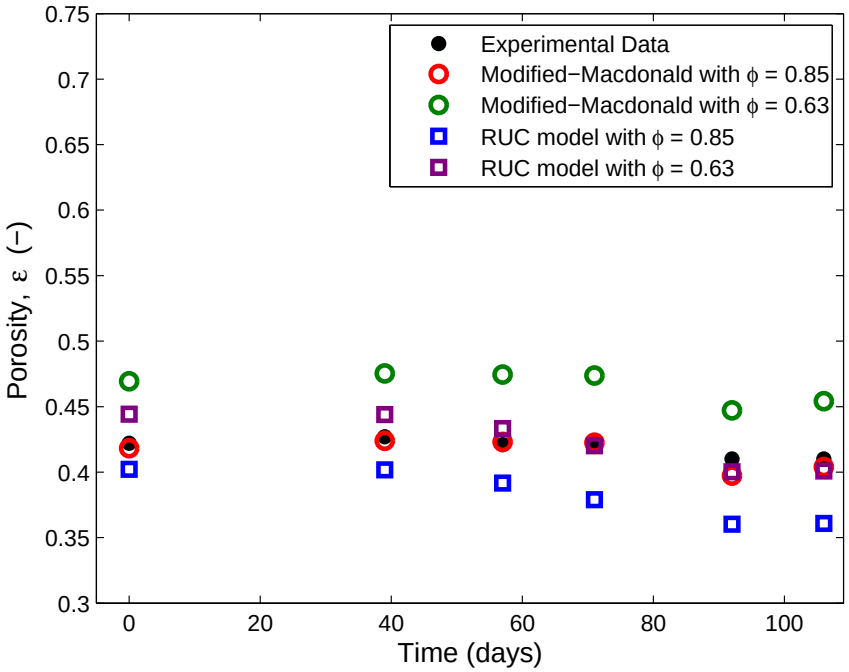

Figure B1. Biofilter 2: Comparison between optimized porosity values for $\phi = 0.85$ and $\phi = 0.63$.

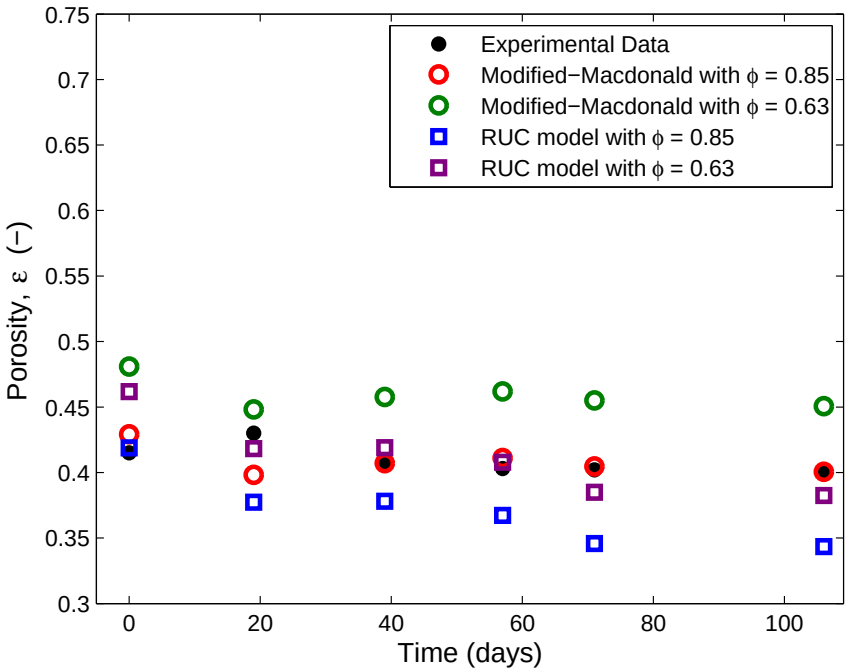

Figure B2. Biofilter 3: Comparison between optimized porosity values for $\phi = 0.85$ and $\phi = 0.63$.

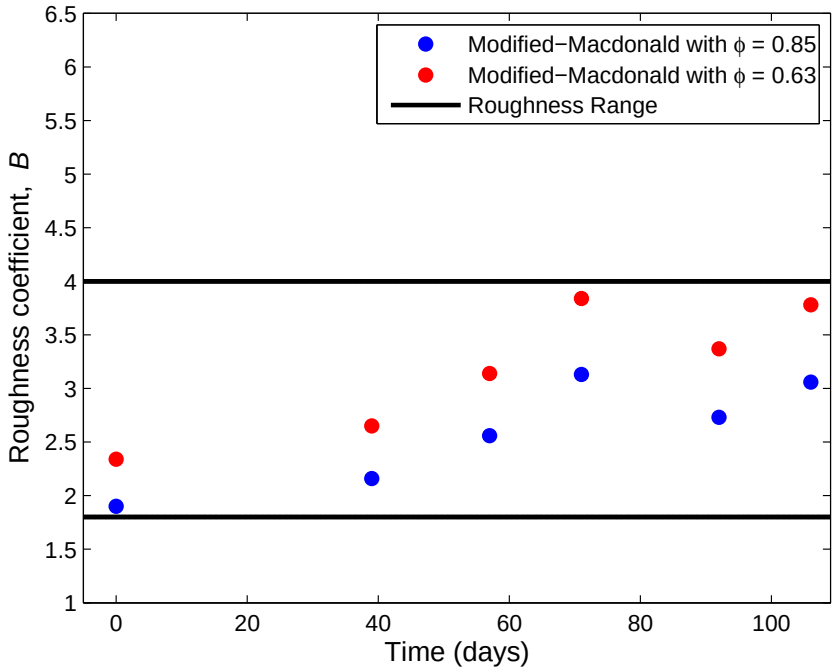

Figure B3. Biofilter 2: Comparison between optimized B-values for $\phi = 0.85$ and $\phi = 0.63$.

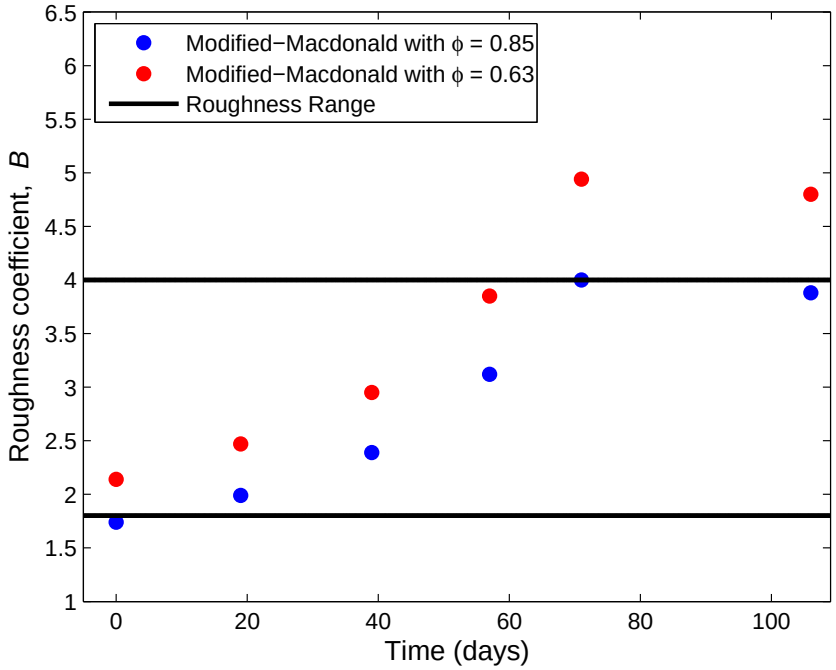

Figure B4. Biofilter 3: Comparison between optimized B-values for $\phi = 0.85$ and $\phi = 0.63$.

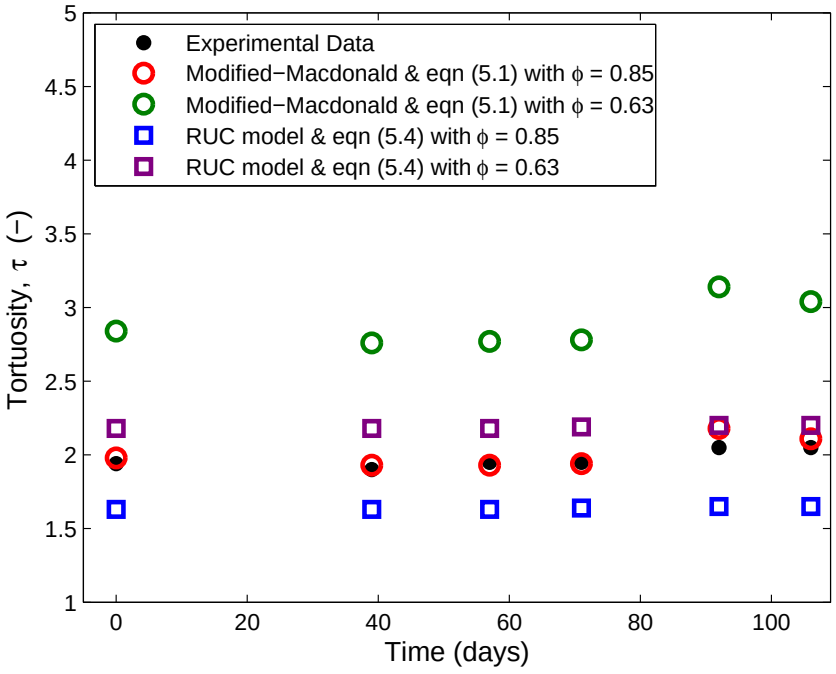

Figure B5. Biofilter 2: Comparison between optimized τ-values for $\phi = 0.85$ and $\phi = 0.63$.

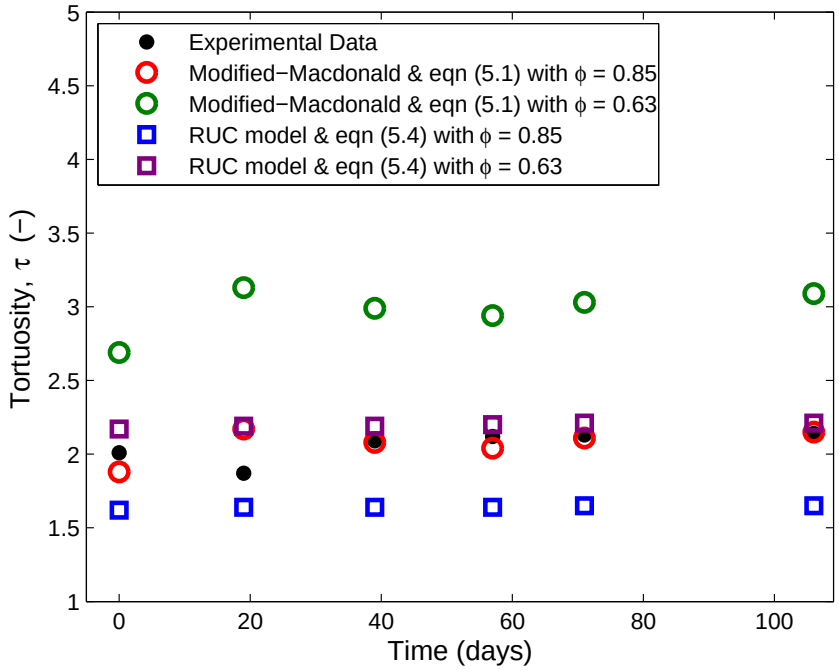

Figure B6. Biofilter 3: Comparison between optimized τ-values for $\phi = 0.85$ and $\phi = 0.63$.

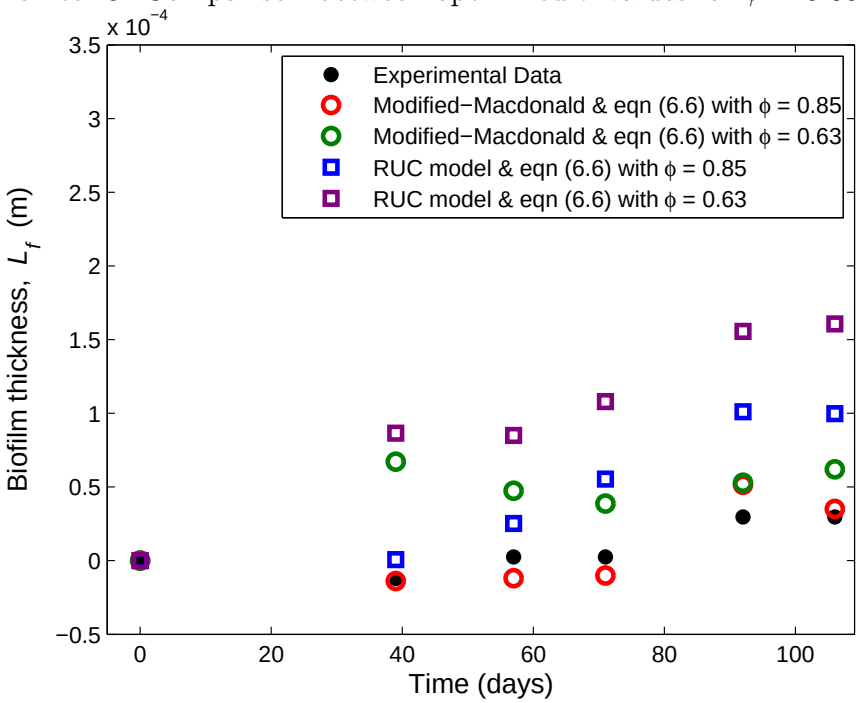

Figure B7. Biofilter 2: Comparison between optimized L_f-values for $\phi = 0.85$ and $\phi = 0.63$.

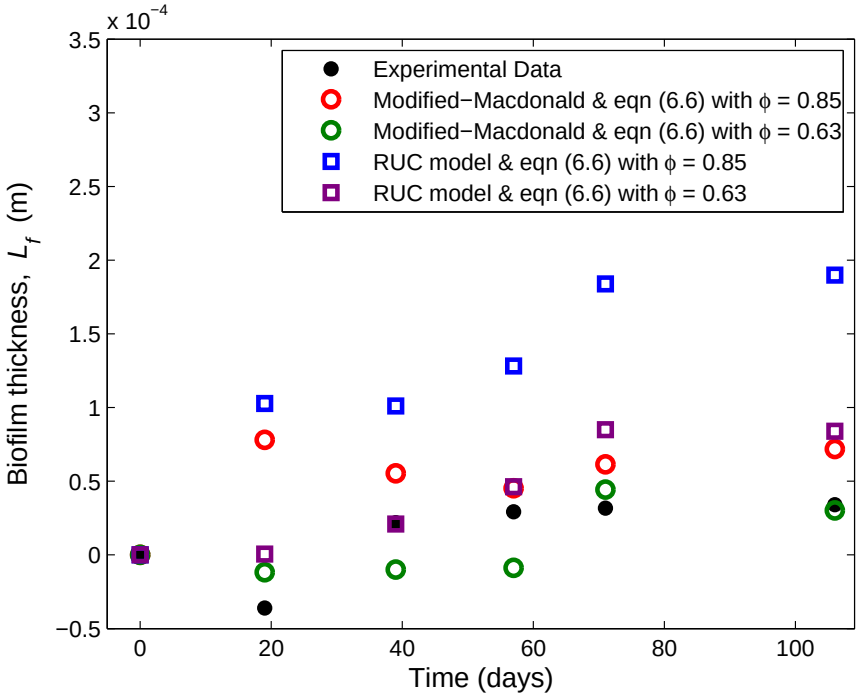

Figure B8. Biofilter 3: Comparison between optimized L_f-values for $\phi = 0.85$ and $\phi = 0.63$.

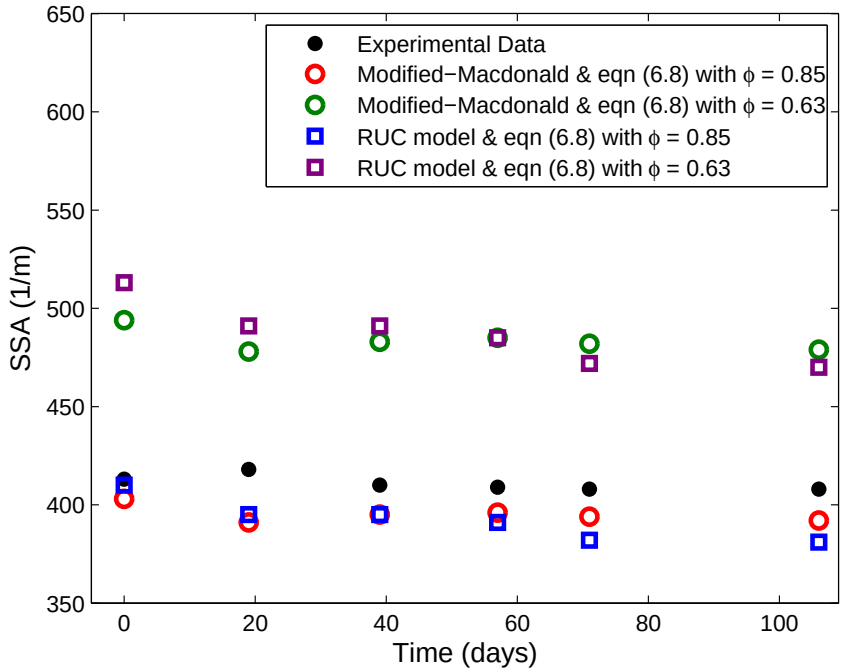

Figure B9. Biofilter 2: Comparison between optimized SSA values for $\phi = 0.85$ and $\phi = 0.63$.

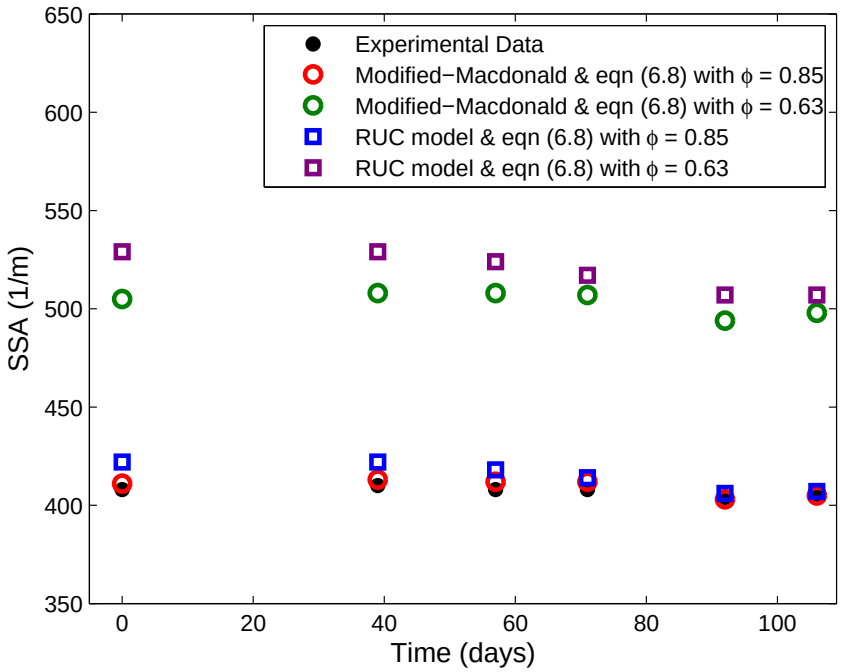

Figure B10. Biofilter 3: Comparison between optimized SSA values for $\phi = 0.85$ and $\phi = 0.63$.

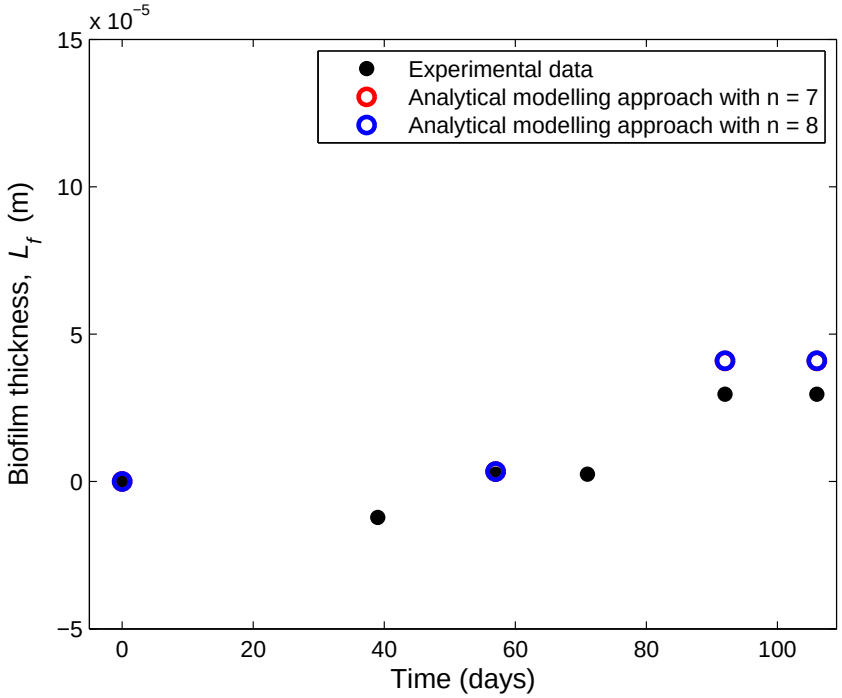

Figure B11. Biofilter 2: Comparison between L_f-values for $n = 7$ and $n = 8$.

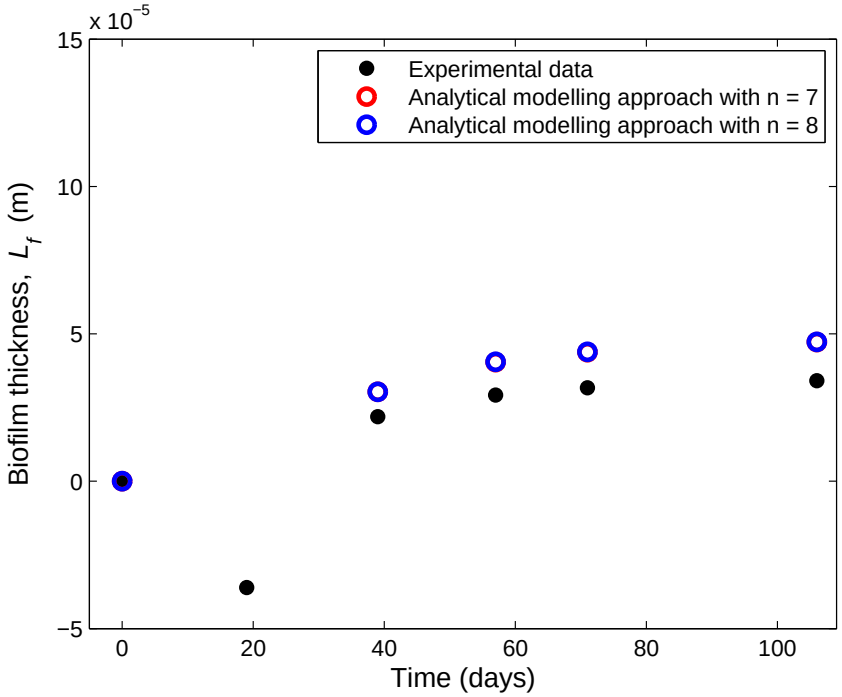

Figure B12. Biofilter 3: Comparison between L_f-values for $n = 7$ and $n = 8$.

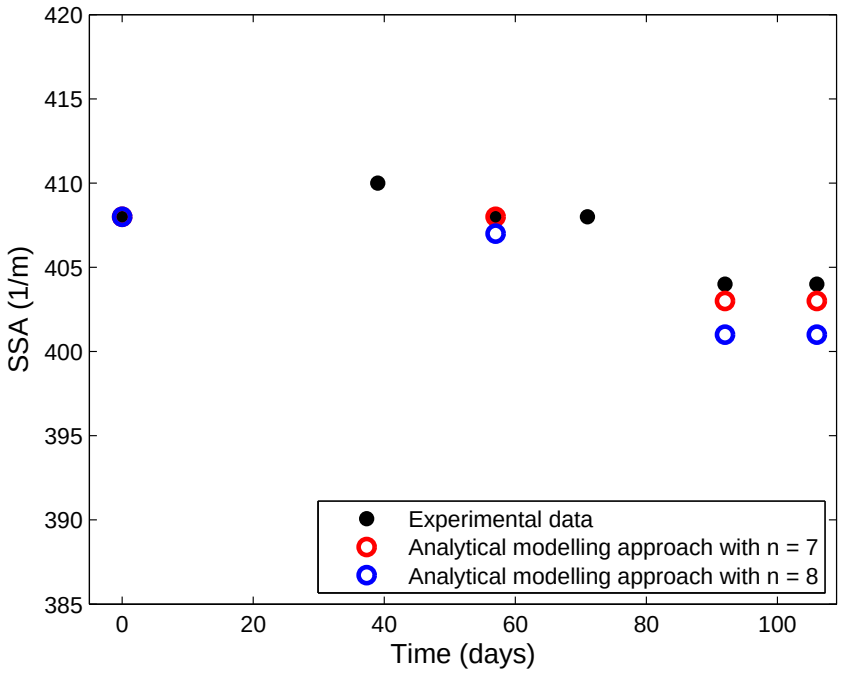

Figure B13. Biofilter 2: Comparison between a_f-values for $n = 7$ and $n = 8$.

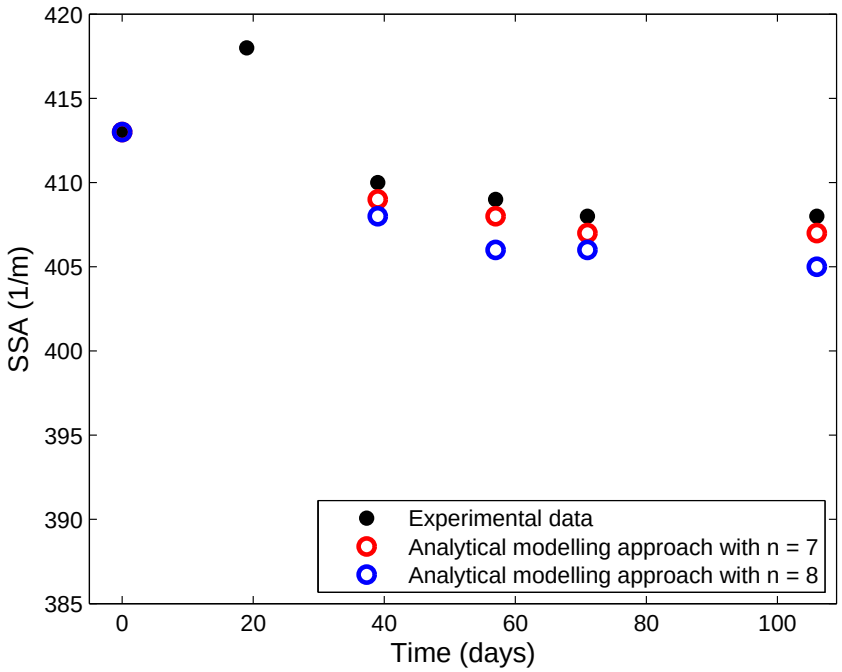

Figure B14. Biofilter 3: Comparison between a_f-values for $n = 7$ and $n = 8$.

Appendix C

Final Pressure Drop Predictions

The following graphs contain the pressure drop predictions made by the Modified-Macdonald equation compared to those made by the adapted RUC model.

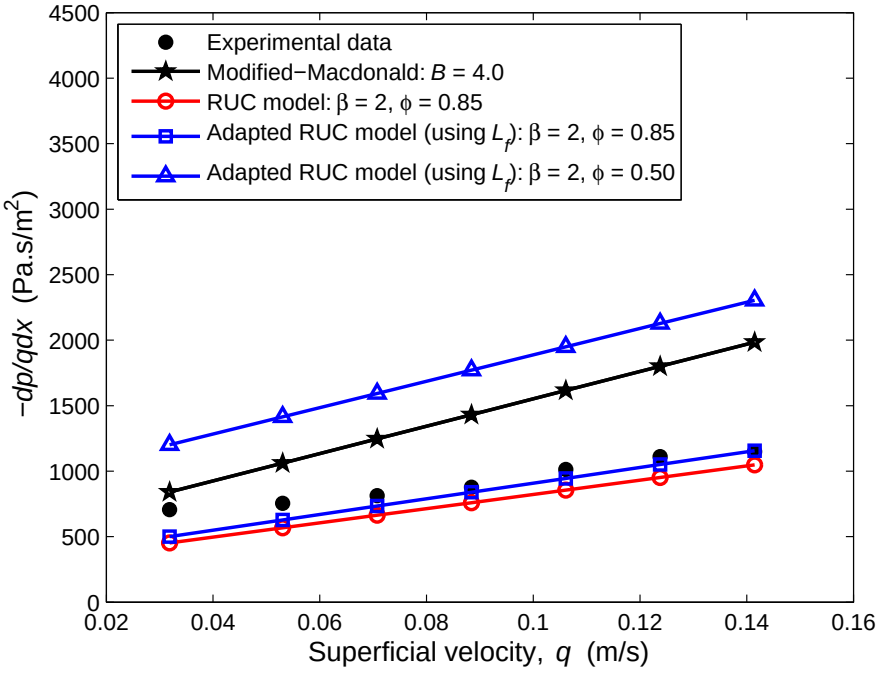

Figure C1. Biofilter 1: Adapted RUC model vs Modified-Macdonald equation for day 19.

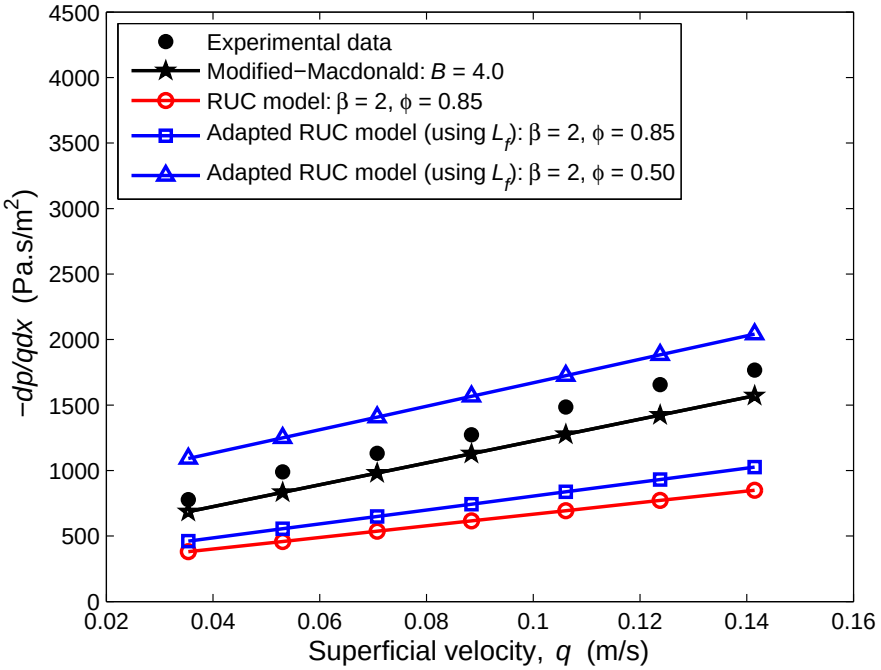

Figure C2. Biofilter 1: Adapted RUC model vs Modified-Macdonald equation for day 57.

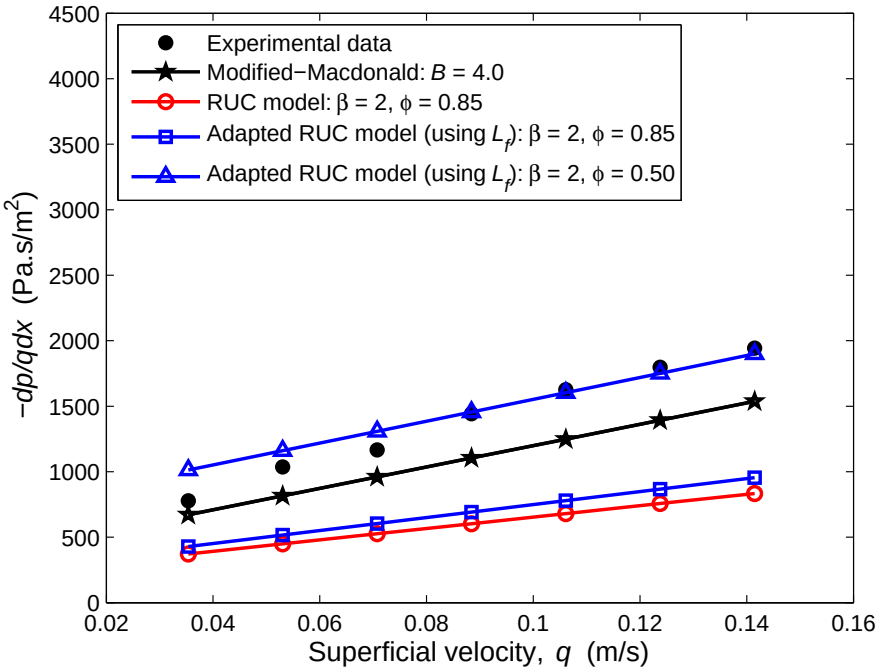

Figure C3. Biofilter 1: Adapted RUC model vs Modified-Macdonald equation for day 71.

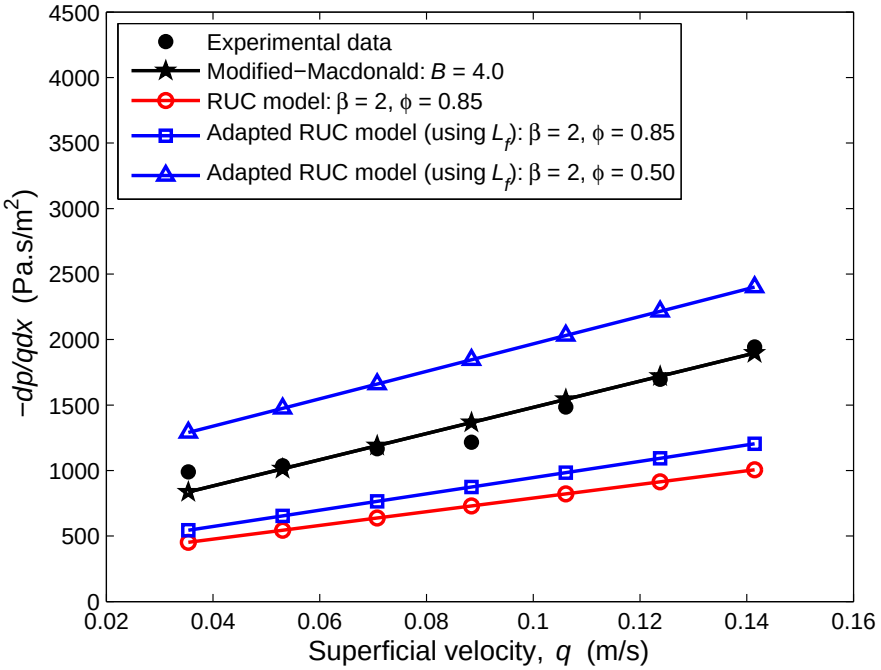

Figure C4. Biofilter 1: Adapted RUC model vs Modified-Macdonald equation for day 92.

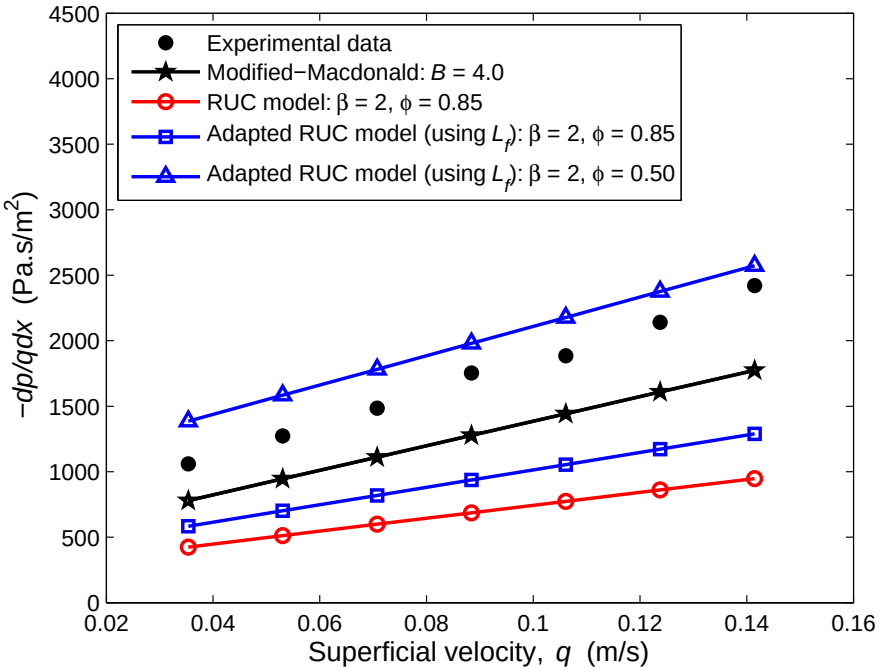

Figure C5. Biofilter 1: Adapted RUC model vs Modified-Macdonald equation for day 106.

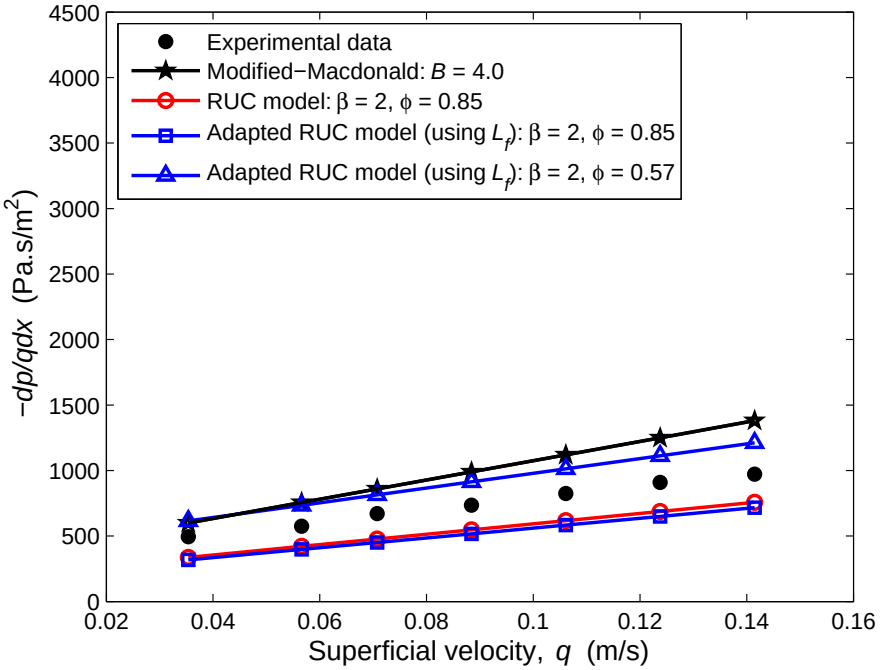

Figure C6. Biofilter 2: Adapted RUC model vs Modified-Macdonald equation for day 57.

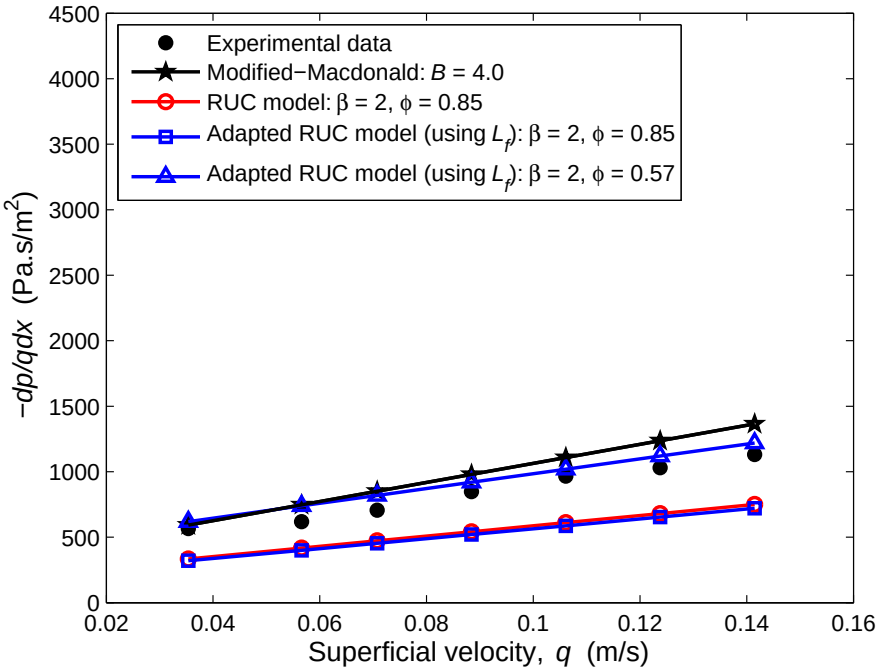

Figure C7. Biofilter 2: Adapted RUC model vs Modified-Macdonald equation for day 71.

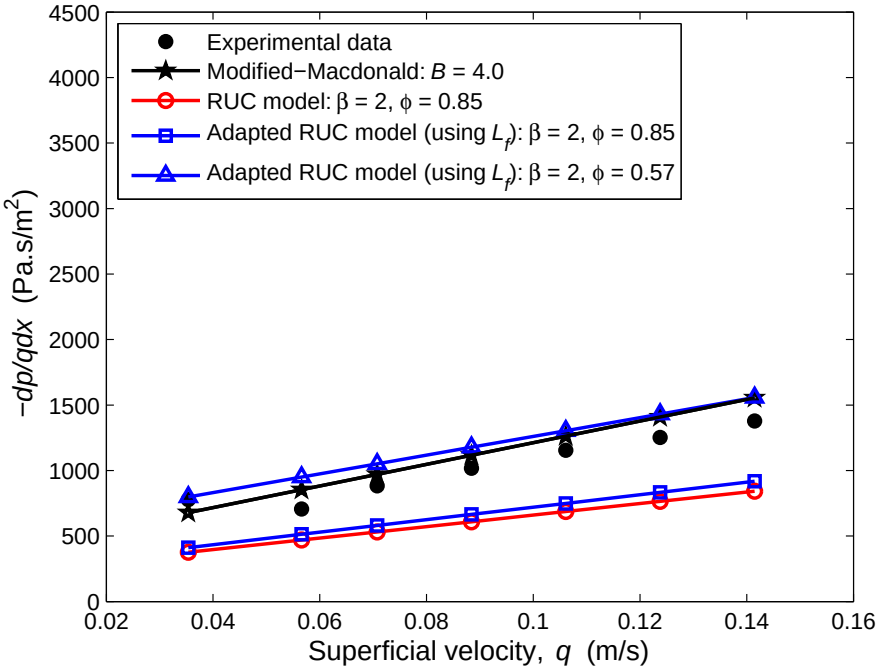

Figure C8. Biofilter 2: Adapted RUC model vs Modified-Macdonald equation for day 92.

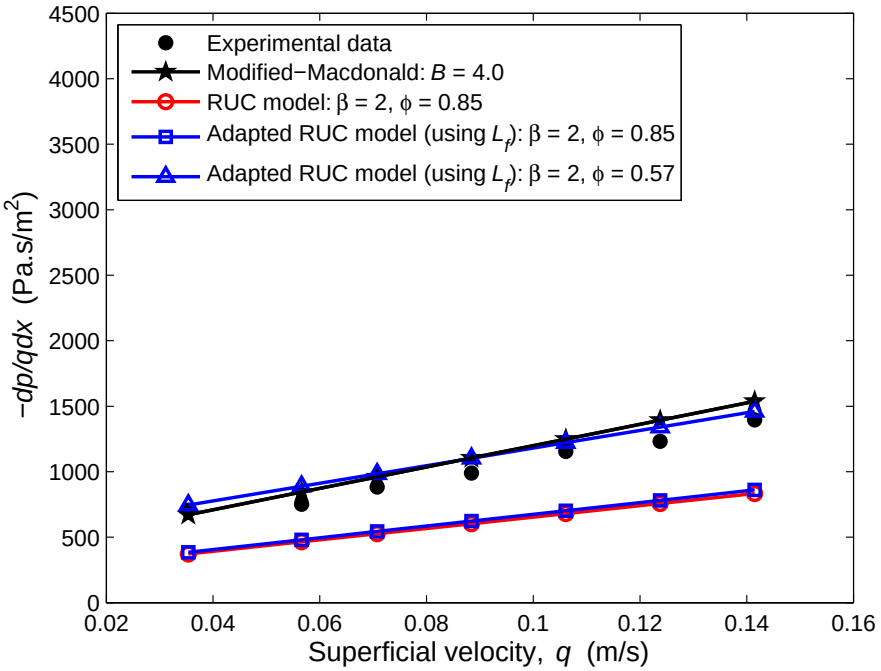

Figure C9. Biofilter 2: Adapted RUC model vs Modified-Macdonald equation for day 106.

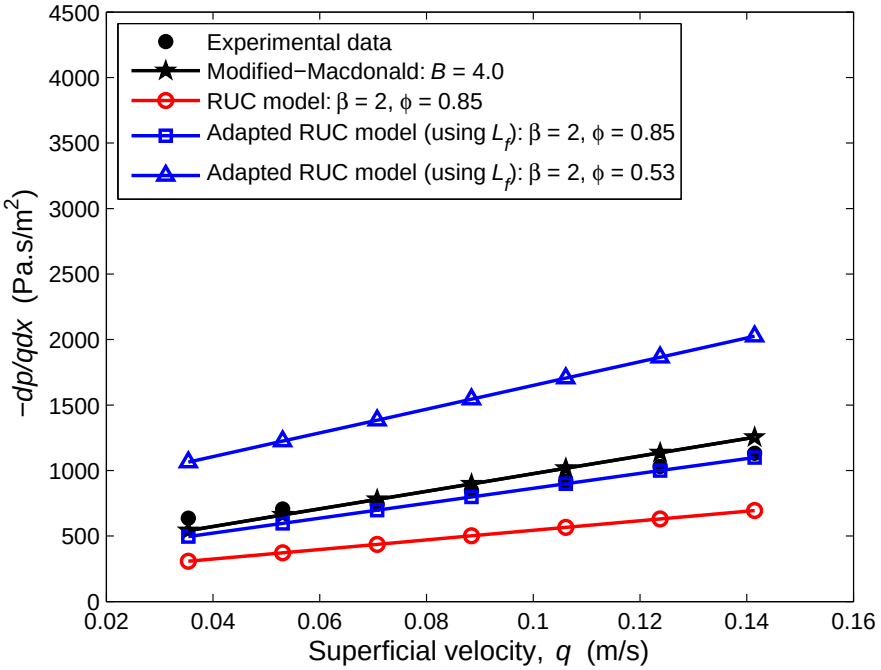

Figure C10. Biofilter 3: Adapted RUC model vs Modified-Macdonald equation for day 19.

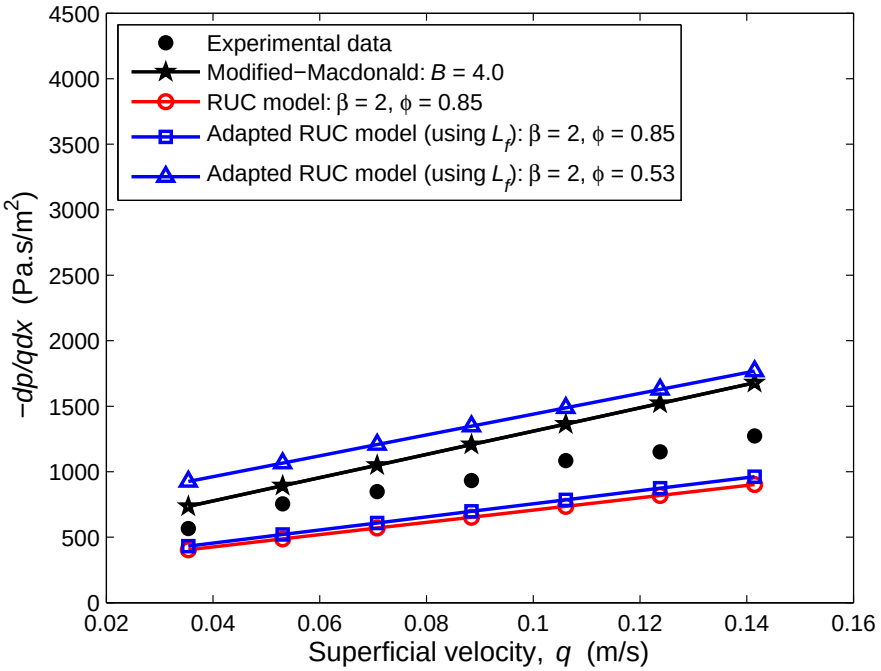

Figure C11. Biofilter 3: Adapted RUC model vs Modified-Macdonald equation for day 57.

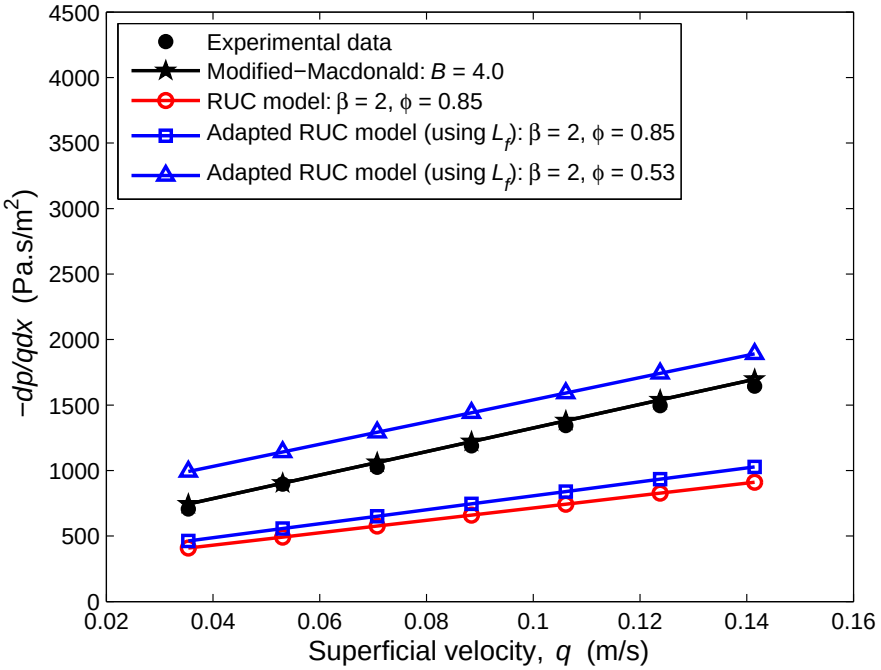

Figure C12. Biofilter 3: Adapted RUC model vs Modified-Macdonald equation for day 71.

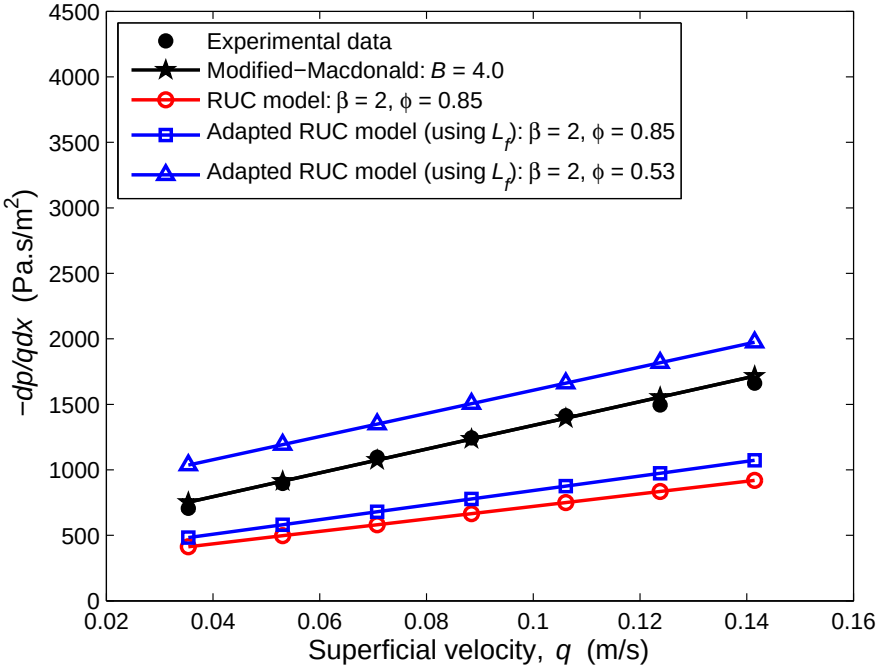

Figure C13. Biofilter 3: Adapted RUC model vs Modified-Macdonald equation for day 106.